UNIVERSITY OF CAPE COAST

THREE-DIMENSIONAL IMAGING WITH LONG INFRARED DIGITAL HOLOGRAPHY

PHILIP KWASI MENSAH

2016

Digitized by UCC, Library

UNIVERSITY OF CAPE COAST

THREE-DIMENSIONAL IMAGING WITH LONG INFRARED DIGITAL HOLOGRAPHY

BY

PHILIP KWASI MENSAH

Thesis submitted to the Department of Physics of the school of Physical Sciences, College of Agriculture and Natural Sciences, University of Cape Coast in partial fulfillment of the requirements for the award of Doctor of Philosophy degree in Physics.

JULY, 2016

Digitized by UCC, Library

DECLARATION

Candidate's Declaration

I hereby declare that this thesis is the result of my own original research and that no part of it has been presented for another degree in this university or elsewhere.

Signature: …… Date: …….

Candidate's Name: Philip Kwasi Mensah

Supervisors' Declaration

We hereby declare that the preparation and presentation of the thesis were supervised in accordance with the guidelines on supervision of thesis laid down by the university of Cape Coast.

Signature: …… Date: ……..

Principal Supervisor's Name: Professor Riccardo Meucci

Signature: ……. Date: ……..

Co-Supervisor's Name: Professor P. K. Buah-Bassuah

Digitized by UCC, Library

ABSTRACT

A three-dimensional (3D) laser imaging system based on digital holography has been used as a tool for testing digital holography (DH) in the infrared (IR) range in several configurations; transmission and reflection mode. The feasibility of digital holography in the infrared region was demonstrated using two beam interferometric technique for recording holograms both in reflection and transmission type geometry which employs a pyroelectric sensor array detector. The materials used are two euro coins, marble plate, earthenware tree, Aluminum plate, Lens mount, Bronze statues of Augusto and Traiano, lens mount, Bronze statue and human size mannequin. Their sizes ranges from 2.3 cm to 170.0 cm. Images from these different objects were acquired with high resolution miricle thermoteknix cameras. The recorded images in the form of fringes were transferred to a computer for analysis using MATLAB software. By making use of image processing tools and Fast Fourier Transform (FFT) technique, the 3D images of the samples were analyzed and decoded, to the original real object from the fringes. IR digital holography has many advantages whenever large object and hard materials of high depth penetration, recording and reconstruction is required with respect to digital holography in the visible region. A long wavelength radiation has a lower sensitivity to sub micrometric vibrations- use of larger angles, smaller distances between the object and the recording device- this peculiarity provides a higher fringe visibility when large samples are investigated.

Digitized by UCC, Library

ACKNOWLEDGEMENTS

I would like to gratefully acknowledge the supervision of Prof. Riccardo Meucci and Prof. P.K Buah-Bassuah during this work. I thank Dr. Massimilliano Locatelli for the technical support on the equipment selections and helpful corrections of the data. Other colleagues in the Istituto Nazionale di Applicata (INOA) Research Group in Firenze, Italy, also provided valuable service, especially Andrea Geltrude who was always patient and helpful to answer questions about the MATLAB programming and the formation of the holograms. My gratitude also goes to the Head of Department, Prof. M. J. Eghan, for his support and encouragement. My thanks go to Prof. J.J Fletcher, Dr. Alfred Owusu, and all Senior Members and Senior Staff of the Physics Department who contributed in various ways towards the successful completion of this work. I acknowledge the massive support of all colleagues especially Kwadwo Anokye Dompreh and Matthew Amekpewu. I thank all members of the Mensah family who have contributed greatly towards my education. My last but not the least thanks go to the Office of External Activities (OEA) of the International Center for Theoretical Physics (I.C.T.P), and the TRIL programme for financial support at CNR-INOA in Firenze, Italy. Throughout my life as a graduate student, their regular support, advice and friendship has been a very vital factor in seeing this day.

Digitized by UCC, Library

DEDICATION

This doctoral thesis is dedicated to all members of the Mensah family, past, present and generations to come.

Digitized by UCC, Library

TABLE OF CONTENTS

Digitized by UCC, Library

Digitized by UCC, Library

Digitized by UCC, Library

Digitized by UCC, Library

Digitized by UCC, Library

LIST OF FIGURES

Digitized by UCC, Library

Digitized by UCC, Library

Digitized by UCC, Library

Digitized by UCC, Library

Digitized by UCC, Library

Digitized by UCC, Library

Digitized by UCC, Library

Digitized by UCC, Library

LIST OF PLATES

Digitized by UCC, Library

LIST OF TABLES

Digitized by UCC, Library

LIST OF SYMBOLS

3D	Three dimensional
2D	Two dimensional
CCD	Charge coupled device
CMOS	Complimentary Metal-Oxide Semiconductor
PSD	Position sensitive detector
IR	Infrared
DH	Digital holography
IRDH	Infrared digital holography
FPA	Focal plane array
CO_2	Carbon dioxide
NIR	Near-infrared
PC	Personal computer
CW	Continuous wave
U_o	Complex amplitude of the object wave
U_r	Complex amplitude of the reference wave
Eo	Real amplitude of the object wave
E_r	Real amplitude of the reference wave
φ_o	Phase of the object wave
φ_r	Phase of the reference wave
U_h	Digital hologram
β	Constant dependent on the exposure characteristics of the hologram recording media.

Digitized by UCC, Library

τ	Exposure time of recording the hologram
h_0	Amplitude transmission of the unexposed plate
FFT	Fast Fourier transforms
θ_{max}	Maximum angle between the object wave and the reference wave
f_{max}	Maximum spatial frequency that can be resolved
λ	Wavelength
Δx	Distance between neighbouring pixels of a CCD/CMOS camera in *x* axis
Δy	Distance between neighbouring pixels of a CCD/CMOS camera in *y* axis
THz	Terahertz
µm	micrometer
cm	Centimeter
nm	Nanometer
Ge	Germanium
InSb	IndiumAntimony
HgCdTe	Mercury cadium telluride
LiTaO3	Lithium tantalate
BS(1&2)	Beam splitters
ZnSe	Zinc Selenide
USB	Universal serial bus
TEM_{00}	Transverse electromagnetic (lowest-order mode)

Digitized by UCC, Library

70T/30R	70% Transmittance and 30% Reflectance
50T/50R	50% Transmittance and 50% Reflectance
Laser	Light amplification by stimulated emission of radiation
(ξ, η)	Point in the object plane
(x, y)	Point in the hologram plane
(ξ', η')	Point in the image plane
Γ	Diffracted field
ρ'	Distance between a point in the hologram plane and a point in the reconstruction plane
ρ	Distance between a point in the object plane and a point in the hologram plane
Q	Inclination factor
d	Recording distance between the object plane and the hologram plane
d′	Reconstruction distance between the reconstruction plane and the hologram plane
I	Intensity
φ	Phase
Re	Real part
Im	Imaginary part
*	Conjugate function
f	Focal length of a lens
$L(x, y)$	Lens function in the hologram plane

Digitized by UCC, Library

$P(\xi', \eta')$	Phase correction factor when introduced a lens
$\Delta\xi$	Distance between neighbouring pixels in *x* axis of the reconstruction plane
$\Delta\eta$	Distance between neighbouring pixels in *y* axis of the reconstruction plane
	Convolution operation
USAF	United States Airforce target
ASi	Amorphous Silicon
LiF	Light-in-flight
HUD	Head-up-display
HOE	Holographic Optical element
A/D	Analogue-digital converter
	Forward Fourier Transform
$^{-1}$	Inverse Fourier Transform

Digitized by UCC, Library

CHAPTER ONE

INTRODUCTION

Interferometers provide a means of measuring optical path differences through the analysis of fringe patterns formed by the interference of coherent light waves. However, in holographic interferometer, a wave front is stored in a hologram and later compared interferometrically with another wave front. Phase differences between these two wave fronts produce fringes that can be analysed to yield a wide range of both qualitative and quantitative information about the system originating these two wave fronts. Long wavelength interferometers have been widely applied in different fields, such as infrared optics, infrared transmitting materials, and high-reflective multilayer dielectric coatings for high power laser systems (Beaulier, et al., 1978 and Decker,et al.,1972).

In optical metrology, long-wave interferometers are also employed for shape measurement of reflective rough surfaces and for testing optical systems that requires deep aspheric. An advantage of using long wavelength is that the aspheric departure from the best fit reference-sphere, in unit of the probing wavelength, is reduced at longer wavelength, thus allowing one to obtain an interferogram of the deep aspheric under test (De Nicola, 2008). Optical methods have been used as a metrological tool for a long time. They are non-contact, non-destructive and very accurate. With the use of computers and other electronic devices, they have become faster, more reliable, more convenient and more robust.

Digitized by UCC, Library

Holography is one of the optical methods. Since the early stage of holography, many efforts have been devoted to find reliable materials to record holograms using Infrared (IR) wavelengths of 770 nm to 1 mm (Prevost et al, 1989 and Rioux, et al,1977 &1978). This spectral range could open new and interesting opportunities. It was envisaged that many materials, opaque to visible radiation but transparent to IR could be tested in this way (Beaulier, et al., 1978). For instance, using the $10\mu m$ wavelength, holography could allow the inspection of infrared glasses, such as Ge, InSb and HgCdTe which are impossible to control in the visible and near-IR ranges (Rukman, et al., 1978). Also, it was known that such long IR wavelength is appropriate to investigate plasma, since the interferometric sensitivity of interferometric measurement of electron concentrations increases with the wavelength of the probing radiation (Rukman et al, 1978).

On the other hand, the use of long IR wavelengths reduces the sensitivity of interferometric measurements and therefore IR holography is well suited for optical testing of aspheric optics, or to measure the optical path variation, dispensing from the use of multiple wavelengths in the visible region (Ferraro et al., 2005 and Chivian et al, 1969). It is also of particular significance in those digitally holographic-based applications, where the flexibility of the numerical reconstruction process allows refocusing the numerically reconstructed images of a 3D object at different planes over a range of distances usually larger than the source wavelength.

Digitized by UCC, Library

In industry there is the need for accurate measurement of three-dimensional (3D) shape of objects to speed up product development and ensure manufacturing quality. Also, in medical field knowledge of the 3D shape and other biological features of the suspected objects are helping medical experts to make correct diagnoses, choose appropriate treatments and to effectively evaluate such treatments. In this chapter, an overview of 3D shape measurement is initially presented. The conception and the development of holography as important tool to fulfil the task of 3D shape measurement are also presented. The disadvantages and limitations of this technology are introduced in this thesis. The objective and scope, contribution and structure of the thesis are presented in the last section of this chapter.

An overview of 3D shape measurements using optical methods

Various optical techniques have been developed for measuring 3D shape from a single position (Tiziani, 1997 and Chen et al., 2000). For instance the time –of- flight technique measures the flight time of pulse from a laser or other light source to an object and back. The flight time for two pulses, one of which is reflected from the surface of the object to the receiving sensor and the other passing through an optical fiber are measured and compared to determine the distance. A typical resolution of this technique is approximately 1mm (Juptner, et al., 1996). Although with improvements in the equipment, the resolution can be better than 30μm at a standoff distance of about 1 m. Another similar technique is called Light-in-Flight (LiF) holography.

Digitized by UCC, Library

Holographic recording of LiF was first proposed by Abramson (1983, 1984a, 1984b and 1985). He observes that a hologram can only image the distance in space where the optical path of the reference wave matches that of the object wave. Digital holography has been applied to LiF recordings (Pomarico et al., 1996). Either short temporal coherence light or very short light pulse is used to generate a motion image of propagating optical wave front. The depth resolution may be estimated to be 6.5 μm (Nilsson and Carlsson, 1998). The active triangulation technique is a powerful tool for 3D shape measurement. A laser spot is projected on the surface of the object and is imaged through a Charged Coupled Device (CDD) or a Position Sensitive Detector (PSD). The lateral displacement of the spot image is related to the depth of the object. Its typical measurement range is 5 mm to 250 mm and accuracy is about 1 part in 10,000 with measurement frequency of 40 kHz or higher (Ji and Leu, 1989; Keferstein and Marxer, 1998). Sensors based on the triangulation principle are suitable for inspection and measurement in industrial environment.

However, both laser speckle and differences in the surface characteristics of the measured object from that of the calibration surface, limit the accuracy of measurements. Structured light techniques may also be categorised amongst the active triangulation methods, as they project either coded the light or sinusoidal fringes onto the object. The height distribution of the surface of the object is encoded into a deformed fringe pattern which is captured by an image acquisition

Digitized by UCC, Library

sensor (Srinivasan et al., 1984). The shape is directly decoded from this recorded image according to the calibrated system parameters.

This technique is easy to implement in an industrial environment. By the use of a computer controlled projector and camera, no moving parts have to be used and the full field measurement can be done within less than a second. In an optimized structured light projection system, the measurement accuracy may achieve 1 part in 20,000. However, the problem of shading which is inherent to all triangulation techniques is also a limitation of the structured light techniques. Moiré can be traced back over many years as a measurement technique. The key to this technique is the Moiré effect. When two sinusoidal gratings, are superimposed with a small angle between the grating lines, a fringe pattern of much lower frequency than the individual gratings can be generated and resolved by a CDD camera.

It is often termed as mechanical interference, because the mathematical description of a Moiré pattern is the same as the interference pattern formed by electromagnetic waves (Cloud,1995). Rapid image acquisition and phase shifting techniques have been introduced to Moiré systems to overcome environmental perturbations and to analyse the fringe pattern produced (Kujawinska et al., 1991; Van Haasteren and Frankena, 1994). The typical measurement range of the phase shifting Moiré method is 1mm to 500mm with a resolution similar to that of structured light projection at 0.1 to 0.01 of a fringe. Laser interferometer is probably one of the most commonly used techniques in metrology for high-resolution and high-precision measurement. The idea behind interferometric

Digitized by UCC, Library

shape measurement is that the fringes are formed by variation of the sensitivity matrix that relates the geometric shape of an object to the measured optical phase.

The matrix contains four variables, wavelength, refractive index, and illumination and observation directions. These are the dual or multiple wavelength methods (Haddad, 1965), the refractive index change methods (Zelenka and Varner, 1969), and the illumination direction variation/ two sources methods (Abramson, 1976). There are also other methods for optical 3-D shape measurement, such as laser speckle pattern sectioning (Dresel et al., 1992), photogrammetric, laser tracking systems and confocal microscopy (Wilson, 1990). Different methods have been developed to fulfill the requirements of various applications. For optically rough surfaces, the Moiré and fringe projection methods are widely used as they are less sensitive to environmental effects and can perform fast full field measurements. Also, their measurement range is much larger than that of interferometers. However, if the size of the object is smaller than a few centimeters and the high accuracy is needed, interferometers are a more appropriate option. It was a barrier for holography that there was a necessary intermediate photographic recording set-up and wet-chemical processing stage. But with the advent of digital holography, holography can be performed nearly in real time and there is no longer any requirement for this time-consuming photographic process involved. The background of holography will be discussed first before describing the application of digital holography to the measurement of surfaces of real.

Digitized by UCC, Library

Principle of digital holography

Holography is a method which records and reconstructs not only the irradiance of each point in an image, but also the direction in which the wave is propagating at that point. That is what its name means, which is a whole record as compared to photography which only records the intensity of the optical wave at each point. Holography records both amplitude and phase of light field, whereas in photography all information about the relative phases of the light waves from the original three-dimensional scene is lost.

However, holography is quite different. It does not record an image of the object wave, but the object wave itself. Since all recording media, for example photographic emulsions or photonic detectors, only respond to irradiance, it is necessary to convert the phase information of the object wave into variations of irradiance. This makes holography an essentially different process from that of photography.

Correlation between holography and photography

Holography may be better understood via an examination of its differences from ordinary photography: A hologram represents a recording of information regarding the light that come from the original scene as scattered in different angle of directions rather than from only one direction as in photography. This allows the scene to be viewed from a range of different angles, as if it were still present. A photograph can be recorded using normal light sources (sunlight or electric lighting) whereas a hologram is recorded using laser sources.

Digitized by UCC, Library

Holographic recording requires registering an interference pattern to be recorded using diffraction principles. A photograph can be viewed in a wide range of lighting condition, whereas holograms can only be viewed with specific forms of illumination, when a photograph is cut in half, each piece shows half of the scene; however, a hologram when cut in half the whole scene can still be seen in each piece. This is because whereas each point on a photographic recording includes information about light scattered from every point in the scene. A photograph is a 2D representation that can only reproduce a rudimentary 3D effect. Whereas the reproduced viewing range of hologram adds many more depth perception cues that were present in the original scene.

The basic procedure in holography consists of two beams; a reference beam and a reflected beam from the object to form an interference pattern of the object. What was actually recorded was the interference pattern formed by the light scattered from the surface of the object and a coherent beam called the reference wave as shown in figure 1a and 1b in transmission and reflection configuration modes. The coherent beam ensures that the interference is displayed stably in time. The object cannot be recognise directly from its hologram, because it is in the form of bright and dark microscopic fringes. These micro fringes are not visible to the human eye due to the high spatial frequencies involved.

Digitized by UCC, Library

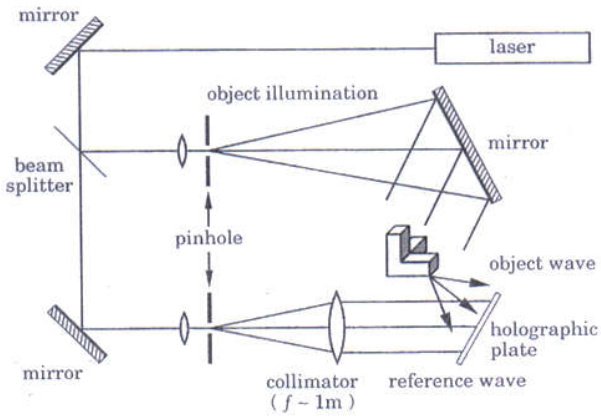

Figure 1a: An arrangement for recording reflection holograms. (Lauterborn, et al., 2013)

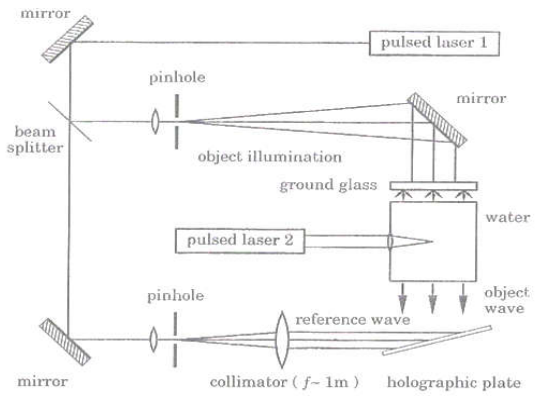

Figure 1b: Arrangement for recording transmission holograms. (Lauterborn, et al.,2013)

The hologram is usually recorded on flat surfaces but contains 3D information. A reconstruction beam is used to illuminate the hologram and it is positioned at the same angle as the reference beam that was used as shown in figure 1c, during recording phase.

Digitized by UCC, Library

When the reconstruction beam was at a right angle, three beams of light will emerge through the hologram. An undiffracted beam (zeroth order) will pass directly through the hologram. The second beam forms the primary (virtual) image (first order) that is diffracted at the same angle as the incoming object beam that was used during recording. The third beam forms the secondary (real) image (first order). Figure 1c, which form the images are diffracted at the same angle α , from the undiffracted beam. Between the image beams, the angle is twice as large (2α).

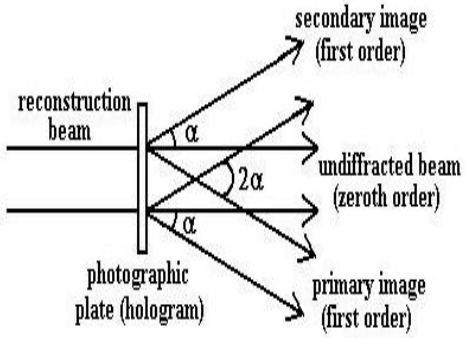

Figure 1c: Image reconstruction. (Lauterborn, et al.,2013)

Looking at the hologram at the same angle as the primary image beam, a virtual image of the object located behind the hologram was observed as shown in figure 1d. Also, looking at the hologram at the same angle as the secondary image beam, a real image of the object located in front of the hologram can be observed as shown in figure 1e.

Digitized by UCC, Library

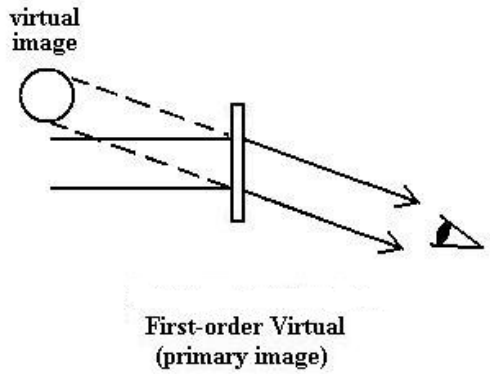

Figure 1d: Image reconstruction of the first order (primary image). (Lauterborn, et al.,2013)

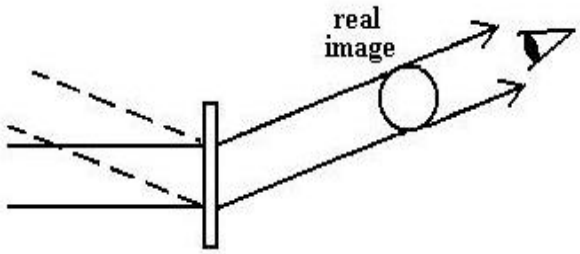

Figure 1e: The image reconstruction of first order real (secondary image). (Lauterborn, et al.,2013)

Digitized by UCC, Library

When sufficiently long exposure time has elapsed, depending upon the laser power employed and the sensitivity of the film/plate the photographic film was developed by a wet chemical method. Subsequently, the hologram is placed back in the recording geometry, and it is illuminated with a reference wave similar to the original reference wave that was used to record the hologram. A virtual image was then located in the same position that was previously occupied by the object. This virtual image formed by part of the transmitted light, exhibits all the normal attributes of perspective and depth of focus that the object would exhibit if it were still there.

To explain the basic principle of holography more clearly, the holographic process may be described mathematically. Assume that the coordinate system of the hologram plane is the x y plane. In recording the hologram, the complex amplitude of the object wave can be written as:

$$U_o(x,y) = E_o(x,y)\exp[i\varphi_o(x,y)] \qquad (1)$$

Where E_o is the real amplitude and φ_o is the phase of the object wave.

Similarly, the reference wave can be written as

$$U_r(x,y) = E_r(x,y)\exp[i\varphi_r(x,y)] \qquad (2)$$

where E_r is the real amplitude and φ_r is the phase of the reference wave.

When both waves interfere with each other at the surface of the recording medium, the intensity is given by:

Digitized by UCC, Library

$$U_h(x,y) = |U_0(x,y) + U_r(x,y)|^2 = [U_0(x,y) + U_r(x,y)].[U_0(x,y) + U_r(x,y)]$$
$$= |U_0(x,y)|^2 + |U_r(x,y)|^2 + U_0(x,y)U_r(x,y)$$
$$+ U_0(x,y)U_r(x,y) \qquad (3)$$

where * represents complex conjugate.

The amplitude transmission of the developed photographic plate is proportional to $U_h(x,y)$:

$$I(x,y) = h_0 + \beta\tau U_h(x,y) \qquad (4)$$

The constant β is dependent on the exposure characteristics of the light- sensitive material, τ is the exposure time and h_o is the amplitude transmission of the unexposed plate. $I(x,y)$ is called the hologram function. From equations (1),(2), (3) and (4), the hologram function can be written as:

$$I(x,y) = h_o + \beta\tau[E_o^2 + E_r^2 + U_o(x,y)U_r(x,y) + U_o(x,y)U_r(x,y)] \qquad (5)$$

In the reconstruction process, the hologram function is multiplied by the complex amplitude of the original reference wave:

$$U_r(x,y)I(x,y) = [h_o + \beta\tau(E_o^2 + E_r^2)]U_r(x,y) + \beta\tau E_r^2 U_o(x,y)$$
$$+\beta\tau U_r^2(x,y)U_o(x,y) \qquad (6)$$

The first term on the right- hand side of equation (6) is the undiffracted wave passing through the hologram. Since the hologram can be regarded as a diffraction grating, this term indicates the zero order diffraction term of the hologram. The second term is the reconstructed object wave, whose brightness is affected by the real constant E_r^2 , this is a virtual image. The third term is a

Digitized by UCC, Library

distorted real image of the object. For in-line holography, where the axes of the object wave and the reference wave are parallel, these three terms superpose together and cannot be separated spatially. However, in off-axis holography, these three terms are spatially separated and may be isolated.

The reason for the distortion of the real image was that the spatially varying complex factor U_r^2 , which modulates the image forming conjugate object wave U_0.

An undistorted real image can be generated by using the conjugate reference beam U_r for reconstruction:

$$U_r(x,y)U_h(x,y) = [h_0 + \beta\tau(U_r^2 + U_0^2)]U_r(x,y) + \beta\tau U_r^2 U_0(x,y) + \beta\tau U_r^2(x,y)U_0(x,y) \quad (7)$$

The development of optical holography

The history of holography shows a rapid development of the technology. The first idea of two- stage imaging process was proposed by Bragg (1939, 1942) in his X-ray microscope. In his experiment, an X-ray diffraction pattern of the crystal lattice was first recorded photographically. Then the photograph was illuminated by a filtered mercury arc lamp to implement the second diffraction process. The core of Bragg's method is a double diffraction process, which is also the key to the holographic process. It was observed that diffraction field of an object can be represented as a Fourier transform of the light distribution at the

Digitized by UCC, Library

object and so the first recording is a Fourier transform of the object and the second diffraction is a Fourier transform of the object, which is an image of the object itself. If all the diffracted information of amplitudes and phase are preserved, the diffraction from the hologram will reproduce the object wave.

The preservation of object phase was realised by the choice of crystals that possess a center of symmetry as they are able to produce a diffracted field that would be real. Another constriction of this method was the strong magnification differential for the different wavelengths, X-ray and visible light, used in each stage respectively. Gabor (1948) extends this idea and built the foundation of optical holography when he tried to improve the resolution of the electron microscope. He named this new technology 'holography' which was a major innovation in the optical imaging field.

In the process of what is now called 'in-line interferometric holography', the photographic plate was illuminated by a plane wave through a low contrast transparent phase object, where the axes of both the object wave and the reference wave were collinear. The reference wave was used to interfere with the diffracted object wave, in order to keep the phase information of the object wave in an intensity- based interference pattern. Both waves were assumed to be mutually coherent. This interference pattern was recorded by the photographic film in order to generate a hologram and the light diffracted from this hologram during reconstruction constituted the second diffraction stage, having the effect of restoring the original object wave. When Gabor applied this method to the electron microscopy, it failed for various reasons. The most serious problem was

Digitized by UCC, Library

the twin image in the reconstruction. As the photographic plate does not record the absolute phase, two possible objects contribute to the single exposure that generates the hologram.

One object is the original object and the other is a virtual object located symmetrically behind the hologram. Through reconstruction, the diffracted light forms two waves: the original object wave and a 'twin' wave caused by the virtual object. The reconstructed object wave was so seriously disturbed by the twin wave that various researchers worked on resolving this problem (Gabor, 1949, Bragg and Rogers, 1952, Gabor, 1951, Baez, 1952). Gabor's approach and Bragg's X-ray microscope are similar, however, the difference between them are extremely significant.

In Bragg's microscope, no phase information is lost and an exact reconstructed image can be obtained but the object must be symmetrical. In Gabor's approach, an object which does not have symmetrical structure can be handled. But the loss of phase information, though tolerable, leads to information of an additional conjugate image. Rogers (1950, 1952) and Kirkpatrick and El-Sum (1956) made efforts to significantly extend the theory and conceptual understanding of holography, it was not until the early 1960's that significant progress was made in this field. Leith and Upatnieks (1966) proposed a new method to completely remove the twin conjugate wave. The method was simple and utilises an off-axis reference wave. The experimental geometry is shown in figure 1a. From an optical viewpoint, the interference between the diffracted object wave and off-

Digitized by UCC, Library

axis reference wave would form a hologram with the structure of a diffraction grating.

When light is diffracted from this hologram in the reconstruction process, it will yield two waves representing the first two orders of the grating. In so doing physical separation is achieved and the previously tilting of the reference wave, dramatic improvement is achieved and this started a new era of holographic applications. Another advantage of this method is that the film can be processed with reduced requirement for a linear transfer of exposure to amplitude transmission. Also, it has the ability to eliminate the self-interference effects between points of the object. Finally, it removes the restrictions on the use of objects which do not transmit a large proportion of light. Although a number of advantages were provided by this new method, the real potential of research in holographic field was not realised until another two important advances emerged.

The advent of the gas laser, which the coherent source, with strong irradiance, was one of the important advances. It significantly increased the resolution of holography and gives the ability to make holograms of very large objects. Furthermore, another advance by Leith and Upatnieks (1964) was diffuse illumination holography. The diffuse illumination on the object, this technology has the ability to record holograms of diffuse reflecting, 3D objects as compared to the previous technology, which only records holograms of very thin transparent objects. Diffuse illumination

Digitized by UCC, Library

holography also has the capability to superpose multiple holograms on the same holographic plate.

This phenomenon is very helpful enabling multi-exposure methods in the application of holographic interferometer. Denisyuk (1962) invented the thick reflection hologram for which the images are viewed in the light that is reflected from the hologram. As shown in figure 2, the beam reflected from the object and the reference beam must arrive at the photographic plate from opposite sides to record a reflected hologram.

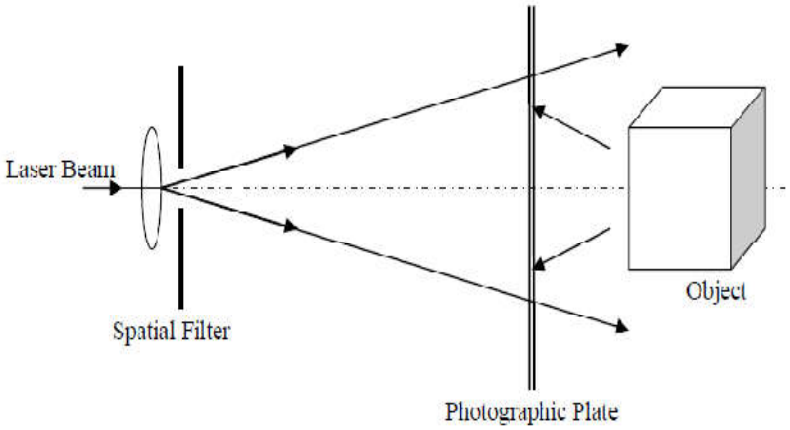

Figure 2: A simple geometry for recording one-beam reflection hologram (Denisyuk, 1962)

This type of hologram has a very good wavelength selectivity which allows it to be illuminated by white light to reconstruct the image. Due to the great potential of holography, it has been applied to many scientific and engineering fields. These includes high- resolution imaging of aerosols (Thompson et al., 1967), imaging through diffusing and aberration media (Leith and Upatnieks,

Digitized by UCC, Library

1966, Kogelnik, 1965), multiple imaging (Lu, 1968 and Groh, 1968), computer generated holograms (Lohmann and Paris, 1967), the production and correction of optical elements (Upatnieks et al., 1966), information storage and processing (Stroke et al., 1965, and Vander Lugt et al., 1965).

Amongst these, Holographic Interferometry (HI) is a major application of holography, which was discovered by several groups working independently (Brooks et al., 1965, Burch, 1965, Collier et al., 1965, Haddad, 1965, Powell and Stetson, 1965). It became possibly, for the first time, to map the displacements of a relatively rough surface with an accuracy of a fraction of a micrometre (Amadesi et al., 1974); it was possible to make an interferometric comparison of stored wave fronts that existed at different times. The explosive growth of optical holography since the advent of the laser in the 1960's was restricted with the beginning of a digital era in the late 1990's. Conventional optical holography uses photographic film as a recording medium which cannot be processed in real-time. The wet chemical procedure made the applications of holography to be complex. A new type of holography, digital holography emerged, becoming an increasingly active field for optical researchers.

The development of digital holography

Leith and Upatnieks proposed off-axis holography; Rogers reasoned that the interference pattern of on-axis hologram could be calculated analytically for some simple objects (wire). He fabricated the holograms and reconstructed the images. But this method could go no further until the computing power was

Digitized by UCC, Library

dramatically increased and the Fast Fourier Transform (FFT) algorithm was invented. Brown and Lohmann (1966) were successful in using detour phase and the FFT algorithm to create binary computer generated holograms. Later, the computer generated holograms were transferred to a transparency by plotting or printing device and they were then optically reconstructed.

This offers a great advantage in that the hologram of an object can be created accurately; even it never existed in the physical world. Limitations of this method include the feasibility of creating the object mathematically in the first place, the acceptable duration for the calculations involved and the performance of the device used to transfer the numerical hologram to a suitable transparent medium (Lee, 1978, Bryngdahl and Wyrowski, 1990). The development of computer technology made possible not only the digital recording process in the computer but also the numerical reconstruction process as well. The idea of numerical reconstruction was proposed by Goodman and Lawrence (1967) and by Kronrod et al. (1972). A hologram on the photographic plate is optically enlarged and sampled and then this digitised hologram is reconstructed numerically.

Improved reconstruction algorithm and its application applied to various fields, for instance, particle measurement (Onural and Scott, 1987 and Onural and Ozgen, (1992), shape measurement (Ma et al., 2004) and Microscopy (Haddad et al., 1965). Schnars and Juptner (1993) used a CCD camera to record a hologram and perform numerical reconstruction in order to reconstruct this digital hologram. It was named ‘direct holography’ originally, but later the term ‘digital

Digitized by UCC, Library

holography' was widely accepted by the metrology community for this method. It was a method that moved directly from optical recording to numerical processing.

It has been successfully applied to deformation analysis (Pedrini et al., 2003 and Rastogi,1997), shape measurement (Yamaguchi et al., 2006), microscopy (Cuche et al., 1999), particle distribution measurement (Koek et al., 2005), light-in–flight holography and other short-coherence-length applications (Nilsson and Carlsson, 1998), comparative digital holography (Osten et al., 2002), holographic tweezers (Reicherter et al., 2006) and encryption of information (Meng et al., 2005). Digital holography adds to some exciting new features to tradition optical science. It allows the simulation of experiments on a computer and even the ability to perform scenarios that cannot be realised by real experimentation. The phase information can be obtained directly, which is a significant contribution to optics.

Some problems in digital holography

Although digital holography has some significant advantages over conventional optical holography, there are some important restrictions on this new technique.

The spatial frequency requirements

In the last four decades, the development of solid-state image sensors, like CCD or CMOS, which are capable of recording signals in the visible range up to about 1100 nm, enabled the development of Digital Holography (DH). In order to numerically simulate the reconstruction process achievable with traditional films, a number of suitable algorithms have been developed, and to them several post-

Digitized by UCC, Library

processing possibilities have been added, like plane of focus adjustment (Ferraro et al.,2009 and Ferraro et al.,2005), amplitude and phase images computing from a single hologram (Grilli et al.,2001), recording aberration compensation (Ferraro et al.,1978 and Stadelmaier,2000).

However, only lately the technology of pyrocameras, and focal plane array (FPA) microbolometers offered digital sensors that do not require cryogenic cooling and have enough pixels, of appropriate size, to make the extension of DH to the long IR range feasible (Saugnac &Contencin,1989). In particular, the last generation microbolometers have a number of a useful pixel over 300K and the pixel size has been reduced up to 25μm. The above technological progress stimulated further exploration of DH at IR long wavelengths (Allaria et al., 2003 and De Nicola et al., 2008). In digital holography, a CCD or CMOS camera are used as a recording medium to take the place of the high- resolution photographic film or plates used in optical holography.

The interference pattern produced by the superposition of the reference wave from the object points has to be resolved in order to restore the intensity and phase information of the object.

The maximum angle θ_{max} between these waves:

$$f_{max} = \frac{2}{\lambda} \sin\frac{\theta_{max}}{2} \qquad (8)$$

where f_{max} is the spatial frequency and λ is the wavelength.

Digitized by UCC, Library

Photographic emulsions used in optical holography have resolutions up to 5000 line pairs per millimetre (Lp/mm). Using these materials, holograms with angles of up to 180^0 between the reference and the object, wave can be recorded. In order to obtain good reconstructed image quality and measurement accuracy, each micro fringe in the hologram must be represented by at least two pixels. Then the corresponding maximum resolvable spatial frequency is calculated by:

$$f_{max} = \frac{1}{2\ x} \qquad (9)$$

However, the distance between neighbouring pixels of a high- resolution CDD camera is only of the order of $x \approx 5\mu m$. From equation (9), the maximum resolvable spatial frequency of a CCD camera is about 100 line pairs per millimetre (Lp/mm).

Combining equations (8) and (9) leads to;

$$\theta_{max} = 2ar\,csin\left(\frac{\lambda}{4\ x}\right) \approx \frac{\lambda}{2\ x} \qquad (10)$$

where the approximation is valid for small angles. Therefore the distance between neighbouring pixels is the quantity that limits the maximum angle between the reference and object wave. For off-axis holography, half of the full resolution of the hologram was occupied by the twin image, which means the valid resolution for the off-axis hologram is only half of the results in equation (9).

The limited resolution of the CCD device restrict digital holography being applied to large objects or small objects that are very close to the CCD device. In

Digitized by UCC, Library

digital holography, both the size of the object and the distance of the object to the CCD have to be carefully chosen to ensure the validity of the experimental results. A lot of effort has been made to increase the resolution of digital holography. For all set ups the maximum spatial frequency has to be adapted very carefully to the resolution of the CCD. If too high spatial frequencies occur, the contrast of the entire hologram decreases or, in the extreme case, it vanishes totally. These issues will be discussed in the latter part of this thesis.

Charged Coupled Device (CCD) for digital hologram recording

The sensitivity of CCD cameras is typically in the range of ≤ 70 mK, which is better than the sensitivity of photographic emulsion used for classical holography. The spectral range reaches approximately $8\ \mu m \quad 12\ \mu m$, based on amorphous silicon as a chip material. In conventional holography with photographic plates the intensity ratio between the reference wave and object wave should be in the range of 5:1 to 10:1 in order to avoid nonlinear effects due to the recording medium (Schnars &Juptner, 1993). However, from interference theory, it is known that the maximum contrast in an interference pattern is achieved if the intensity ratio is 1:1. The intensity ratio can be controlled by covering one- half of the expanded reference wave by an aperture. The brightness in that half of the CCD being illuminated by reference and object wave together should be twice as high of the brightness in the other half, which is illuminated only by the object wave.

Digitized by UCC, Library

As for classical holography using the photographic material, the total light energy impinging on the CCD can be controlled by varying the exposure time (Tiziani, 1997). This is usually done with mechanical or electronic camera shutter which in this case is shutter- less. The CCD-cameras typically have a dynamic range of 4 bit digital input, which is comparable to the dynamics of photographic materials and fully sufficient for hologram recording. Even objects with brightness variations exceeding the dynamic range of the recording medium by far can be stored and reconstructed, because the object information is coded as interference pattern (hologram).

Stability requirements

A stable optical set-up is necessary for digital as well as conventional holography. Any change in the optical path difference between the interfering beams will result in a movement of the fringes and reduced contrast in the hologram. During hologram exposure, the path variations should not exceed $^1/_4$, better $^1/_{10}$ of a wavelength. In contrast to conventional holography disturbances due to vibrations are visible in digital holography even in the recording process: the hologram visible on the monitor of the recording system appears flat and has a low modulation, which is easy to monitor the stability of the set up against vibrations (Schnars & Juptner, 2005).

Digitized by UCC, Library

The algorithm for numerical reconstruction

Fresnel- Kirchhoff integral is used to describe the diffraction of light wave at an aperture which is mounted perpendicular to the incoming beam. In the case of holography, the hologram is the aperture. The numerical calculation of the Fresnel- Kirchhoff integral is of vital importance in performing the numerical reconstruction of the digital hologram. There are some algorithms available to realise this process, but different algorithms vary in the quality of the reconstructed image.

The zero order term and twin image

Since the inception of holography, virtual or twin images were considered as a limitation to holography. They are defocused images of the holographic objects that are superimposed on the real images of the objects either in optical or numerical reconstruction. We can trace its origin from the principle of in-line holographic set up. The twin-image problem has received a lot of attention since Gabor's pioneering work on holography. It is a matter of concern to research in holography, since it is widely used in the fields like; optical holography, soft X-rays and electronic microscopy. Basically, there are two classes of approaches which have been proposed to tackle this problem; involving a change in the hologram recording set up and an attempt to numerically suppress the twin-image. The best known method is the off-axis holography, first suggested by Leith and Upatnieks (1962).

Digitized by UCC, Library

An off-axis hologram leads to spatially separated real and twin images at the reconstruction step. The real image can then be selected by spatially filtering the reconstructed planes (Cuche, et al., 2000a and 2000b).

The digital off-axis set up, however, proves less relevant for the study and collection of small objects due to sampling constraints (Xu, et al., 2000) and practical considerations. Therefore, in-line digital holography is preferred in this context and the twin image problem still relevant and has to be addressed. The CCD/ CMOS only records the intensity of the interference pattern, as the photographic film does in optical holography. Similarly, what was illustrated in the previous section, after numerical reconstruction in the computer, it will be the case that the zero- order term and the twin image also exist together with the desired image.

Due to the limited resolution and dynamic range of CCD sensor, the zero-order term and the twin image will severely affect the quality of the reconstructed object image. They must be suppressed in order to gain useful results from digital holography.

Comparisons of analogue and digital holography

Digital holography (DH) is an emerging technology of new paradigm in general imaging applications. By replacing the photochemical procedures of conventional holography with electronic imaging, a door opens to a wide range of new capabilities. Although many of the remarkable properties of holography have been known for decades, their practical applications have been constrained

Digitized by UCC, Library

because of cumbersome procedures and stringent requirements on equipment (Gyimesi,et al.,2009). Digital holography offers a number of significant advantages, such as the ability to acquire holograms rapidly, availability of complete amplitude and phase information of the optical field, and versatility of the interferometric and image processing techniques. Most obviously, DH does not involve photochemical processing (Fuzessy, et al., 2006). Therefore, DH is orders of magnitude faster and can be performed at video rates. Additional hardware required in DH is the CCD camera and a computer, while the need for dark room facilities and supply of chemicals is unnecessary.

Furthermore, due to the high sensitivity of CCD compared to photographic emulsion, the exposure time is reduced by orders of magnitude. For instance, a CCD pixel area of 100 $\mu m,^2$ can detect as few as several photons, whereas a similar area of a high-sensitivity photographic plate requires many millions of photons. In analogue holography (AH), however, to properly read out the magnified or demagnified hologram, the wavelength also needs to be scaled proportionately, a task that is highly cumbersome at the least and infeasible in most cases (Kim,2011). The familiar parallax effect of display holograms of AH is currently not feasible in DH (Yu, et al., 2002). Most often the superposed holograms are illuminated with single wavelength, and the resulting aberrations are unavoidable. In DH, however, the superposition simply consists of addition of several numerical arrays. There is no limitation on the number of arrays and furthermore, there are ways to pre-process the arrays to compensate for chromatic and other aberrations if present.

Digitized by UCC, Library

The critical aspects in digital hologram reconstruction

The distance of the object camera is significantly large than the digital recording device aperture, the numerical reconstruction of object wavefront amplitude can be performed according to the discretization of well-known Fresnel approximation of Fresnel-Kirchhoff equation (Schnars and Juptner,2005), using rather simple algorithms. In order to reconstruct large objects holograms, a number of analytical conditions occurring in digital holography have to be taken into account. The digital recording and reconstruction process of hologram has an important drawback compared with its analogue counterpart, which is the general lack of resolution of digital recording devices compared to films.

This is crucial, since in order to satisfy the Whittaker-Shannon sampling theorem, the fringe period of the interference pattern P has to satisfy the following inequality:

$$\mathrm{p} \geq \frac{\lambda}{2 \sin\frac{\theta}{2}} = 2\mathrm{d_p} \qquad (11)$$

This establishes that the fringe period P has to be larger than two times the detector pixel pitch(d_p), θ is the angle between the reference and the object beam as shown in the figure 3.

Digitized by UCC, Library

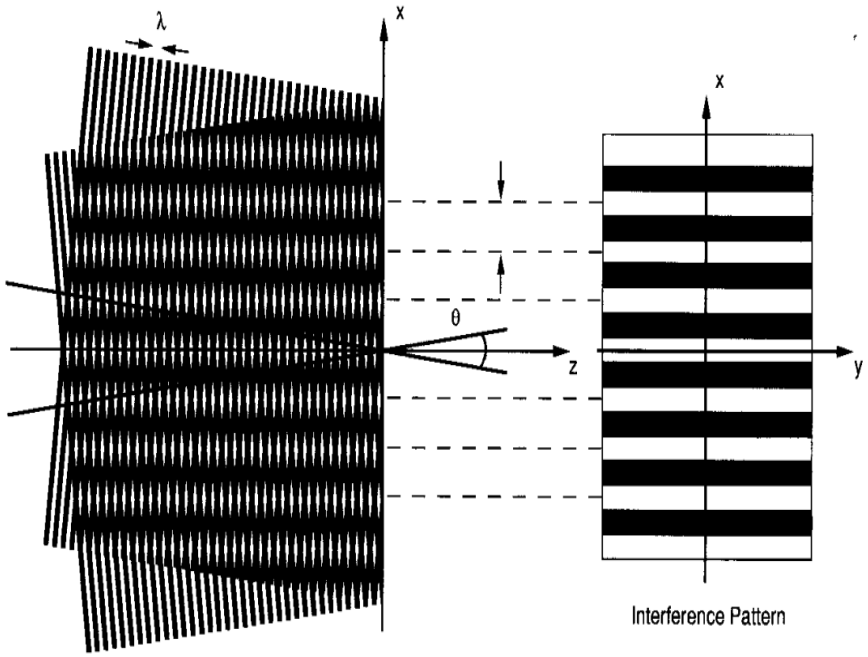

Figure 3: Fringe formation process (Pelagotti, et. al., 2010).

This limitation fixes a minimum value for θ, when considering small values, this will reduce to (λ) lambda over two times the pixel pitch in equation (11). It is noteworthy that θ represents an inverse proportionality to $d_p$and a direct relation to the wavelength.

$$\theta = 2\sin^{-1}\left(\frac{\lambda}{4\,d_p}\right) \approx \frac{\lambda}{2d_p} \qquad (12)$$

Recording set up

From this maximum value of the θ angle it follows a minimum distance value between the object and the detector, in the simplest configuration shown in figure 3, that is with reference and object beams collinear with the axis of the detector.

Digitized by UCC, Library

In the off-axis configuration shown in figure 4, the maximum angle and the minimum distance can be easily computed by geometrical considerations.

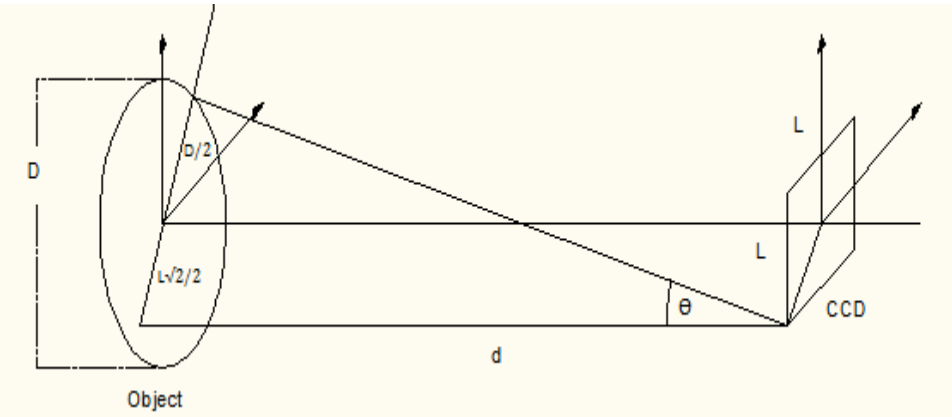

Figure 4: Digital recording minimum distance. (Pelagotti, et al., 2010)

In particular, for large objects, the expression for the minimum distance further simplify as indicated in the last expression, from which we can see that this value is in inverse proportion to the wavelength in use as shown in equation (13);

$$\theta_{max} = \tan^{-1}\left(\frac{\frac{D}{2}+\frac{L\sqrt{2}}{2}}{d_{min}}\right) \approx \frac{D + N d_p\sqrt{2}}{2d_{min}}$$

$$d_{min} = \frac{d_p\left(D + N d_p\sqrt{2}\right)}{\lambda} \approx \frac{d_p D}{\lambda} \qquad (13)$$

Where D is the lateral dimensions of the object and $L=Nd_p$, the CCD lateral dimension.

Digitized by UCC, Library

Despite the important drawback connected with the current dimensions of the thermal camera pixels, the use of longer wavelengths in digital holography has several advantages, especially in hologram recording of large objects: the stability of the system becomes a less critical factor, also, from equationn (13), the angle between the reference beam and the object beam increases with the wavelength. Consequently, the distance between the camera and the object can be reduced to suitable laboratory conditions for large objects. Moreover, with CO_2 lasers it is possible to obtain very high power outputs and this makes it easier to expand the beam to irradiate large objects. Furthermore, the resolution of the reconstruction image at minimum distance is not influenced by the wavelength in use.This renewed interest could have further implications also in homeland security, night vision and biological science as it is extending 3D imaging capabilities from visible to far IR towards the THz region (George, et al,2006).

Types of holograms

A hologram is a recording in two- or three- dimensional medium of the interference pattern formed when a point source of light, the interference beam, of fixed wavelength encounters light of the same fixed wavelength arriving from an object (object beam). When a hologram is illuminated by the reference beam alone, the diffraction pattern recreates the wave fronts from the original object. Thus, the viewer sees an image indistinguishable from the original object. There are many types of holograms which can be classified in many ways. Basically, we can divide them into two types: reflection holograms and transmission holograms.

Digitized by UCC, Library

The reflection hologram is a truly three-dimensional image which is seen near its surface. This is the most common type which is shown in galleries. The hologram is illuminated by a 'spot' of white incandescent light, held at a specific angle and distance which is located at the viewer's side of the hologram. Thus the image consists of light reflected by the hologram. Typical transmission hologram is viewed with laser light, usually of the same type used for the recording. This light was directed from behind the virtual image can be very sharp and deep. For instance, through a small hologram, a full- size room with people in it can be seen as if the hologram were a window. Supposing this hologram was broken into pieces, one can still see the entire scene through each piece. Depending on the location of the piece (hole) a different perspective was observed. Furthermore, if an undiverged laser beam was directed backwards (relative to the direction of the reference beam) through the hologram, a real image can be projected onto a screen located at the original position of the object.

In between the reflection and transmission type of holograms, many variations can be made such as embossed holograms, integrated holograms, holographic interferometry, multichannel hologram and computer-generated holograms.

Applications of holograms

Holography represents one of a fascinating examples of recombining of scattered radiation to produce pictures/images. It has been a well-used method to produce image, and an important tool in science and technology. Holography is

Digitized by UCC, Library

now spreading from the research laboratory to industry, and finds wider employment in communication and other engineering problems.

A hologram can store numerous quantities of information. Holograms are able to hold a vast amount of data, which does not necessarily have to be in a visible image format. A single image can contain a lot of information that may be accessed by reflecting light from different angles.

Traditional optical storage methods such as compact discs can be accessed from one angle. Several companies are researching into the use of holograms as high capacity data storage devices for entertainment and computing purposes. Holography can also be used in security applications. Complex holograms are much more difficult to reproduce compared to static images. In view of this, holograms are often placed on valuable items to reduce forgery. Common security applications of holography include labels on credit cards and images embedded on currencies. Important documents such as passports and identification cards also often used them to discourage illegal reproduction, has made holograms a well-known concept. Holograms show up more and more often on tickets and on original covers on software computer programs. An example of an important area of application is bar-code readers in shops, warehouses, libraries to mention but few.

A code reader like this is based on the application of holographic components like optical gratings. This large important industry has contributed to make holography an industrial success. In the aircraft industry head-up displays (HUD) are an important example of holographic technology.

Digitized by UCC, Library

HUD helps the pilots so that they do not need to look down onto the instrument panels, because the instruments are projected onto the windscreen with help of holographic technology, and thus make flying easier. Also, holography is used for making holographic optical elements (HOE), based on interference; this technique is used in bar-code readers

Objectives of this thesis

The objective of this thesis is to explore the feasibility of digital holography at long IR wavelength and apply it to large macroscopic objects.

Specific objectives

- To reconstruct various sizes of objects: between 1 mm to about 40 cm and more.
- To test the possibilities of reconstructing larger objects by means of two negative lenses.
- Investigated the algorithms for performing numerical reconstruction, especially Fresnel approximation and convolution approach and applied them to both stimulated ideal holograms and real holograms obtained from the optical system.
- Explore the methods to enhance reconstruction results of the digital holograms including the reduction of speckle noise, improvement of the resolution of the reconstruction results.

Digitized by UCC, Library

Scope of the thesis

In this work, we report an investigation on IR at 10.6 μm and also demonstrate, by means of experiments, how to exploit the advantages and possibilities offered by this wavelength range. In order to test the reliability of DH at long IR wavelength, we experiment six different set-ups and imaged objects of increasing sizes, made of several materials. The experiments were performed in both transmission and reflection mode. The high power output makes it easier to expand the beam and irradiate large objects, which results in good fringe contrast. It is also intended to find out whether it can be adopted for fire- fighters and first responders with a way to see through the fire in order to save human lives.

Organisation of work

Now a brief introduction of 3-dimensional imaging with long infrared digital holography and the background of the techniques for shape measurement is given. A historical review of holography has shown the roots of holography, the subsequent development of digital holography. The problems to be investigated in this thesis have been proposed. Also, the objectives and contributions of this work have been given in chapter one, the rest of this thesis is organsed into four parts.

In chapter two, the background and basic principle, the theory and principle of operation of digital holography and the techniques to suppress the zero-order term and twin image are discussed. The different algorithms for numerical reconstruction of digital holograms are shown in this chapter. Results based on

Digitized by UCC, Library

these algorithms are presented and analysed. Different algorithms are compared and also presented.

In chapter three, Experimental methods for the various configurations and experimental components are presented in detail.

In chapter four, digital holography as applied to shape measurement of macroscopic objects, the results of the experiments and analysis for the six configurations are discussed in this chapter. Chapter five provides an overall conclusion of this thesis. The results are analysed and some recommendations for further research direction are offered.

Digitized by UCC, Library

CHAPTER TWO

LITERATURE REVIEW

Background and basic principles

Early in the field of holography, considerable effort was expended to increase the range of holography beyond the visible wavelengths. Although efforts were made to record the hologram at 10.6 μm, they were not successful due to lack of suitable recording media, such as Silver Bromide or dichromatic gelatine in the visible region(Calixo,1988). In a comprehensive review of media for holography at 10.6 μm , more than twelve separate recording materials were described, including photochromic film, gelatin film, wax film and photoresist (Beaulieu & Lessard,1997). In an early work (Chivian et al.,1969), successful recordings at 10.6 μm were obtained using a thermochromic material, cuprous mercuric iodide to record an on-axis interference pattern and later a two-step photographic process was used to view the reconstruction using He-Ne laser(Kobayashi & Kurihara,1971).

Another important early media study is the infrared holography experiments with thermal bleaching of organic photochromic films also in a two-step process (Izawa et al., 1969). Related rough surface Interferometry at 10.6 μm has been studied, to test IR transmitting materials, for optical metrology of aspheres and to study rough surfaces (Kwon et al., 1980). Digital holography became feasible with the emergence of high- resolution CCD/CMOS devices. The basic principle of digital holography is the same as in the conventional

Digitized by UCC, Library

holography, which was discussed in chapter one. It consists of two procedures: a recording stage and a reconstruction stage. However, in digital holography the process of recording the hologram uses a CCD/CMOS camera, replacing photographic film as a recording medium. In equation (5), the parameter h_o can be neglected for a CCD/CMOS camera. The CCD/CMOS camera transfers the captured image to the computer connected to and this image was saved as a digital hologram.

In the process of reconstruction, this hologram is digitally accessed and numerically reconstructed by a virtual reference wave which effectively stimulates the reference wave used in the process of recording. As the reconstruction procedure is being performed in the computer, its speed depends only on the implementation of the numerical reconstruction algorithm and the speed of the computer processor. Since the reference has to be generated virtually in the computer, a plane wave or a spherical wave is usually used in the process. The object is either transparent or a 3D body with a diffusely reflecting surface, which is at a certain distance from the CCD/CMOS device. A typical set-up of digital holography is shown in figures 5a, 5b and 5c.

In figure 5a, a plane reference wave and the wave reflected from the object are interfering at the surface of a CCD. The resulting hologram was electronically recorded and stored. In this case, the object, in general, was a 3D body with diffusely reflecting surface located at a distance d, from the CCD.

Digitized by UCC, Library

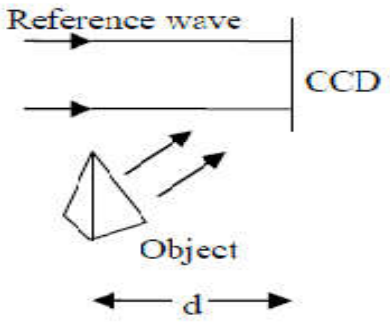

Figure 5a: The concept of digital hologram recording (Schnars &Juptner, 2005)

In optical reconstruction the virtual image appears at the position of the original object and the real image is formed at a distance d, as well, but in the opposite direction from the CCD as shown in figure 5b.

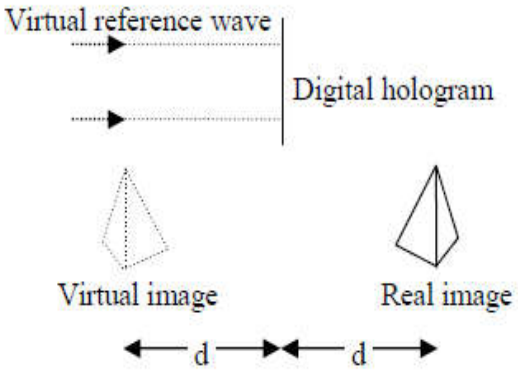

Figure 5b: The reconstruction with reference wave (Schnars &Juptner, 2005)

A hologram can be assumed as an aperture and the reconstructed images are the results of diffraction of a reference wave by this aperture. To obtain a real image, a conjugate reference wave was used in the reconstruction as shown in figure 5c.

Digitized by UCC, Library

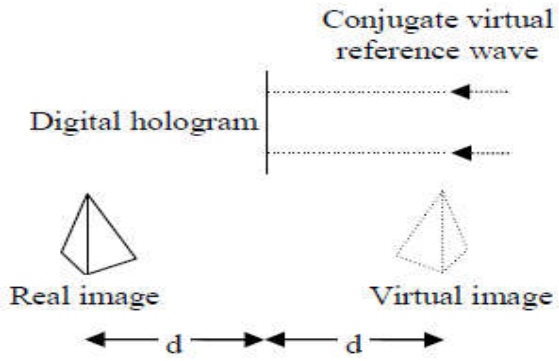

Figure 5c: The reconstruction with conjugate wave (Schnars &Juptner, 2005).

Huygens's principle illustrates that every point of a wavefront can be considered as a source point for secondary spherical waves. The Huygens' Principle would allow that secondary waves not only propagate in forward direction, but also backwards into the direction of the source. But, experiment demonstrates that the wavefronts always propagate in one direction. To ignore this unphysical situation formally, the inclination factor Q, defined in equation (14) was introduced in the Fresnel- Kirchoff integral. The wavefront at any other place is the coherent superposition of these secondary waves. Suppose the coordinate system as shown in figure 6a, then the diffraction by the aperture or hologram in the distance d along the propagation direction of the wave can be quantitatively described by Fresnel-Kirchhoff integral (Schnars and Juptner, 2005):

$$\Gamma(\xi',\eta') = \frac{i}{\lambda}\int_{-\infty}^{\infty}\int_{-\infty}^{\infty} A(x,y)\frac{\exp\left(-i\frac{2\pi}{\lambda}\rho'\right)}{\rho'} Q\, dx\, dy \qquad (14)$$

Digitized by UCC, Library

where

$$\rho' = \sqrt{(x \quad \xi)^2 + (y \quad \eta)^2 + d^2} \qquad (15)$$

and

$$Q = \frac{(\cos\theta + \cos\theta')}{2} \qquad (16)$$

The light source lying in the source plane with complex coordinate (ξ,η) radiates spherical waves. A(x,y) is the complex amplitude of such a wave in the aperture plane. At first an opaque aperture with only one hole at the position (x,y) was considered. Such a hole was considered as the source for secondary waves. The field at the position (ξ', η') of the diffraction plane is proportional to the field at the entrance side of the aperture A(x,y) and to the field of the secondary spherical waves emerging from (x,y) described by $\exp\left(\frac{-i2\pi}{\lambda\rho'}\right)/\rho'$ as shown in figure 6a.

Digitized by UCC, Library

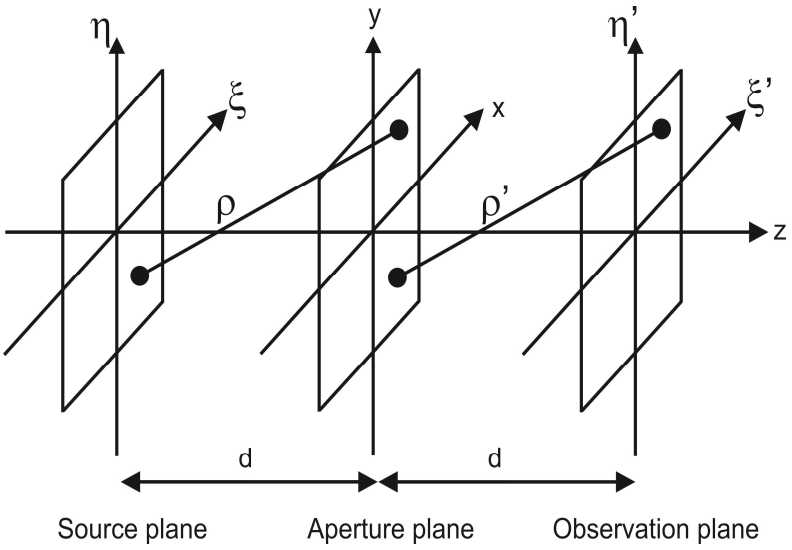

Figure 6a: The coordinate system for the diffraction (Schnars &Juptner, 2005)

In equation (14), $A(x,y)$ is the complex amplitude in the plane of the aperture bending as shown in figure 7. $\Gamma(\xi',\eta')$ is the diffracted field in the observation plane and ρ' represents the Euclidean distance between a point in the aperture plane and a point in the observation plane as shown in figure 7 can be evaluated from equation (15).The inclination factor, Q depends on the angles θ and θ' in accordance with equation (16). θ is the angle between the incident ray from the source and the unit vector $\bar{n}$ perpendicular to the aperture plane and θ' is the angle between the diffracted ray and $\bar{n}$ as shown in figure 6b.

Digitized by UCC, Library

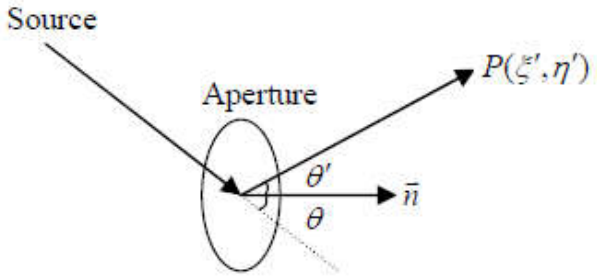

Figure 6b: Diffraction angles with inclination factor Q (Schnars &Juptner, 2005)

The inclination factor Q is approximately zero for $\theta \approx 0$ and $\theta' \approx \pi$. This prevents the waves from travelling into the backwards direction. The inclination factor Q is set to unity because of the angles θ and θ' areas approximately zero in practical digital holography – a consequence of the relatively low resolution of the detector. The use of a ''+'' sign in the argument of the exponential function of the Fresnel-Kirchoff integral in equation (14) instead of ''-'' sign used, depends on the definition of the harmonic wave equation, which can be defined either as $\exp(+i\varphi)$ or $\exp(-i\varphi)$. However, using the ''+'' sign in equation (14) leads to the same expressions for all measurable quantities, as the intensity and magnitude of the interference phase used in digital holographic interferometers. If the reference wave is set up to be normal incident to the hologram, then the diffracted light is approximated by the Fresnel-Kirchhoff integral as:

Digitized by UCC, Library

$$\Gamma(\xi',\eta') = \frac{i}{\lambda}\int_{-\infty}^{\infty}\int_{-\infty}^{\infty} U_h(x,y)U_r(x,y)\frac{\exp\left(-i\frac{2\pi}{\lambda}\rho'\right)}{\rho'}dx\,dy \tag{17}$$

where $U_h = (x,y)$ is the digital hologram captured by the CCD camera; λ is the wavelength of the light in the virtual reference beam used in the reconstruction; ρ' is the distance between a point in the hologram plane and a point in the construction plane, which has the same form as equation(15); $U_r(x,y)$ is the function describing the reference wave. For a uniform plane reference wave, it has real amplitude with the simple equation:

$$U_r(x,y) = a_r + i0 = a_r \tag{18}$$

For a spherical reference wave whose point source is at the original point of the object plane, it can be described as:

$$U_r(x,y) = \frac{\exp\left(-i\frac{2\pi}{\lambda}\sqrt{d^2+x^2+y^2}\right)}{\sqrt{d^2+x^2+y^2}}$$

$$U_r(x,y) \approx \frac{1}{d}\exp\left(-i\frac{2\pi}{\lambda}d\right)\exp\left[-i\frac{\pi}{\lambda d}(x^2+y^2)\right] \tag{19}$$

In equation (17), $\Gamma(\xi'\eta')$ is the diffraction pattern calculated at a distance d behind the CCD plane as shown in figure 7, which means it reconstructs the complex amplitude in the plane of the real image. Therefore, both the intensity and the phase information can be obtained after numerical reconstruction.

Digitized by UCC, Library

However, in optical reconstruction, only the intensity is visible. So this new facility potentially sheds new light in many applications of holography.

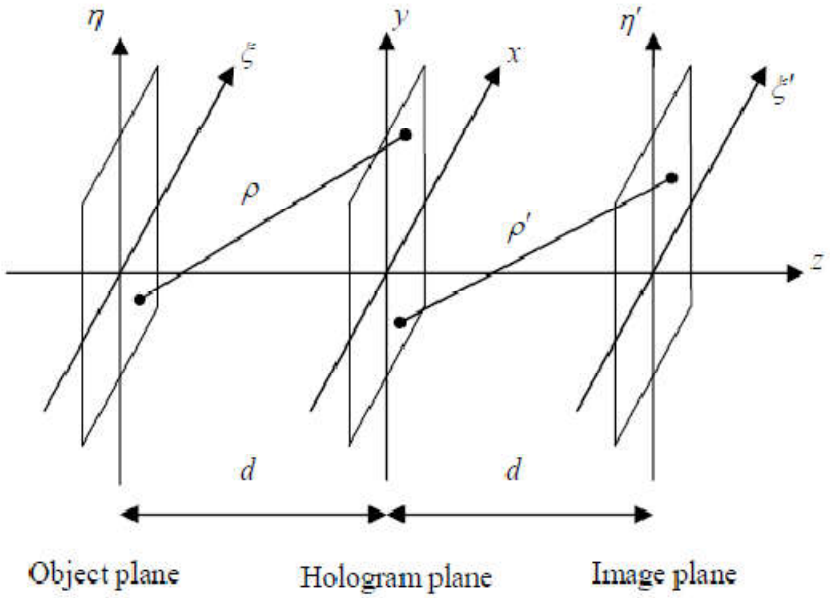

Figure7: Coordinate system for numerical hologram reconstruction (Schnars &Juptner, 2005)

The reconstructed intensity is written as:

$$I(\xi',\eta') = |\Gamma(\xi',\eta')|^2 \qquad (20)$$

And the reconstructed phase is:

Digitized by UCC, Library

$$\varphi(\xi',\eta') = \arctan\frac{\mathrm{Im}|\Gamma(\xi',\eta')|}{\mathrm{Re}|\Gamma(\xi',\eta')|} \qquad (21)$$

where Re denotes the real part and Im denotes the imaginary part.

It is worth noting that the calculated diffraction pattern is the complex amplitude at a distance d behind the CCD plane where the real image is reconstructed. However, the real image could be distorted by the reference wave in equation (6). In order to overcome this effect and to ensure that undistorted real images are left, a conjugate reference wave has to be introduced in the reconstruction as shown in figure 5c. Contrary to the situation depicted in figure 6b, an undistorted real image swaps with the virtual image and is located at the position where the object was recorded. Then the calculated diffraction pattern is rewritten as:

$$\Gamma(\xi\eta) = \frac{i}{\lambda}\int_{-\infty}^{\infty}\int_{-\infty}^{\infty} U_h(x,y)U_r(x,y)\frac{\exp(-i\frac{2\pi\rho}{\lambda})}{\rho}dxdy \qquad (22)$$

with

$$\rho = \sqrt{(x-\xi)^2 + (y-\eta)^2 + (d^2)} \qquad (23)$$

where $U_r(x,y)$ is conjugate to the original reference wave$U_r(x,y)$. But for the plane reference wave defined in equation (16), both results from equation (17)

Digitized by UCC, Library

and equation (22) are equivalent because $U_r(x,y) = U_r(x,y)$. The virtual image can be reconstructed by adding a numerical lens in the process of numerical reconstruction. The simplest scheme is shown in figure 8 where the numerical lens is located directly behind the hologram.

The lens introduced functions as an eyepiece for the observer, viewing the optical reconstruction. Suppose the lens has a focal length of f, the imaging formula of the lens is:

$$L(x,y) = \exp\left[i\frac{\pi}{\lambda f}(x^2 + y^2)\right] \qquad (24)$$

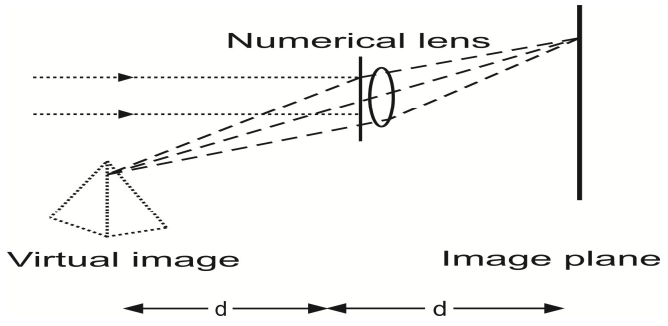

Figure 8: The reconstruction of the virtual image (Schnars &Juptner, 2005).

For the magnification to be 1, f=d/2 is the usually used in equation (24). The phase aberrations caused by the introduced lens should be corrected to avoid phase errors in the reconstructed image. The phase correction factor is described as(Laporta,2007) :

$$p(\xi',\eta') = \exp\left[i\frac{\pi}{\lambda f}(\xi'^2 + \eta'^2)\right] \qquad (25)$$

Digitized by UCC, Library

According to equation (17), equation (24) and equation (25), the combined equation for virtual image reconstruction through a numerical lens of focal length f is:

$$\Gamma(\xi',\eta') = \frac{i}{\lambda} P(\xi',\eta') \int_{-\infty}^{\infty}\int_{\infty}^{\infty} U_h(x,y) U_r(x,y) L(x,y) \frac{\exp\left(-i\frac{2\pi}{\lambda}\rho'\right)}{\rho'} dxdy \tag{26}$$

This combination of conventional holography and electronic devices allows holograms to be taken and reconstructed in the near real time. Using CCD/CMOS cameras, the hologram can be recorded directly and stored digitally, since no wet chemical or other time- consuming processes are required. Numerical reconstruction also offers greater flexibility than optical processing. Without using the phase shifting methods, the phases of the stored light wave can be calculated directly from the digital holograms under numerical reconstruction, as shown in equation (24). Also, other optical metrology methods, for example, shearography, can be derived numerically from digital holography (Schnars and Juptner, 1994).

Digitized by UCC, Library

The theory and principle of operation of digital holography

The principle of the optical recording and reconstruction in classical holography is illustrated in figure 9a and figure 9b.

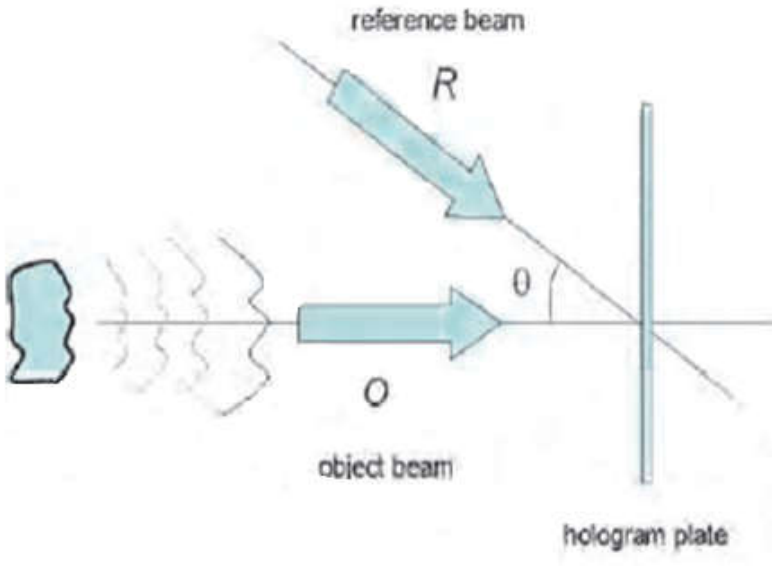

Figure 9a: Optical configuration for recording and reconstruction of holograms (De Nicola, et. al., 2011)

Digitized by UCC, Library

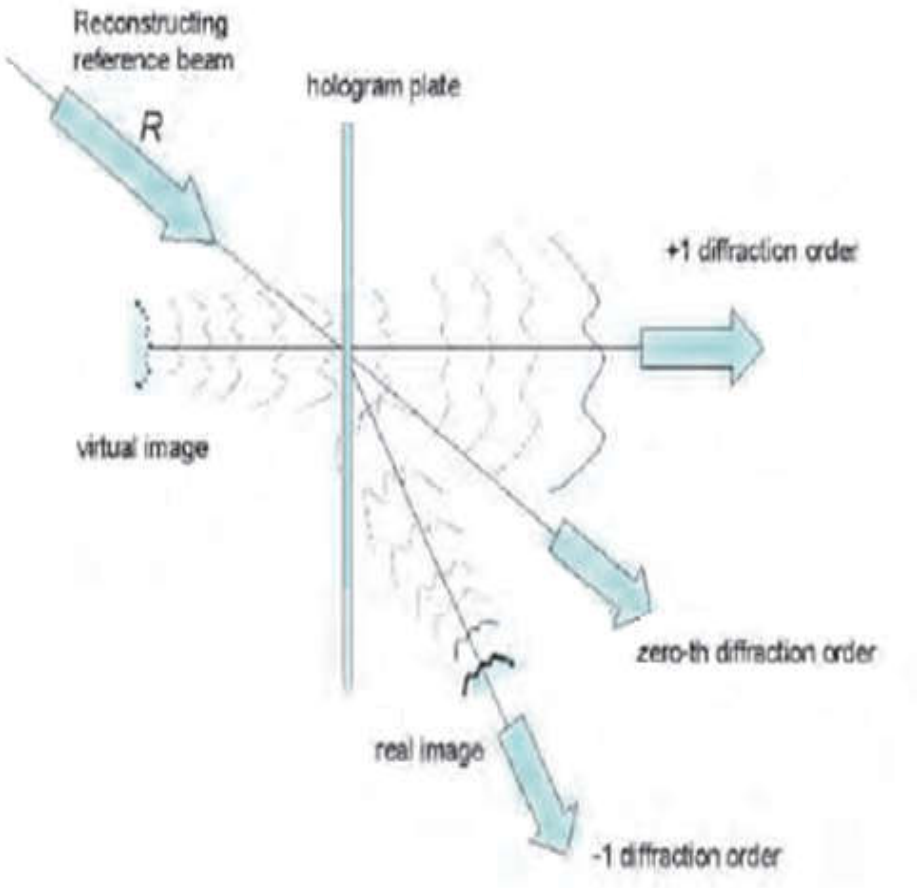

Figure 9b: Optical configuration for recording off-axis hologram (De Nicola,et. al., 2011)

The reference beam R interferes at the plane of the holographic plate at off-axis angle θ with respect to the object beam O. In this set up the reconstructed image is spatially separated from zero-order diffraction and the second image, the so called twin image. These three diffraction orders propagate along different directions and can be observed separately, leading to significant improvement compared to the original in-line configuration originally developed by Gabor (Gabor, 1948 and Goodman, 1996) where the zero-order and the two conjugate images overlap.

Digitized by UCC, Library

The intensity distribution $I(x, y)$ across the x y holographic recording plane can be written as the modulus squared of the complex superposition $O(x, y) + R(x, y)$, namely;

$$I(x, y) = |O(x, y) + R(x, y)|^2$$

$$= |R(x, y)|^2 + |O(x, y)|^2 + R(x, y)O(x, y) + R(x, y)O(x, y). \quad (27)$$

where the symbol * denotes complex conjugation; $O(x, y) = |O(x, y)|\exp[i\varphi_0(x, y)]$ is the complex amplitude of the object wave with real amplitude $|O(x, y)|$ and phase $\varphi_0(x, y)$ and $R(x, y) = |R(x, y)|\exp[\varphi_R i(x, y)]$ is the complex amplitude of the reference wave with real amplitude $|R(x, y)|$ and phase $\varphi_R(x, y)$. Equation (27) is modified to the form;

$$I(x, y) = (|R(x, y)|^2 + |O(x, y)|^2) + 2|R(x, y)||O(x, y)|\cos(\varphi_0(x, y) - \varphi_R(x, y)) \quad (28)$$

which shows explicitly that the recorded hologram contains a term with amplitude and phase modulated the spatial carrier. For numerical reconstruction of the recorded hologram, the interference pattern $I(x, y)$ is illuminated by the reference wave $R(x, y)$, so that we have;

$$R(x, y)I(x, y) = R(x, y)|R(x, y)|^2 + R(x, y)|O(x, y)|^2 + |R(x, y)|^2O(x, y) + R^2(x, y)O(x, y) \quad (29)$$

Digitized by UCC, Library

The first term on the right side of this equation is proportional to the reference wave field, the second one is spatially varying 'cloud' surrounding the first term. These two terms constitute the zero order diffraction or dc term. The third represents, apart for a constant, an exact replica of the original waveform $O(x,y) = |O(x,y)|\exp(i\varphi_0(x,y))$ for which it is called virtual image, or simply image of the object. The last term is the so- called twin image of the original object wave or real image. In holography, the hologram can be regarded as an amplitude transmittance that refracts the reference wave.

Suppression of zero-order term and twin image

Hologram formation corresponds to the recording the intensity pattern of the free propagated waves diffracted by the objects. Hologram reconstruction, however, does not exactly solve the inverse propagation problem but rather propagate further the intensity pattern. It is well known that the in-line configuration, originally developed by (Gabor, 1949 and Leith&Upatniek 1966), zero order diffraction and the two conjugate images overlap. In classical holography, the influence of the conjugate image was removed by the off-axis geometry invented by Leith and Upatniek (1962) since in this case the three diffraction orders propagate along different directions and can be observed separately. In digital holography, the recorded intensity distribution of the hologram is multiplied by the reference wave field in the hologram plane and the diffracted field in the image plane is determined by the usual Fresnel-Kirchoff integral (Goodman, 2005) to calculate the amplitude and phase distribution of the reconstructed real image.

Digitized by UCC, Library

In digital off-axis holography the zero order of diffraction, the so- called dc term, and the conjugate virtual image appear at different locations and the elimination of these two undesired terms results in an enhancement of the image quality. Several new methods have been recently been proposed to solve the issue of the twin-image problem (Onural and Scott, 1987). Takaki et.a,l(1999) used an electro-optical holographic microscopy recording system involving the acquisition of two or three phase shifted holograms for suppressing the zero-order and the conjugate image.

In the method discussed in Kreis and Juptner (1997), the dc term was partly eliminated by averaging the intensity distribution of the hologram, while keeping the twin image unaltered. Cuche et. al,(2000b) developed a method based on spatial filtering for removing the dc term and twin image by properly filtering the corresponding spatial frequencies in the computed Fourier transform of the hologram. Recently, a method of recording four quadrature-reference wave holograms and of reconstructing the object wave- front it was also proposed in the case of in-line holography (Lai et.al, 2000).

Electronic holography

Even with the use of thermoplastic recording media, holographic interferometry remains a challenging and, in many cases, an unacceptable technique for industrial applications those that involve on-line quality testing in a production environment. Speckle-pattern interferometric (Jones and Wykes, 1983), another technique closely associated with holographic interferometry,

Digitized by UCC, Library

alleviates many shortcomings of the traditional holographic approach when combined with electronic image recording and processing equipment. Speckle is the course granular or mottle intensity pattern observed when a diffuse surface is illuminated with coherent light. The intensity of light scattered by the surface fluctuates randomly in space, dark and bright spots appear. These spots forming the entire image constitute the speckle pattern.

A speckle pattern develops if the height variations of the rough surface are larger than the wavelength of the beam. Speckles result from the interference of light scattered by the surface points. The phases of the waves scattered by different surface point fluctuate statistically due to the height variations. If these waves interfere with each other, a stationary speckle pattern develops. The speckle of the object surface is superimposed on the target with a spherical reference wave. The source point of the reference wave should be located in the center of the imaging lens. Due to this in-line configuration, the spatial frequencies are resolvable by the sensor. In practice, the reference wave is coupled into the set up by a beam splitter or guided through an optical fibre, which is mounted directly in the aperture of the lens system.

The intensity on the target is:

$$I_A(x,y) = \left|a_R(x,y)\exp\left(i\varphi_R\right) + a_0(x,y)\exp\left(i\varphi_0\right)\right|^2$$

$$= a_R^2 + a_0^2 + 2a_R a_0 \cos\left(\varphi_0 \quad \varphi_R\right) \qquad (30)$$

Digitized by UCC, Library

where: $a_R \exp(i\varphi_R)$ is the complex amplitude of the reference wave and $\varphi_0 \exp(i\varphi_0)$ is the complex amplitude of the object wave in the image plane. The term $(\varphi_0 \quad \varphi_R)$ is the phase difference between reference and object wave, which varies randomly from point to point. This speckle interferogram was recorded and electronically stored. After the deformation a second speckle pattern was recorded:

$$I_B(x,y) = |a_R(x,y)\exp(i\varphi_R) + a_0(x,y)\exp(i\varphi_0 + \quad \varphi|^2$$

$$= a_R^2 + a_R^2 + 2a_R a_0 \cos(\varphi_0 \quad \varphi_R + \quad \varphi) \qquad 31$$

These two speckle pattern are subtracted to give:

$$I = |I_A \quad I_B| = |2a_R a_0(\cos(\varphi_0 \quad \varphi_R) \quad \cos(\varphi_0 \quad \varphi_R + \quad \varphi))|$$

$$= 2\varphi_R\varphi_0 \left|\sin(\varphi_0 \quad \varphi_R + \frac{\varphi}{2})\sin\frac{\varphi}{2}\right| \qquad (32)$$

The intensity of this difference image is minimal at those positions, where $\varphi = 0, 2\pi, \ldots$. The intensity reaches its maximum at those positions, where $\varphi = \pi, 3\pi, \ldots$. The result is a pattern of dark and bright fringes, similar to a holographic interferogram. However, the differences to digital holography are the speckle appearance of the fringes and the loss of the three-dimensional information in the correlation process.

Digitized by UCC, Library

Numerical reconstruction of digital hologram

Equation (22) is the main formula of digital holography and it is essential to calculate it numerically to perform numerical reconstruction of a digital hologram. The direct approach of equation (22) is not feasible in terms of the calculation complexity and computer run time. Some approximations have to be applied in order to calculate the quadrature of this double integral to making the numerical reconstruction effective and efficient. According to the approximation used in the algorithm, the numerical reconstruction can be classified into three types: Fresnel approximation, convolution approaches and other methods.

Reconstruction by Fresnel approximation

In digital holography, the values of the coordinates x and y as well as ξ and η, are very small compared to the distance d between the reconstruction plane and the CCD/CMOS device. The right hand side of equation (23) can be expanded to a Taylor series:

$$\rho = d + \frac{(\xi - x)^2}{2d} + \frac{(\eta - y)^2}{2d} - \frac{1}{8}\frac{[(\xi - x)^2 + (\eta - y)^2]^2}{d^3} + \qquad (33)$$

The fourth term can be neglected, if it is small compared to the wavelength (Klein et. al., 1986):

$$\frac{1}{8}\frac{[(\xi - x)^2 + (\eta - y)^2]^2}{d^3} \ll \lambda \qquad (34)$$

Digitized by UCC, Library

The effect of it and the terms after it are negligible and they can be removed. Thus the distance ρ consists of linear and quadratic terms and can be approximated as:

$$\rho = d + \frac{(\xi \quad x)^2}{2d} + \frac{(\eta \quad y)^2}{2d} \qquad (35)$$

Replacing the denominator in equation (22) with d and inserting equation (35) into it, the following expression results in the reconstruction of the real image:

$$\Gamma(\xi,\eta) = \frac{i}{\lambda d}\exp\frac{i(2\pi d)}{\lambda}\exp\left[\quad i\frac{\pi}{\lambda d}(\xi^2+\eta^2)\right]$$

$$\times \int_{-\infty}^{\infty}\int_{-\infty}^{\infty} u_r(x,y)u_h(x,y)\exp\left[\quad i\frac{\pi}{\lambda d}(x^2+y^2)^2\right]\exp[\, i\frac{2\pi}{\lambda d}(x\xi+y\eta)\,]dxdy \qquad (36)$$

This equation is known as the Fresnel approximation/Fresnel transformation due to its mathematical similarity with the Fourier transform. Similarly, to equation (20) and equation (21), the intensity is calculated by squaring:

$$I(\xi,\eta) = |\Gamma(\xi,\eta)|^2 \qquad (37)$$

Digitized by UCC, Library

And the phase is calculated by

$$\varphi(\xi\,\eta) = \arctan\frac{\mathrm{Im}[\Gamma(\xi\,\eta)]}{\mathrm{Re}[\Gamma(\xi\,\eta)]} \qquad (38)$$

To convert the Fresnel approximation in equation (36) to a digital implementation, two substitutions are applied (Yaroslavsky & Merzlyakov, (1980)) :

$$\nu = \frac{\xi}{\lambda d}; \qquad \mu = \frac{\eta}{\lambda d} \qquad (39)$$

Therefore, equation (37) turns into:

$$\Gamma(\nu,\mu) = \frac{i}{\lambda d}\exp(\ \ i\frac{2\pi}{\lambda}d)\ \exp\,[-i\lambda\pi d\,(\nu^2+\mu^2)]$$

$$\times \int_{-\infty}^{\infty}\int_{-\infty}^{\infty} U_r\,(x,y)U_h(x,y)\,\exp\left[\ \ i\frac{\pi}{\lambda d}(x^2+y^2)\right]\exp\,[i2\pi(x\nu+y\eta)]\,dx\,dy$$

$$= \frac{i}{\lambda d}\exp\left(\ \ i\frac{2\pi}{\lambda}d\right)\exp[\ \ i\pi\lambda d(\nu^2+\mu^2)]$$

$$\times\ \ ^{-1}\left\{U_r(x,y)U_h(x,y)\,\exp\left[\ \ i\frac{\pi}{\lambda d}(x^2+y^2)\right]\right\} \qquad (40)$$

This shows that the Fresnel approximation is equal to the multiplication of a spherical phase factor and the inverse Fourier transformation of the function:

$$U_r(x,y)U_h(x,y)\,\exp\left[\ \ \frac{i\pi(x^2+y^2)}{\lambda d}\right] \qquad (41)$$

Digitized by UCC, Library

Suppose that there is a rectangular raster of $N \times N$ points with steps x and y along the coordinate axes. x and y are the spacing of two adjacent pixels on the CCD/CMOS devices in the horizontal and vertical directions respectively.

The calculated diffraction function $\Gamma(\nu, \mu)$ is sampled with this raster so that the infinite integral in equation (39) is converted to finite sums given by:

$$\Gamma(m,n) = \frac{i}{\lambda d}\exp(\ \ i\frac{2\pi}{\lambda}d)\exp[\ \ i\lambda\pi d(m^2\ \ \nu^2 + n^2\ \ \mu^2)]$$

$$\times \sum_{k}^{N-1}\sum_{l}^{N-1} U_r(k,l)U_h(k,l)\exp\left[\ \ i\frac{\pi}{\lambda d}(k^2\ \ x^2 + l^2\ \ y^2)\right]\exp[i2\pi(k\ \ xm\ \ \nu + l\ \ yn\ \ \mu)]$$

For $m = 0, 1, \ldots, N\ \ \ 1; n = 0, 1, \ldots, N\ \ \ 1$

(42)

This is because the maximum frequency is determined by the sampling interval in the spatial domain according to the theory of the Fourier transform;

$$\nu_{max} = N\ \ \nu = \frac{1}{x};\ \mu_{max} = N\ \ \mu = \frac{1}{y} \qquad (43)$$

The relationship between x, y, ν and μ are:

Digitized by UCC, Library

$$\nu = \frac{1}{N\ x}; \quad \mu = \frac{1}{N\ y} \tag{44}$$

Combining equations (44) and (42) gives the following expression:

$$\Gamma(m,n) = \frac{i}{\lambda d}\exp(\ \ i\frac{2\pi}{\lambda}d)\exp[\ \ i\pi\lambda d\left(\frac{m^2}{N^2\ x^2}+\frac{n^2}{N^2\ y^2}\right)]$$

$$\times\sum_{k}^{N-1}\sum_{l}^{N-1} U_r(k,l)U_h(k,l)\exp\left[\ \ i\frac{\pi}{\lambda d}(k^2\ \ x^2+l^2\ \ y^2)\right]\exp[\ \ i2\pi\frac{(km+ln)}{N}]$$

$$= \frac{i}{\lambda d}\exp(\ \ i\frac{2\pi}{\lambda}d)\exp[\ \ i\pi\lambda d\left(\frac{m^2}{N^2\ x^2}+\frac{n^2}{N^2\ y^2}\right)]$$

$$\times\ \ ^{-1}\{U_r(k,l)U_h(k,l)\exp\left[\ \ i\frac{\pi}{\lambda d}(k^2\ \ x^2+l^2\ \ y^2)\right]$$

(45)

This equation (45) is the well-known discrete Fresnel transform. The evaluation of the matrix Γ is done by applying an inverse discrete Fourier transform to the product of $U_r(k,l)$ with $U_h(k,l)$ and $\exp[\ \ i\pi(k^2\ \ x^2+l^2\ \ y^2)/(\lambda d)]$.

The calculation can be done effectively using the Fast Fourier Transform (FFT) algorithm. If the intensity is of interest, the factor in front of the sum only affects the overall phase and can be neglected in equation (37). Also, if the wavelength does not change in multiple exposures, this factor can be removed when calculating the phase differences between holograms.

Digitized by UCC, Library

The sizes of the reconstructed pixels ξ and η are different from the sampled pixel in the hologram, x and y as in equations (39) and (44). The relationship between them is given as:

$$\xi = \frac{\lambda d}{N \ x}; \quad \eta = \frac{\lambda d}{N \ y} \qquad 46$$

Similarly, the corresponding discrete formula for reconstruction through a virtual lens with focal length $f = \frac{d}{2}$ is given by the expression:

$$\Gamma(m,n) = \frac{i}{\lambda d}\exp\left(\ i\frac{2\pi}{\lambda}d\right)\exp\left[i\pi\lambda d\left(\frac{m^2}{N^2 \ x^2} + \frac{n^2}{N^2 \ y^2}\right)\right]\sum_{k=0}^{-1}\sum_{l=0}^{N-1} U_r\,(k,l)\exp\left[i\frac{\pi}{\lambda d}(k^2 \ x^2 + l^2 \ y^2)\right]\exp\left[i2\pi\left(\frac{km}{N}+\frac{ln}{N}\right)\right]$$

For $m = 0, 1, \ldots, N \quad 1$; $n = 0, 1, \ldots, N \quad 1$. (47)

Reconstruction by the convolution approach

The numerical processing of the Fresnel-Kirchoff integral without approximation is very tedious and time-consuming. Also, besides the Fresnel approximation, another approach which is widely used in the field of digital holography is to perform the numerical reconstruction. For numerical processing

Digitized by UCC, Library

a different but equivalent is much more suitable. This method makes use of the convolution theorem. It was first applied to process the numerical reconstruction of sub-optical holograms by Demetrakopoulos and Mitta (1974). Later, this approach was introduced to digital holography by Kreis and Juptner (1997). We can interpret equation (22) as a superposition integral given by:

$$\Gamma(\xi,\eta)\int_{-\infty}^{\infty}\int_{-\infty}^{\infty} U_h(x,y)U_r(x,y)g(\xi,\eta,x,y)\,dx\,dy \qquad (48)$$

Where the impulse response $g(\xi,\eta,x,y)$ is given by;

$$g(\xi,\eta,x,y)=\frac{i}{\lambda}\frac{\exp\left[-i\frac{2\pi\sqrt{d^2+(x-\xi)^2+(y-\eta)^2}}{\lambda}\right]}{\sqrt{d^2+(x-\xi)^2+(y-\eta)^2}} \qquad (49)$$

According to equations (48) and (47), the linear system characterised by $g(\xi,\eta,x,y)=g(\xi-x,\eta-y)$ is space-invariant. Therefore, the equation (48) can be regarded as a convolution and the convolution theorem can be applied (Appendix A). The two-dimensional convolution of two functions $f(x,y)$ and $g(x,y)$ is defined as:

$$(f\ast g)(x,y)=\int_{-\infty}^{\infty}\int_{-\infty}^{\infty} f(\xi,\eta)g(x-\xi,y-\eta)\,dx\,dy \qquad (50)$$

Where $\ast$ denotes the convolution operation. The convolution theorem states that the Fourier transform of the convolution of two functions is equal to the product of the Fourier transform of the individual functions:

$$\{f(x,y)\ast g(x,y)\}=\{f(x,y)\}\{g(x,y)\}=F(u,v)G(u,v) \qquad (51)$$

Digitized by UCC, Library

It will be appropriate to say that the convolution of two functions in the spatial domain can be easily obtained through the multiplication of them in another domain, namely spatial frequency domain. We can now apply the convolution theorem to equation (22) to yield this result:

$$\Gamma(\xi,\eta) = \quad ^{-1}\{ \ \left(U_h(x,y).U_r(x,y)\right). \ \left(g(x,y)\right)\} \tag{52}$$

Equation (52) includes two forward Fourier transformations and one inverse Fourier transformation; all these can be practically implemented through the FFT algorithm. Considering the digitisation, the numerical impulse response function is described as in equation (53). The shift of the coordinates by $\frac{N}{2}$ is to make the reconstructed area symmetrical with respect to the optical axis.

$$g(k,l) = \frac{i}{\lambda}\frac{\exp\left[\ \ i\frac{2\pi\sqrt{d^2+\left(k\ \ \frac{N}{2}\right)^2\ \ x^2+(l\ \ \frac{N}{2})^2\ \ y^2}]}{\lambda}\right.}{\sqrt{d^2+\left(k\ \ \frac{N}{2}\right)^2\ \ x^2+(l\ \ \frac{N}{2})^2\ \ y^2}} \tag{53}$$

The Fourier transform of $g(k,l)$ can be calculated and expressed analytically (Goodman, 2005) as in equation (54):

$$G(n,m) = \exp\quad i\frac{2\pi d}{\lambda}\sqrt{1\quad \frac{\lambda^2\left(n+\frac{N^2\ \ x^2}{2d\lambda}\right)^2}{N^2\ \ x^2}\quad \frac{\lambda^2\left(m+\frac{N^2\ \ y^2}{2d\lambda}\right)^2}{N^2\ \ y^2}}$$

(54)

This saves one Fourier transform for the reconstruction of the real image:

Digitized by UCC, Library

$$\Gamma(\xi,\eta) = \quad ^{-1}\{ \quad (U_h \quad U_r) \quad G\} \tag{55}$$

For the construction of the virtual image, a lens transmission factor $L(x,y)$ according to equation (23) and the phase correction factor $P(\xi',\eta')$ as in equation (25) should be considered:

$$\Gamma(\xi',\eta') = P(\xi',\eta') \quad ^{-1}\{ \quad (U_h . U_r . L) . G\} \tag{56}$$

The pixel distance of the images reconstructed by this algorithm is the same as that of the CCD:

$$\xi = \quad x; \quad \eta = \quad y \tag{57}$$

The area to reconstruct which is not symmetrical to the optical axis, can be shifted by introducing two integer variables are introduced to shift the reconstructed area:

$$g(k + s_k, l + s_l) = \frac{i}{\lambda} \; \frac{\exp\left[\quad i\frac{2\pi}{\lambda}\sqrt{d^2 + \left(k \quad \frac{N}{2} + s_k\right)^2 \quad x^2 + (l \quad \frac{N}{2} + s_i)^2 \quad y^2}\right]}{\sqrt{d^2 + \left(k \quad \frac{N}{2} + s_k\right)^2 \quad x^2 + (l \quad \frac{N}{2} + s_l)^2 \quad y^2}} \tag{58}$$

The convolution approach enables us to change the image magnification in the reconstruction process. With the introduction of the focal length of the introduced lens and the reconstruction distance, the distance between the hologram plane and the image plane, are changed to the required magnification. The enhanced reconstructed image can be resolved and adjusted to:

$$d' = d . m \tag{59}$$

Digitized by UCC, Library

where d is the recording distance and m the magnification factor. A magnification of $m = 1$ conforms to $\xi = x$; $\eta = y$. The focal length of the numerical lens can be evaluated by the use of the Gaussian formula from geometrical optics (Hecht,1998):

$$f = \left(\frac{1}{d} + \frac{1}{d'}\right)^{-1} \qquad (60)$$

where d and d' are the object and image distances respectively

From equation 27 the lens function becomes:

$$L(x, y) = \exp\left[i\frac{\pi}{\lambda}\left(\frac{1}{d} + \frac{1}{d'}\right)(x^2 + y^2)\right] \qquad (61)$$

Invoking equation (59) for d' and the lens function formula in equation ((61) with equation (56) yields a magnified image.

Digital Fourier holography

Lensless Fourier holography is a special form of holographic recording which is being realised in digital holography. If a spherical wave is used as the reference wave of the holographic system, the point source of the spherical reference wave is located in the plane of the object, and then it is referred to as lensless holography or Fourier holography (Wagner, 1999). The reference wave at the CCD plane is therefore, described by:

$$U_R = \frac{\exp\left(-i\frac{2\pi}{\lambda}\sqrt{(d^2 + x^2 + y^2)}\right)}{\sqrt{(d^2 + x^2 + y^2)}} \approx \frac{1}{d}\exp\left(-i\frac{2\pi}{\lambda}\right)\exp\left(-i\frac{\pi}{\lambda d}(x^2 + y^2)\right) \qquad (62)$$

Digitized by UCC, Library

The term $\sqrt{d^2 + x^2 + y^2}$ is the distance between the source point and the point with coordinates (x, y) in the CCD plane. The spherical wave can be described in equation (22), the reconstruction formula for the virtual image as shown in equation (48) leads to the equation:

$$\Gamma(\xi\,\eta) = C\exp\left[i\frac{\pi}{\lambda d}(\xi^2 + \eta^2)\right] \qquad (63)$$

C is a complex constant. That is the reconstruction of lensless hologram simplifies the calculation of the Fourier transform of the digital hologram. On the other hand, it is not possible to focus on different areas within the object volume with lensless Fourier holography because the reconstruction distance d does not appear in equation (63). The spherical phase factor $\exp\left(i\frac{\pi}{\lambda d}(x^2 + y^2)\right)$ associated with the Fresnel transform is eliminated by the use of a spherical reference wave with the same curvature. The overall effect is that this technique is unable to perform numerical focusing. In addition, this method yields valid diffraction images at short distances, down to zero.

In lensless Fourier, both the object and a focused light spot are still located on the same plane. It is not possible to focus on different areas within the object volume with lensless Fourier holography because the reconstruction distance does not appear as in equation (63). In the case of lensless Fourier micro holography, the object can be placed near to the sensor, which increases the numerical aperture and improves resolution but this introduces aberration in the reconstruction because of violation of the Nyquist frequency requirement. However, a hologram

Digitized by UCC, Library

with the lens, an imaging lens can be used to form a magnified or demagnified image of the object, which then propagates to the hologram plane. For instance, a negative lens is used to form demagnified image of a large object, thus reducing the spatial frequency bandwidth.

Furthermore, using a lens the complex field at the back focal plane of the lens contains three terms: the zero order located on the back focal plane, the inverted constructed image and the conjugate image. In reconstruction, a plane reference wave and a lens will produce the inverse transform which is the image, and the numerical lens is used to focus images at varying distances. For lensless holography, however, it can well assure the precise superposition of the reconstructed images. The allowable minimum recording distances are proportional to the size of the object, and aberration free high- resolution image (Upatnieks, et al., 1966).

Angular spectrum approach

In Fresnel approximation and the convolution method, the object under observation should be placed farther away than the minimum distance. If it is placed within that minimum accepted distance, the spatial frequency of the detector will be too low and aliasing occurs. At long wavelength, if the object is placed within the minimum accepted distance, the spatial frequency of the detector will be high and aliasing will not occur as in equation (64). The minimum distance is given by the expression:

Digitized by UCC, Library

$$d_{min} = \frac{(N \quad x)^2}{N\lambda} \qquad (64)$$

where N and x are the number and size of the pixels respectively (Hecht, 1998). At long wavelength, increasing the size N x of the window function tends to increase d_{min}.

Maintaining N as a constant may lead to the badly sampled reconstructed image if the reconstructed distance does not satisfy equation (64). However, the angular spectrum method is able to overcome this problem. It is comparable with other methods in terms of computational efficiency but has the potential of higher accuracy (Kim et al., 2006). Consider the wave field at the plane d=0 is $U_0(x, y; 0)$, the angular spectrum $A(k_x, k_y; 0)$ at this plane is obtained by taking the Fourier transform:

$$A(k_x, k_y; 0) = \iint U_0(x, y; 0) \exp[\quad i(k_x x + k_y y)]\, dx\, dy \qquad (65)$$

where k_x and k_y are the corresponding spatial frequencies of x and y. If the angular spectrum is at a distance d, $A(k_x, k_y; d)$ is calculated from $A(k_x, k_y; 0)$ as it is given by the relation:

$$A(k_x, k_y; d) = A(k_x, k_y; 0) \exp(ik_z d) \qquad (66)$$

Where $k_z = \sqrt{k^2 \quad k^2{}_x \quad k^2{}_y}$ and the reconstructed complex wavefield at any plane perpendicular to the propagating along the z axis is expressed as:

Digitized by UCC, Library

$$U(\xi,\eta;d) = \iint A(k_x, k_y; d)\exp\left[i\left(k_x\xi + k_y\eta\right)\right] dk_x dk_y$$

$$= \quad ^{-1}[\ \ (U_0)\exp(ikk_z d)] \qquad (67)$$

From equation (67), the resolution of the reconstructed images from angular spectrum method is the same as that of the hologram plane, which means that the pixel size does not vary with changes of wavelength or reconstruction distance.

Phase retrieval approach

Phase retrieval approach permeates many areas of imaging science and other applications including diffraction imaging, optics, astronomical imaging, and microscopy to mention but few. The fundamental problem of recovering a general signal, an image for instance, from the magnitude of Fourier transform is known as phase retrieval, arising in many applications. Its origin comes from the fact that detectors can often times record the squared modulus of the Fresnel or Fraunhofer diffraction pattern of the radiation that is scattered from an object.

In such settings, one cannot measure the phase of the optical wave reaching the detector and therefore, much information about the scattered object or optical field is lost, since as known, phase encodes a lot of structural content of the image we wish to form. Historically, the first application of phase retrieval is X-ray Crystallography (Harrison, 1993 and Pierattini,2003). Over the last century or so, this field has developed a wide array of techniques to recover Bragg's peaks from missing- phase data.

Digitized by UCC, Library

Digital holographic techniques are among the most popular methods that have been proposed to measure the phase of the optical wave. While digital holographic techniques have been successfully applied in certain areas of optical imaging, they are generally difficult to implement in practice (Daudi et. al, 2011 and Zalevsky,2011). Hence the development of algorithms for signal recovery from magnitude measurement is still a very active field of research.

Existing methods for phase retrieval rely on all kinds of a priori information about the signal, such as positivity, atomicity, support constraints, real-value, (Chen et al (2007), and (Fienup, et al.,1982). Direct methods are limited in their applicability to small-scale problems due to their large computational complexity. Oversampling in the Fourier domain has been proposed as a means to mitigate the non-uniqueness of the phase retrieval problem. While oversampling offers no benefit for most one-dimensional signals, the situation is more favourable for multidimensional signals, where it has been shown that twofold oversampling in each dimension almost always yields uniqueness for finitely supported, real-valued and non- negative signals (Bruck and Sodin, 1979 and Hayes, 1982). In other words, a digital image of the form $x = \{[t_1, t_2]\}$ with $0 \leq t_1 < n_1$ and $0 \leq t_2 < n_2$ whose Fourier transform is given by:

$$x[\varphi_1, \varphi_2] = \frac{1}{\sqrt{n_1 n_2}} \sum x[t_1, t_2] e^{-i2\pi\left(\varphi_1 t_1 / n_1 + \varphi_2 t_2 / n_2\right)} \qquad (68)$$

Digitized by UCC, Library

This is usually uniquely determined from the values of $x(\varphi_1, \varphi_2)$ on the oversampled grid $\varphi = \{\varphi_1, \varphi_2\} \epsilon\, \Omega = \Omega_1 \times \Omega_2$ in which $\Omega_1 = 0, {}^1/_2, 1, {}^3/_2, \ldots n_i + {}^1/_2$.

This holds provided x has proper spatial support, is real -valued and non-negative. A nonlinear change of variables was performed so that the reconstruction may be performed by the use of a method that is reminiscent of phase- shifting techniques. The algorithm is based on a local least- squares estimation of the amplitude and phase by summing an a priori model of the phase of the reference wave.

Once the complex object wave is recovered in the acquisition plane, the wave is back- propagated to restore a focused image using digital implementation of the Fresnel transform (Liebling et. al., 2004). An approach to implement numerical reconstruction that uses the Gerchberg- Saxton phase retrieval was proposed (Liu and Scott, 1987). Zhang et al.,(2003) introduced the Yang- Gu phase retrieval algorithm to the numerical reconstruction of in- line digital holograms. Iterations are implemented in both methods until convergence is achieved. The difference between the hologram obtained by the iteration, the real image captured by the camera reaches its minimum value at convergence. The Yang- Gu algorithm takes more time to process than the Gerchberg- Saxton algorithm because of it has two iteration loops. But it can be easily expanded to multiwavelength and mutiple systems and it is not sensitive to choose of the initial value.

Digitized by UCC, Library

The method proposed by Zheng et al., (2005) is based on the processing of a series of holograms of the same object recorded at different distances. What can be recorded on the CCD/CMOS device is the intensity distribution, whiles the phase information is lost completely. Direct application of the Fresnel approximation will produce both the original image and its twin image. The phase of the wave must be retrieved in order to overcome this problem. For instance, a hologram I_1 which is recorded at a distance d_0 from the object, a propagation of this pattern I_1 from d_0 to $d_0 +$ d using Fresnel approximation is calculated to obtain a complex wave field distribution A_2' . Thus keeping the phase distribution of the field A_2' unchanged and using the square root of the hologram I_2 as an amplitude distribution, a new wave field A_2 was performed from $d_0 +$ d to $d_0 + 2$ d. It is also possible to use the inverse Fresnel transform to recover the image of the object.

This is similar to the algorithm for retrieving phase information from two intensity distributions as in Gerchberg- Saxton algorithm and Yang-Gu algorithm but the use of multiple holograms rather than two intensity distributions means that more information was available to recover the image. Furthermore, Zhang et al (2005) proposed a systematic approach from the perspective of generalised sampling theory. An approximation of continuous complex amplitude at CCD/CMOS sensor can be synthesised from a set of basic functions with the recorded samples as weights. Adopting different basis functions and different formulas for describing the diffraction process, an optimal reconstruction algorithm can be developed for various recording conditions and different

Digitized by UCC, Library

diffraction characteristics of the object. A proposed method to numerically extract the object information from the fringe pattern of a hologram was put forth. Then an iterative algorithm is used to imitate an imaging system by focusing on different layers of the object and by the operation in both the spatial domain and frequency domain, the algorithm produces a series of two- dimensional layer image.

The object finally reconstructed layer by layer subject to a constraint condition which must be satisfied (Yu and Cai, 2001). Liebling et al (2003) constructed a new wavelet basis for the processing and reconstruction of digital holograms by taking advantage of the mathematical properties of the Fresnel transform. It permits reconstruction at the various user- specified and wavelength independent scales.

The reconstructions at unrefined stage allow for optimal filtering of the zero- order and twin image which can also result in less noisy images. In this chapter, various algorithms for numerical reconstruction have been presented and discussed. The main focus of these algorithms has been Fresnel approximation and the convolution approach, which are the direct derivatives from scalar diffraction theory. The Fresnel approach is the most cost -effective algorithm because of its use of only one FFT. In the measurement of macroscopic objects at longer distances, for some tens of centimetres, the Fresnel approximation is the best option. However, a microscopic object of smaller size, the convolution approach has a lot of advantages. Measuring macroscopic objects, the recording distance between the object plane and the CCD/CMOS plane is sufficient to

Digitized by UCC, Library

ensure that the Fresnel approximation is equivalent to the angular spectrum algorithm.

Phase retrieval methods can avoid the reconstructed image being severely corrupted by the zero order term and the twin image. They basically remove these terms without the need for any pre or post processing. However, there are complex procedures and the implementation of phase retrieval methods are based on iteration loops, this more complicated and consumes more time than the application of other algorithms. There are other numerical techniques such as:

Apodization

The sharp boundaries of hologram aperture can cause spurious fringes in the reconstruction images especially phase images. The ‘’ringing’’can be reduced by apodization of the boundary of the hologram with a smooth attenuation function (Cuche et. al., 2000).

Focus detection

In a classical imaging system, it is difficult or impossible to recover the focused image from a defocused one. In digital holography, the image can be calculated at any distance from the hologram. To determine if an image is in focus, one can apply subjective judgment to the sharpness of the image or using sharpness metric. A more deterministic method for finding the focus distance if the specimen is either pure amplitude or pure phase object, where a theorem is proven that the sum of absolute values of a complex image array is an extremum at the focal distance (Dubois et. al, 2006).

Digitized by UCC, Library

Super-resolution

Recently, a signal- processing based approach known as super-resolution (SR) image reconstruction has proven useful for overcoming the restrictions involved in obtaining higher resolution images. The term SR, originally used in optics, refers to an algorithm that operates mainly on a single image to extrapolate the spectrum of an object beyond the diffraction limit (Kang and Chaudhuri, 2003). There are two concepts, SR image reconstruction and SR restoration have a common focus in recovering high frequency information that has been lost or degraded during image acquisition.

However, the cause of this loss of high-frequency information differs between these two concepts. SR restoration in optics attempts to recover information beyond the diffraction cut-off frequency, while the SR image reconstruction method stages: registration, interpolation and restoration (Park, et al., 2003). These steps can be implemented separately or simultaneously, according to the reconstruction method adopted. The resolution of digital holography is determined by the pixel count and size of the CCD array. There have been methods developed to overcome the limitation, mainly by synthesising larger apertures of the imaging system, for example by translating the CCD camera to cover a larger area. (Le Clerc, et. al.,2001, Martinez, et. al,2008 and Massig,et.al.,2002). Also, a vertical cavity surface-emitting laser array was used as the laser source, and a number of laser elements were turned on in sequence to illuminate the optical system with varying tilt angles (Mico, et. al., 2006).

Digitized by UCC, Library

The combined hologram then contains larger spectral bandwidth and the results in improved resolution. A grating can be used to redirect diffraction components that otherwise would leave the imaging system, and thus increase the resolution of the digital hologram (Paturzo, et. al., 2008 and Liu, et. al., 2002). In this research experiments were performed in order to compare the Fresnel approximation approach and the convolution algorithm. They are the direct derivatives from the scalar diffraction theory which other algorithms are connected. Fresnel method is the most cost- effective algorithm because of its use of only one FFT. The convolution approach has the advantage of measuring microscopic objects, with their rather small size. The angular spectrum algorithm provides more accurate construction results than both the Fresnel approximation and the convolution approach. The main focus of this thesis is measuring macroscopic objects. The MATLAB codes for performing numerical reconstruction for the formation of the digital holograms are enclosed in appendix E.

Digitized by UCC, Library

CHAPTER THREE

EXPERIMENTAL METHODS

Experimental Components

The optoelectronic components of the experimental set- up comprises of the following:

(a) The laser source

(b) Acquisition system

(c) The software

And these optoelectronic components would be described in the subsequent paragraphs of this section.

The laser source

The laser source was a continuous wave Carbon Dioxide (CO_2) laser, that was an axial gas flow (He and Ne) emitting on the P(20) line at $10.59\ \mu m$. They were in the ratio CO_2 4.5%, N_2 13.5% and He 82%. The model is Blade (EL-EN) 100 a laser class 3A whose cavity, 82 cm long, was defined by a partially reflective flat mirror (R= 95%) and an out-coupling mirror (R=90%) of 3m curvature radius mounted on a piezoelectric translator. The laser active medium is excited by an electric discharge passing through the laser gas. Both N_2 and CO_2 molecules absorb energy from electrons in the discharge but the lowest vibrational level of N_2 easily transfers' energy to CO_2.

Digitized by UCC, Library

Helium helps to maintain the population inversion by facilitating CO_2 molecules drop from the lower levels to the ground state. The output laser beam was horizontally polarised by means of an intra-cavity ZnSe Brewster window. The system, pumped by an electric discharge of 10 mA, when the laser threshold was approximately 7 mA, provides an output power of 190 mW. The spatial profile of the laser was set on a fundamental TEM_{00} Gaussian mode by means of an intra-cavity iris diaphragm. The maximum pressure of the laser was 32 mBar, the voltage used was 220 V and the maximum operating current was 8 A. Due to the high output powers of the laser, they are commonly used in cutting and welding industrial metal profiles, and are frequently employed in surgery and dermatology due to its strong absorbance.

The acquisition system

The cameras used in this research are highly resolution cameras: Spiricon Pyrocam,(model PY-III-C-A, and Miricle Thermoteknix) camera. The Spiricon Pyrocam consists of a $LiTa0_3$ pyroelectric crystal mounted with indium bumps to a solid-state readout multiplexer. This sensor has proven to be the most rugged, stable, and precise IR detector array available. Light impinging on the pyroelectric crystal is absorbed and converted to heat, which creates a charge on the surface. The multiplexer then reads out this charge. For use with short laser pulses, the firmware of the camera creates a very short electronic shutter to accurately capture the thermally generated signal.

Digitized by UCC, Library

The Pyrocam III offers 0.5× 0.5 inch detector array with easy Windows camera setup, direct Windows quantitative and image display, 14- bit digitizer, versatile firewire PC interface, and an integral chopper for CW beams and thermal imaging. The Pyrocam sensor is capable of operation with intensities of about 100 times greater than CCD cameras. This makes the camera ideal for use with high power lasers, as less attenuation is required. Furthermore, the pyocam III has some special features; spectral ranges from 13 to 355 nm and 1.06 to 3000 μm , image CO_2 laser, telecom NIR lasers and other infrared sources up to far IR THz sources. It has a solid state array camera with 100:1 ratio linear dynamic range for accurate profiling as shown in plate 1 and the window assembly as shown in plate 2. Interchangeable windows available for a variety of applications; includes Beam-Gage and beam analysis software for quantitative analysis and image display (OPHIR Photonics,2014).

Plate 1: A picture of Pyrocam III camera (OPHIR Photonics, 2010)

Digitized by UCC, Library

The camera features a high- resolution A/D converter which digitises deep into the camera noise. This enables reliable measurement and analysis of both large signals and low- level signals in the wings of the laser beam. High resolution digitising also enables accurate signal summing and averaging to pull weak signals out of the noise. This is especially useful with fibre optics at 1.3µm and 1.55µm, and in thermal imaging. The camera is also useful in product engineering of CO_2 and other infrared lasers. The Pyrocam is an integral part of the assembly lines of many CO_2 laser manufacturers. Integrators of systems are using the Pyrocam sensor to make sure that optical systems are aligned and operating properly as shown in plate 2.

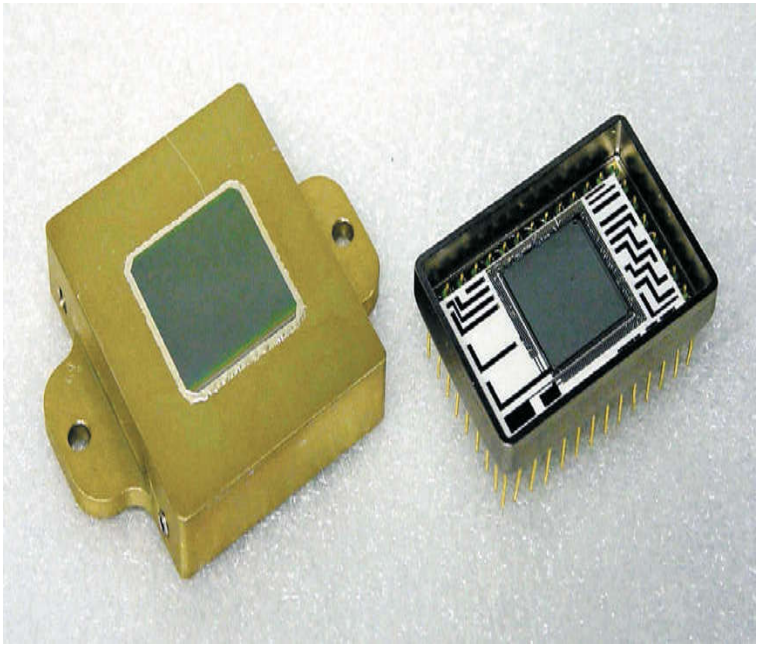

Plate 2: The Pyrocam III sensor array and window assembly (OPHIR Photonics,2014)

Digitized by UCC, Library

The Pyrocam sensor is capable of operation with intensities about 100 times greater than CCD cameras. This makes the camera ideal for use with high power lasers, as less attenuation is required. The second camera as shown in plate 3, is of two types: Thermoteknix Miricle 307K, with 640×480 pixels and $25\ \mu m$ pixel pitch and Thermoteknix Miricle 110K, with 384×288 pixels and $35\ \mu m$ pixel pitch both were used without cameras objective has RS232 composite video (USB or LUDS digital interface) and an 8-bit palletised or full span 14-bit format.

The camera uses a watertight connector and short break-out cable with power. It can operate without the use of a mechanical shutter, no moving parts, are lighter, silent and more robust. This camera lenses normally suffer a loss of focus with variations in environmental temperatures (Thermoteknix systems Ltd., 2014)

Plate 3: Miricle thermoteknix camera (Thermoteknix Systems Ltd, 2014)

Digitized by UCC, Library

The properties of the two cameras used in the experiment; miricle thermoteknix camera and pyrocam III camera are summarised in table 1.

Table 1: The properties of the two cameras: miricle thermoteknix and Spiricon Pyrocam III camera.

Properties	Thermoteknix Miricle 110 K camera	Pyrocam III camera
Power consumption	2.5 W	10 W
Operating temperature	-20ºC to +50ºC	5ºC to50ºC
Weight	1.66 g	1.52 kg
Pixel pitch	35μm× 35 μm	85 μm× 85 μm
Spectral response	8 μ-12 μ	1.06 μ-3000 μ
Sensitivity	≤ 70 Mk	70 μJ/cm²
Array size(pixels)	384 × 288	124 × 124
Detector material	Amorphous Silicon	Zinc Selenide A/R coat
Dimension/mm	57.6 ×45 ×52.5	140×130×60

Digitized by UCC, Library

The Software

The Pyrocam III Windows application incorporates setup software to control all functions of the camera, such as pulsed versus chopped operation, gain, and background reference subtraction, eliminating all controls from the camera housing. Both Pyrocam bundled with Beam-Gage, the state-of-the-art beam profiling system that performs rigorous data acquisition and analysis of laser beam parameters (such as beam size, shape, uniformity, divergence, mode content) and expected power distribution. The Beam-Gage provides high accuracy results, guaranteeing that data baseline (zero-point reference) is accurate to $1/8^{th}$ of a digital count on a pixel-by-pixel basis. Once the Pyrocam is connected to the PC, the Beam-Gage software automatically detects the camera presence and to start taking images and displaying them on the monitor.

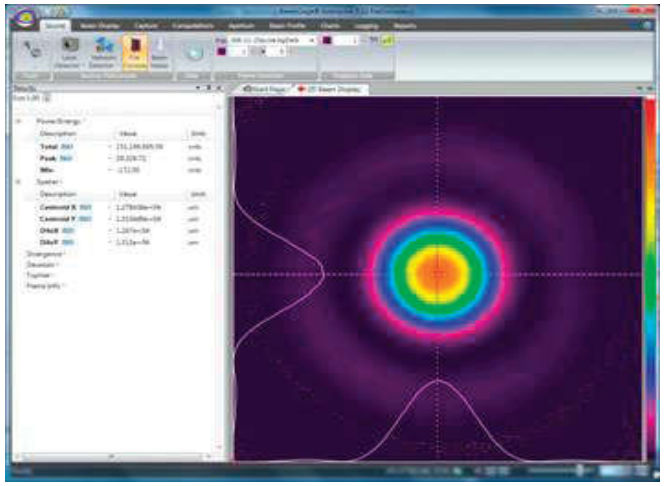

Plate 4: A picture of the Beam-Gage analyser

Digitized by UCC, Library

The images (holograms) are stored in an image file for analysis. The beam-Gage software was used to acquire a video recording of the interferogram and the reconstruction of the interferogram recorded These images are stored in an image file for analysis. Plate 5 shows the interface setup menu which was connected to the Beam-Gage for analysing the laser beam. This software can acquire a video of the interferogram which can be used for reconstruction the hologram using Matlab algorithm (OPHIR Photonics, 2014).

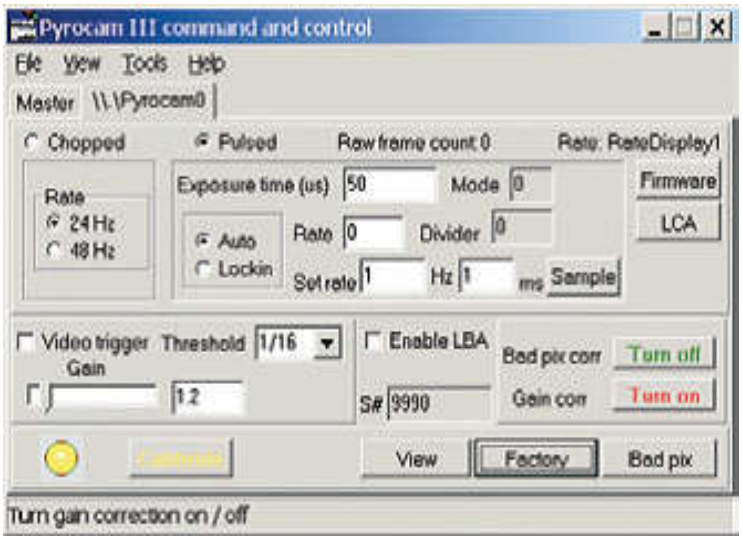

Plate 4: The Pyrocam III windows setup menu

Digitized by UCC, Library

Applications of Pyrocam III sensor

Pyrocam III an ideal camera for use in scientific laboratory investigations of laser beams. This includes physics, chemistry and electronic system designs. The camera is also useful in product engineering of CO_2 and other infrared lasers. It is an integral part of the assembly lines of many CO_2 laser manufactures. Integrators of systems are using pyrocam sensors to make sure that optical systems are aligned and operating properly. There are many medical applications of the pyrocam, such as the analysis of excimer lasers used for eye surgery, dermatology, fibre optic communications for analysing the beams emitted. In many cases, these lasers need alignment to ensure that the eye surgery was performed as expected (OPHIR Photonics, 2014).

Experimental set up

The Optical system consists of a laser beam, ZnSe beam splitters, lenses and gold coated mirrors. The interferogram was recorded by means of two imaging cameras: a $LiTaO_3$ thermal camera, Spiricon Pyrocam III, with 124×124 pixels and 85μm pixel pitch and an amorphous Silicon (ASi) thermal camera, Thermoteknix Miricle 110K, with 384×288 pixel and 35 μm pixel pitch, both used without camera's objectives. Six different setups are discussed in the text with the system calibration performed first, in this case, the test object was a steel plate with four drilled holes each with diameter 700 μm , was placed at a distance of about 400 mm from the sensor array. With the removal of zero-

Digitized by UCC, Library

order term and twin image, the brightness of the image of the resolution target is significantly improved.

Off-axis transmission mode IR holography with low resolution pixel pyroelectric sensor.

In this configuration, the laser beam was characterised by the divergence of 2 mrad. Figure 10 shows digital holography optical setup based on a Mach-Zehnder interferometer configuration. Two mirrors $M_2 \text{and} M_3$ and two beam splitters, BS1 and BS2, were used to form the interferometer. The beam splitters were ZnSe coated windows with a diameter of 50 mm each. The set -up consists of an interferometer in which light scattered from an object interfere with the reference beam on a high- resolution IR camera. The IR camera has a square pixel of $85 \times 85\ \mu m^2$ size and centre- to -centre spacing of the pixel pitch of $100 \times 100\ \mu m$. The reference beam interferes with the object beam at small angle $\alpha \leq \frac{\lambda}{2\ \xi} = 3^0$, as required by the sampling theorem. The IR camera permits the detection of CW infrared laser radiation by means of an internal chopper. This was interfaced to a personal computer to record the digitised fringe patterns and stored in a data file for analysis.

Digitized by UCC, Library

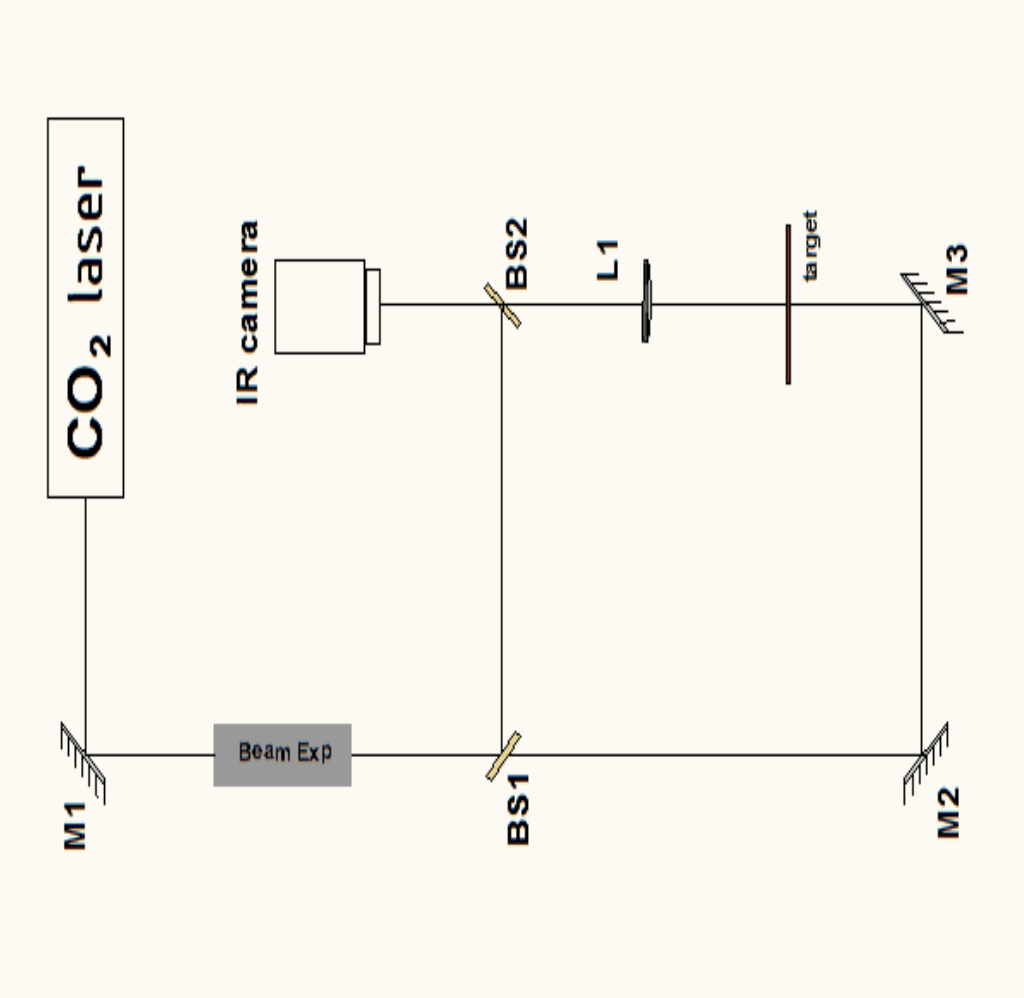

Figure 10: Mach-Zehnder interferometric set -up for recording digital holograms in transmission configuration.

Digitized by UCC, Library

Off-axis reflection mode IR holography with low- resolution pixel pyroelectric sensor

Mach-Zehnder interferometer with low- resolution pixel pyroelectric sensor, for off-axis reflection mode holography was used to obtain reconstructions in digital holography of both amplitude and phase. The system was set to have an optical power in the range of 500-800 mW in order to explore the reflection mode. Figure 14 shows the DH optical set up based on a Mach-Zehnder interferometer in reflection configuration as in figure 11.

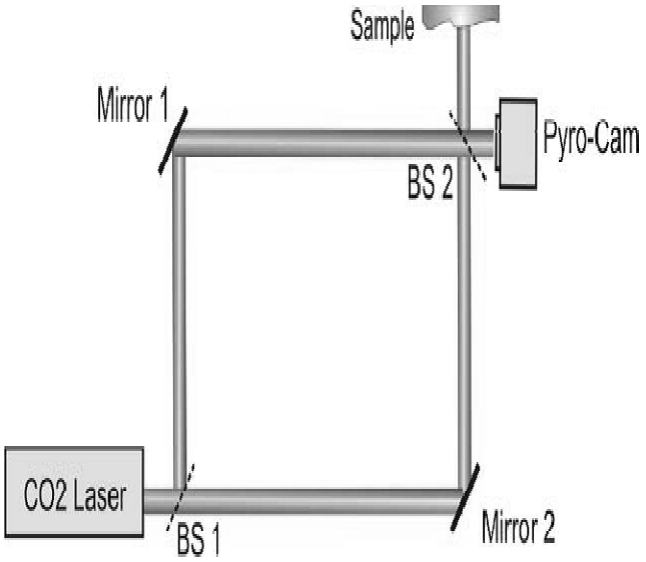

Figure 11: Mach-Zehnder interferometric set up in reflection mode.

The infrared beam was directed to a beam expander with magnification 2.5 times and 15 mm diameter of the output beam. The two mirrors M1 and M2 and the two beam splitters, BS1 (70T/30R at 45^0 of incidence angle) and BS2 (50T/50R at 45^0 of incidence angle) were used to form the interferometer.

Digitized by UCC, Library

The beam splitters were ZnSe coated windows with diameter 50 mm each and as a detector, the same thermal camera was used as in figure 11. The reflective objects used were two opaque Aluminium blocks located at a distance 250 mm from the array. The first object was rectangular in shape with dimensions $20\,\text{mm} \times 35\,\text{mm}$ that have letters inscribed. The letters were ‘’UOR’’ and ‘’XUO’’ each of dimensions about $3 \times 4\,\text{mm}$ inscribed. The second was a disc of the radius of radius 25.4 mm which has inscribed a set of concentric circular tracks. The aluminium blocks are located at a distance, d=250 mm from the array.

Off-axis speckle mode IR holography with a medium resolution pixelated pyroelectric sensor.

The configuration shown in figure 12 was used to obtain the amplitude reconstruction on of one and two euro coins. A simpler interferometric reflection configuration as in figure 12 with a higher resolution camera, amorphous silicon (ASi) thermal Thermoteknix Miricle camera with 384×288 pixels and 35 pixel pitch and a high power CW CO_2 laser, emitting at $10.6\,\mu\text{m}$, attenuated by means of a beam splitter were used.

Digitized by UCC, Library

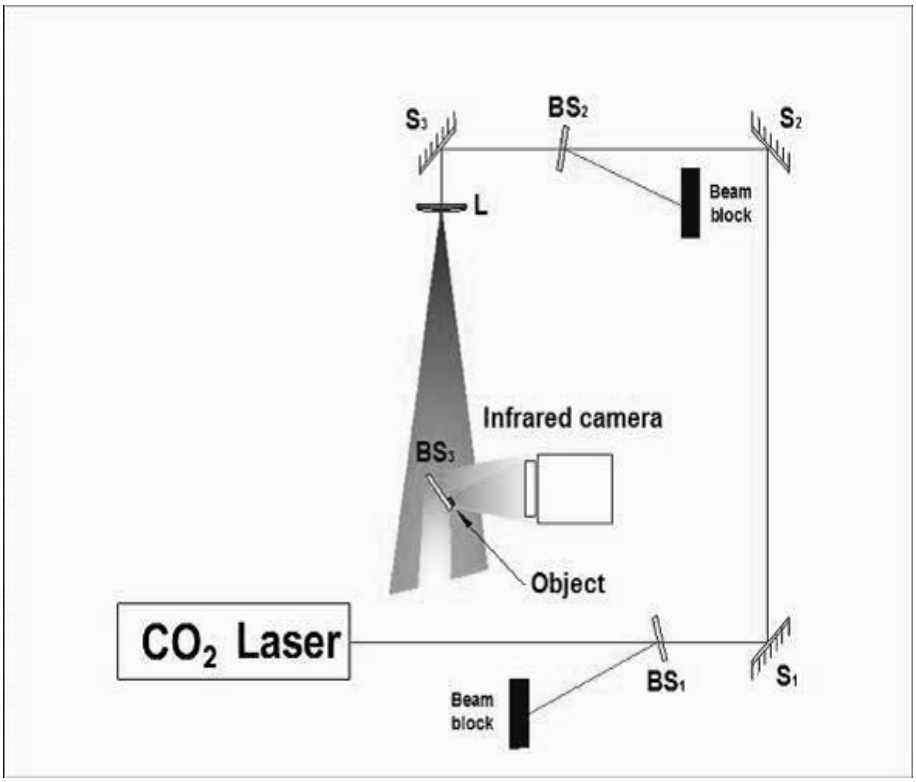

Figure 12: Off-axis interferometric reflection set up in reflection mode.

The object was placed near the beam splitter so that the central part of the laser beam was reflected by the beam splitter towards the camera, thus acting as the reference beam, while the outer part was diffused by the object, thus forming the object beam. Since the beam splitter reflected only 50% of radiation impinging on it, the reference beam intensity was comparable to that of the object beam, as a result a good fringe contrast was obtained. In this configuration, it was also possible to keep the camera very close to the object and obtain rather high-resolution images.

Digitized by UCC, Library

Off-axis speckle mode IR holography with high resolution micro bolometric sensor

A more complex configuration as shown in figure 13 was tested in order to obtain the amplitude reconstruction of a larger object. A CO_2 laser with about 100 W output power and a thermal camera thermoteknix miracle 110k, with 384 x288 Amorphous Silicon (ASi) element and 35 μm pixel pitch was used. In this interferometric set up, the reference beam came from the back of the object, so that, its direction could be easily adjusted to obtain adequate fringe spacing. In order to explore further possibilities offered by IR digital holography, image acquisition of objects made of different materials were tested. Attention was given to metal based items with different finishing

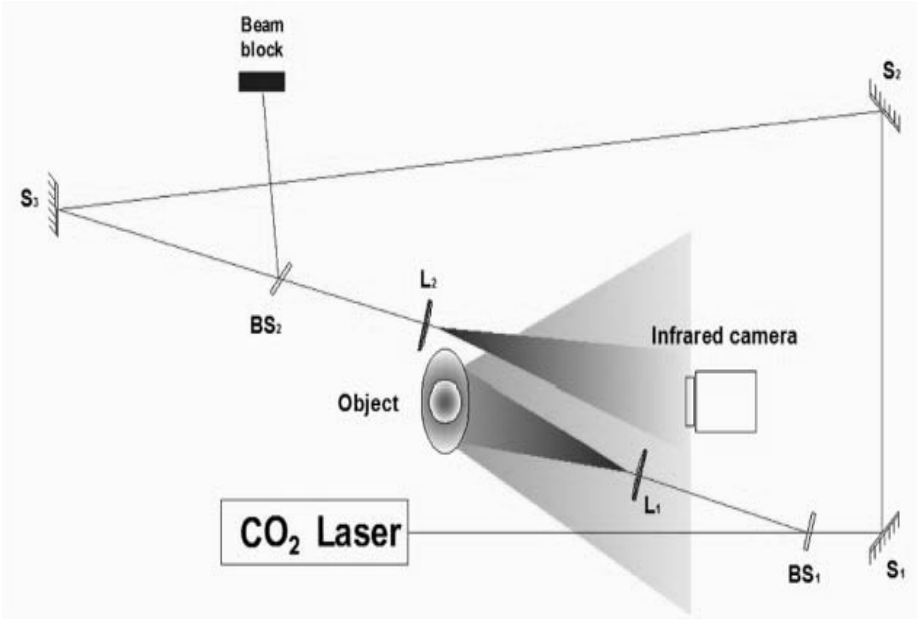

Figure 13: Off- axis interferometric reflection set up in reflection mode.

Digitized by UCC, Library

Some of those items are; Aluminium plate, marble plate, and earthenware tree. Two similar metal objects representing Emperors Augusto and Traiano as shown in plate 6 was sanded in order to remove the finishing; this was to improve the quality of the amplitude reconstruction of the two objects. The two small bronzes were placed at different distances from the detector, with Augusto further away by about 7 cm with respect to Traiano, placed at a distance of about 22 cm from the detector. Using the appropriate distance in the reconstruction formula the two small bronzes could be focused as shown in chapter 4; plate 8 and figure 27 respectively.

Plate 6: Two small bronzes which were used for testing the system.

Digitized by UCC, Library

Interferometer with a large micro bolometric sensor for off-axis speckle mode IR holography.

When objects with larger dimensions have to be recorded, the recording distance increases and this is not feasible in practice. In this case, an interferometer with a negative lens which, was placed in the object arm (between the object and the camera) to reduce the object angle to values with resolvable spatial frequencies spectrum was used. This configuration, as shown in figure 14 was used to further increase the imaged area.

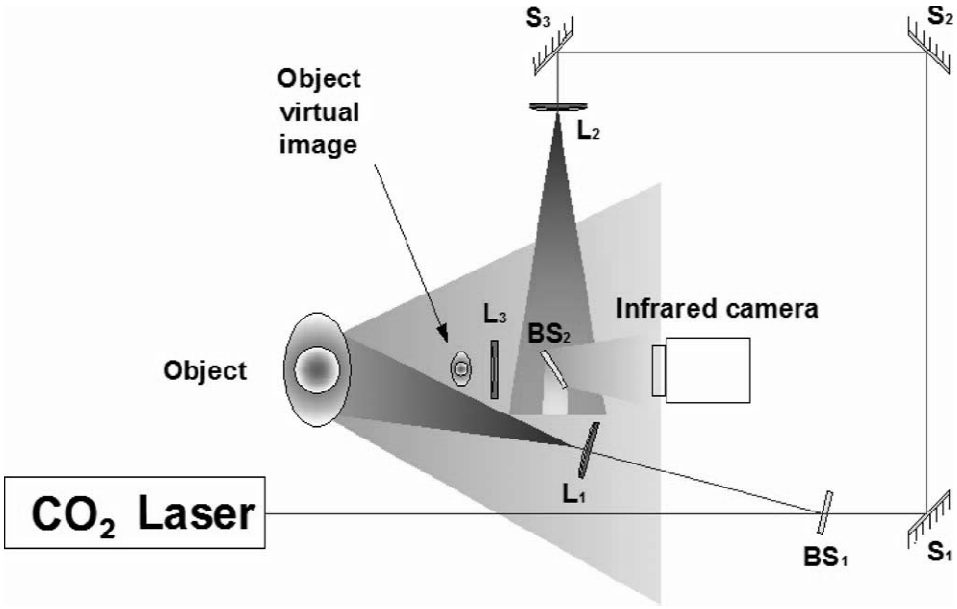

Figure 14: Off- axis speckle interferometric set up in reflection mode, with negative lens.

Digitized by UCC, Library

The wave field emerging from this virtual image is superimposed on the reference wave and the resulting hologram was recorded. The overall effect was to enlarge the field of view of the camera so that larger objects wave fields could be captured.

Off-axis speckle mode IR double-beam holography with a high resolution pixelated micro bolometric sensor.

In order to obtain a more homogeneous distribution of object beam, the ray was split into two beams, pointing to two areas, one above the other, along the vertical direction as shown in figure 15. In this configuration, high resolution camera, an ASi thermal imaging camera, Miricle Thermoteknix 307k, 640x480 detector resolution and 25μm pitch, was employed without the camera's objective.

Digitized by UCC, Library

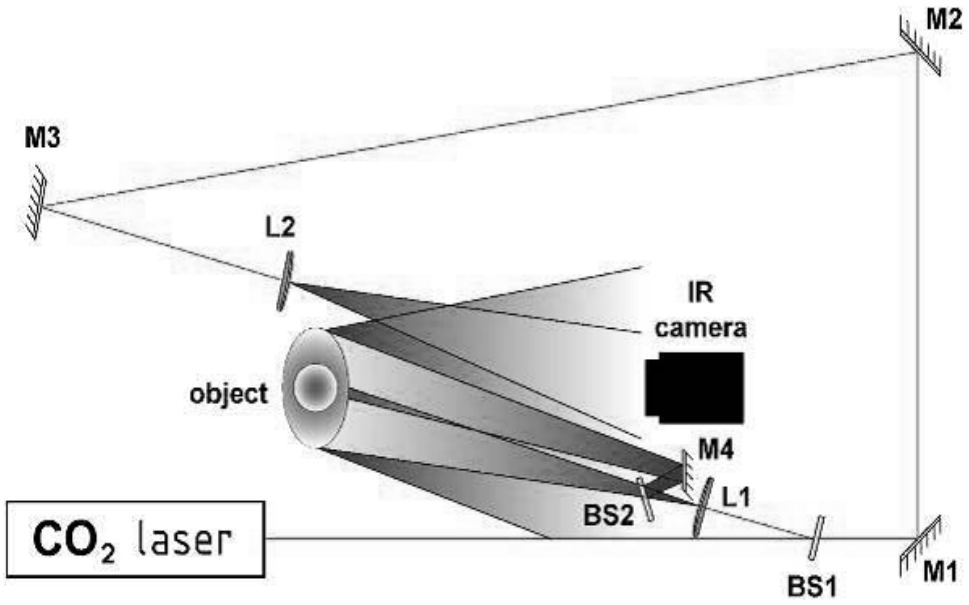

Figure 15: Off-axis interferometric recording set up with object beam split into two.

Table 2 shows the configurations in both off-axis and in-line; transmission and reflection modes.

Digitized by UCC, Library

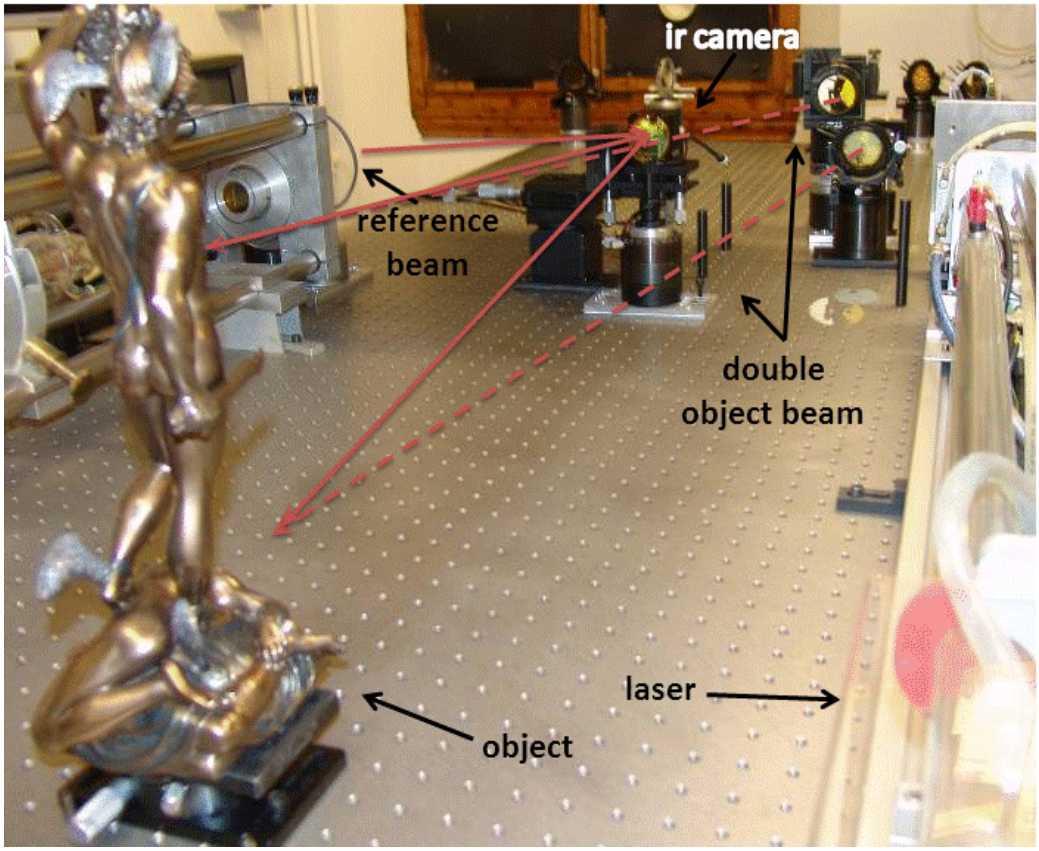

Plate 7: Experimental setup for recording the digital hologram.

Digitized by UCC, Library

Table 2: Summary of the various interferometric set up configurations.

Configuration	Off-axis	In-line
Transmission mode with	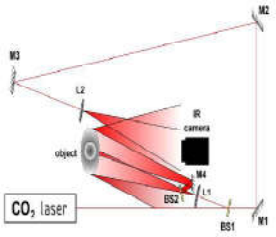	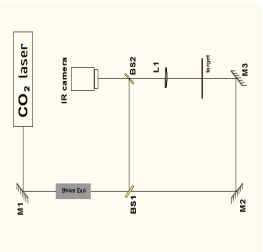
Transmission mode without lens	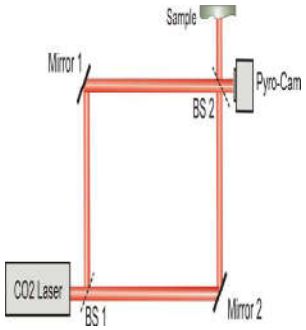	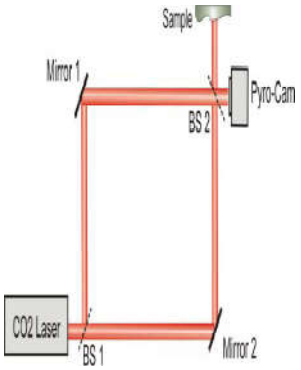
Reflection mode with lens	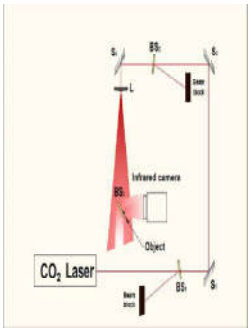	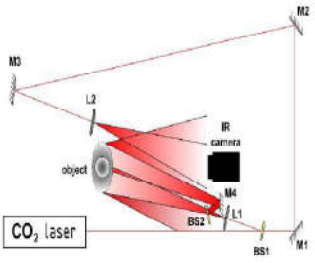

Digitized by UCC, Library

Table 2 continue

Reflection mode without lens	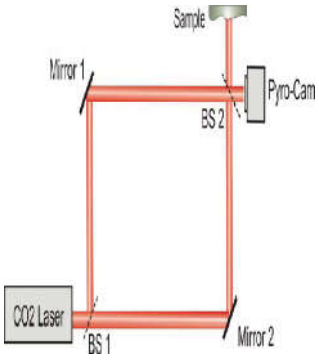	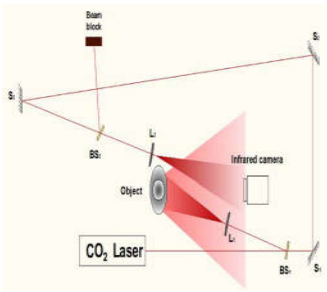
Reflection mode with negative lens	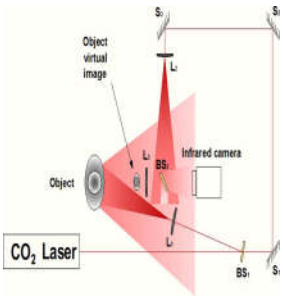	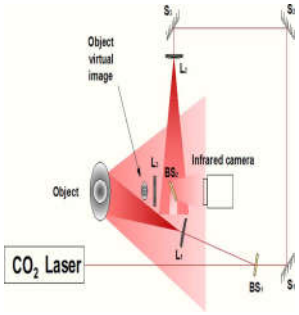

Digitized by UCC, Library

CHAPTER FOUR

RESULTS AND ANALYSIS

The experimental results for the six configurations used to explore digital holography at Infrared (IR) long wavelength are shown in this chapter. Figure 10a shows a hologram acquired with the test object (the steel plate with holes) inserted in the interferometer arm, where one hole is more visible. The fringe pattern of the digitally recorded hologram with the test object as shown in figure 16a and figure 16b shows the amplitude reconstruction of the test object.

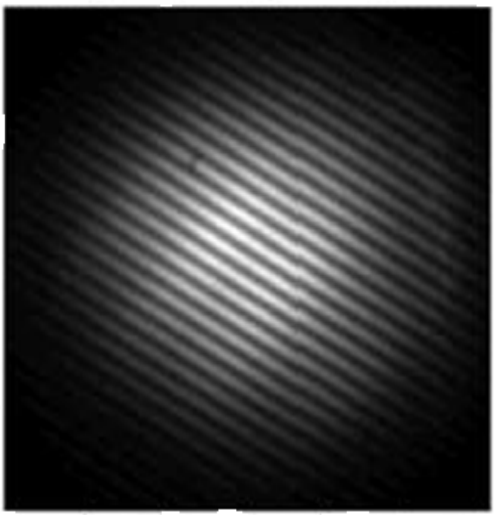

Figure 16a: Digital hologram recorded with amplitude reconstruction.

The three image components resulting from the numerical reconstruction appear separated because of the off-axis geometry: the bright central spot, corresponding to the un-diffracted wave, the four holes of the real image, clearly resolved and out of focus virtual image in figure 16b.

Digitized by UCC, Library

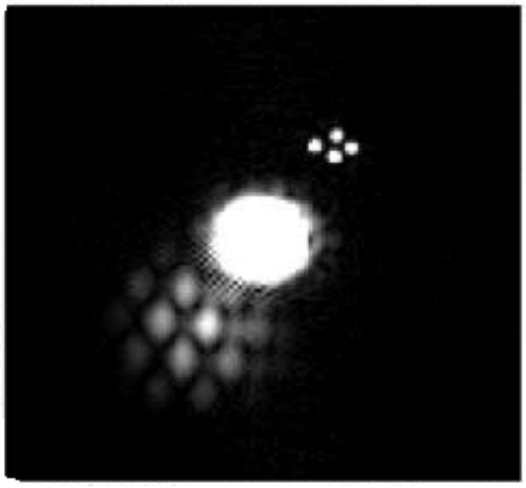

Figure 16b: Digital hologram recorded with amplitude reconstruction.

The current major drawback was due to the size of the pixel pitch of the available thermal cameras which is rather large compared to what would be optimal and possible with analogue films. However, being the infrared laser, the wavelength was fifteen times longer than the average visible light wavelength. Furthermore, a wider view angle and shorter acquisition distances are achievable.

Images of some slits of the United States Air Force (USAF) target were acquired with the interferometric transmission mode as shown in figure 13. A low powered laser and pyrocam III thermal camera were used. By means of a ZnSe lens, with 1- inch focal length, the interferogram was acquired and the amplitude reconstruction of 2.2 squares, a few millimetres area of the target as shown in figure 17 and 18.

Digitized by UCC, Library

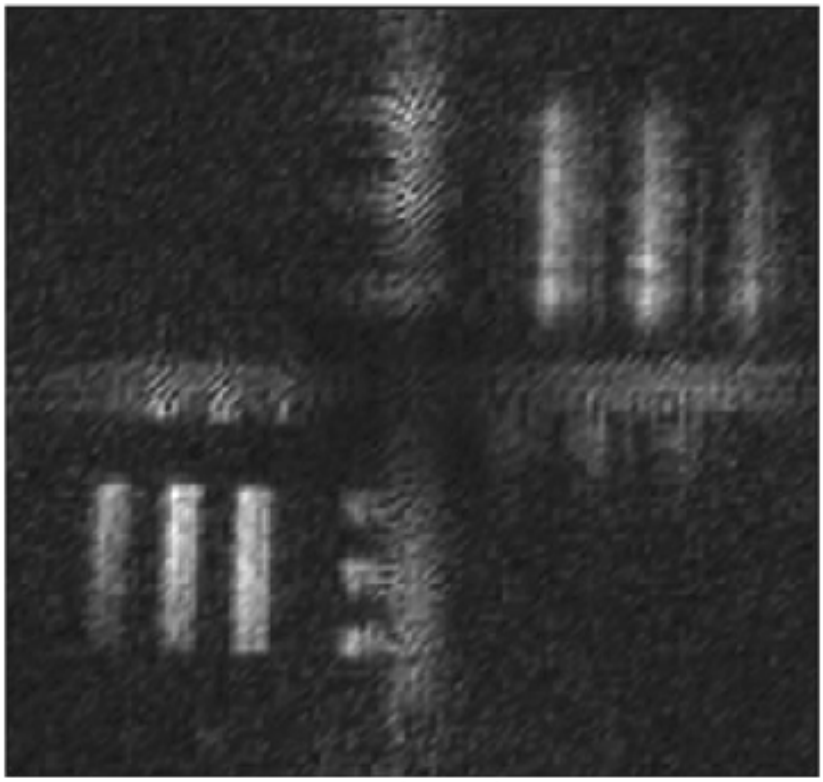

Figure 17: The bottom left corner shows the amplitude reconstruction of 1-2 Slits (2.24 line pair/mm) of United State Air Force (USAF) test target

Digitized by UCC, Library

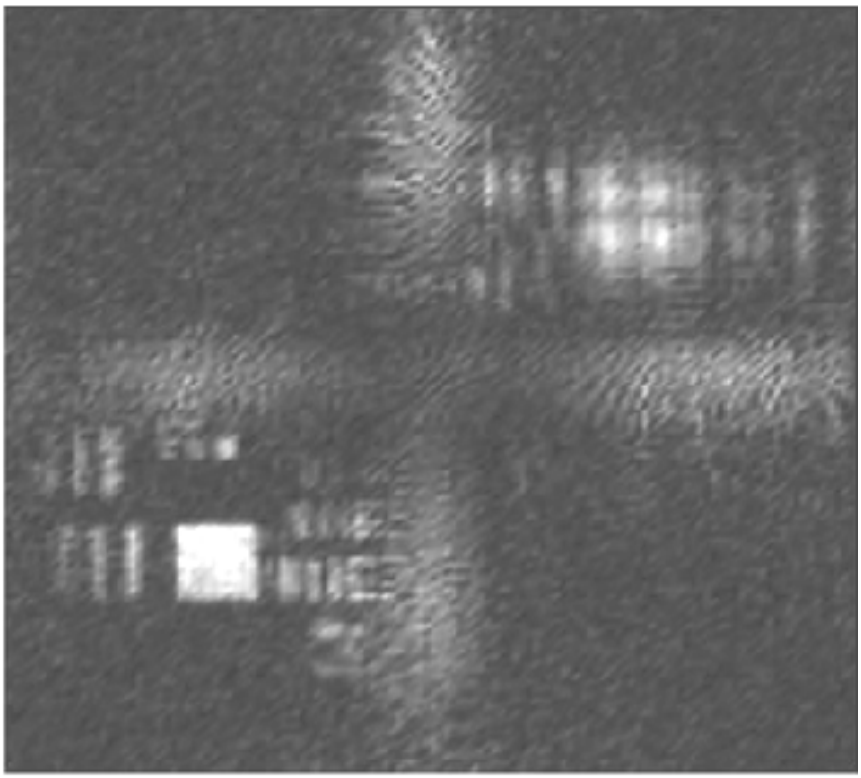

Figure 18: The bottom left corner shows the amplitude reconstruction of 2.2 squares (4.49 line pair/mm) of United States Air Force (USAF) test target.

The background noise has been reduced in figure 16 so that the image is much cleaner than those found in figure 17. A Hanning window has been used to filter the original hologram. The dimensions of the window have to be large enough to avoid the filtering out of the high- frequency information from the object. The choice of too small a size of Hanning window will cause the reconstructed image to be blurred. This effect can be clearly seen in figure 17. Comparing figure 18 and figure 19 carefully, the numbers and the finest bars on the target pattern suggest that some high- frequency information has been lost by filtering process.

Digitized by UCC, Library

This method can also be applied to large opaque objects with a rough surface, but the loss of high- frequency information is more obvious in the case of the well-defined test target. The possibility to obtain reconstructions in digital holography of both amplitude and phase can be used as a quantitative topographic method (De Nicole et al., 2008). Figure 19a shows the interferogram recorded using the off-axis configuration and figure 19b the amplitude reconstruction of the image of the letters inscribed in the first Aluminium block without padding.

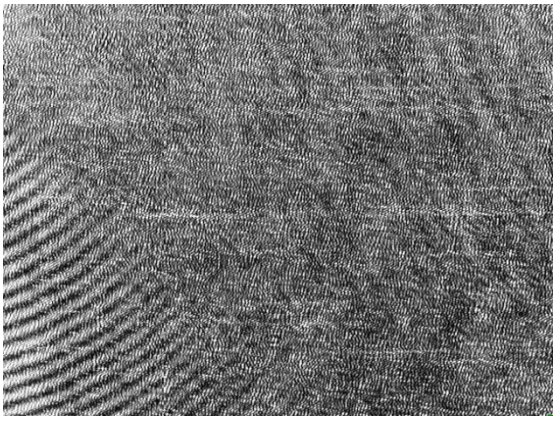

Figure 19a: The interferogram recorded of the letters 'ROU''

Amplitude images were reconstructed from the digitised infrared holograms according to the Fresnel's transform. In figure 19b, 21b the size of the reconstruction pixel was $213\ \mu m \times 213\ \mu m$.

Digitized by UCC, Library

Figure 19b: Amplitude reconstruction of 'ROU'without padding operation.

Figure 19b, 22b shows the corresponding reconstructions without zero padding operations. The size becomes 103 μm × 103 μm which indicates that the resolution was recovered and improved. This can be observed by comparing with the reconstructed images shown in figure 20b and 22b. In this experiment, the object plane was at a distance d=250 mm from the recording plane. To compensate for the loss of resolution with increasing reconstruction distance, d zero padding operation was applied. Before padding as in figure 20b, the 85 μm × 85 μm pixels yielded an image plane pixel size of $\Delta x \times \Delta y$=213 μm× 213 μm.

The digitised hologram, which is a matrix $N \times N$, was then padded with zeros to achieve a larger matrix $N \times N = 256 \times 256$points. The resulting array has a reconstruction pixel of size $x \times y = 103\mu m \times 103\mu m$ at a distance $d = 250\ mm$, this process increases the number of 2D-FFT points. This leads to changing the period, while the spatial sampling rate of the digitised hologram remains constant as shown figure 20b. Similarly, the spatial spectral components

Digitized by UCC, Library

of the reconstructed images, originally hidden from view can be shifted to points where it can be observed as shown in figure 21b.

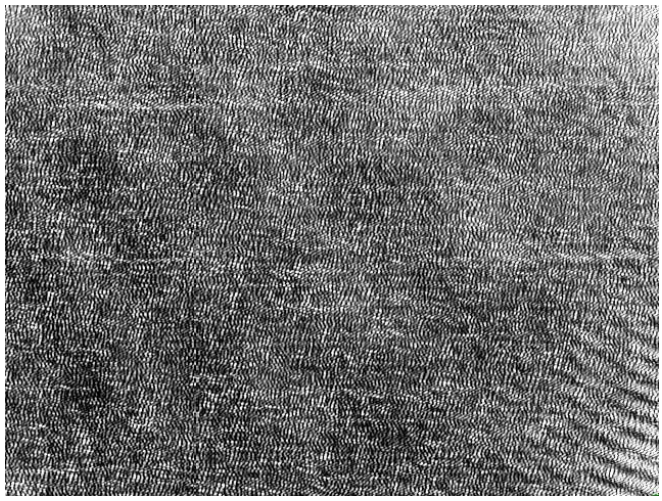

Figure 20a: The interferogram recorded from the aluminium block with 'ROU'' inscription.

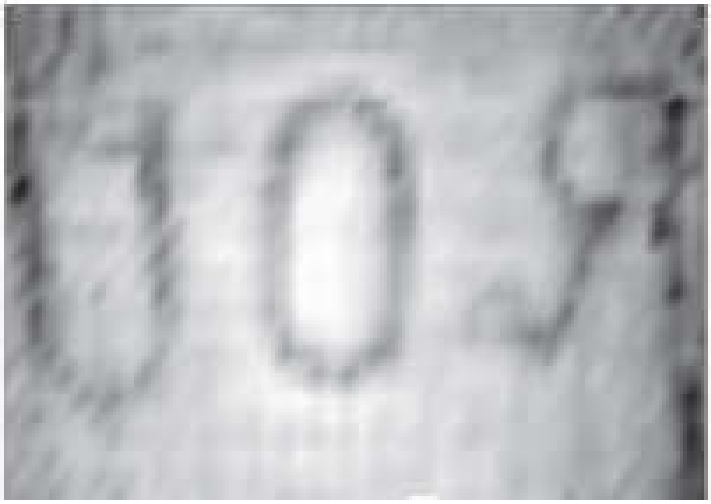

Figure 20b: Amplitude reconstruction of the letters ''ROU'' after zero padding operation

Digitized by UCC, Library

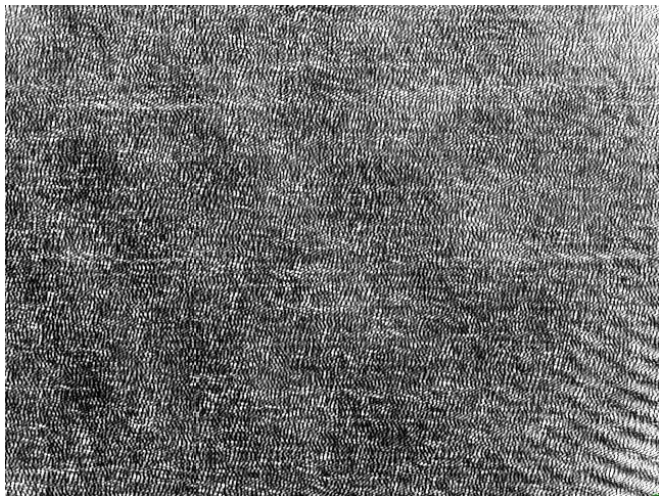

Figure 21a: The interferogram recorded from the aluminium block with 'XOU' inscription.

Figure 21b: Amplitude reconstruction of the letters ''XUO'' after zero padding operation.

Digitized by UCC, Library

In the same way, aliasing created by the use of 2D–FFT resulted from spreading of the spectral components away from the actual frequency leading to undesirable modification of the reconstructed image as shown in figure 22b. Furthermore, aliasing occurs during the numerical reconstruction process, if the distance was less than the minimum object-to-hologram recordable distance; $d_{min} = \frac{N \quad \xi^2}{\lambda}$. This tends to increase the matrix N of the window function leading to an increase in d_{min}. The condition $d > d_{min}$ sets the maximum number of samples with zeros at the end of the digital holograms for a given hologram recording distance. Using an infrared wavelength $\lambda = 10.6\ \mu m$, the condition was satisfied since $d_{min} = 241\ mm$ for $N = 256$. The reconstruction was obtained with a reference beam of the form $R(\xi, \eta) = \exp[i(k_x \xi + k_y \eta)]$, where k_x and k_y of the wave vectors were adjusted to centre the image in the reconstruction plane.

Digitized by UCC, Library

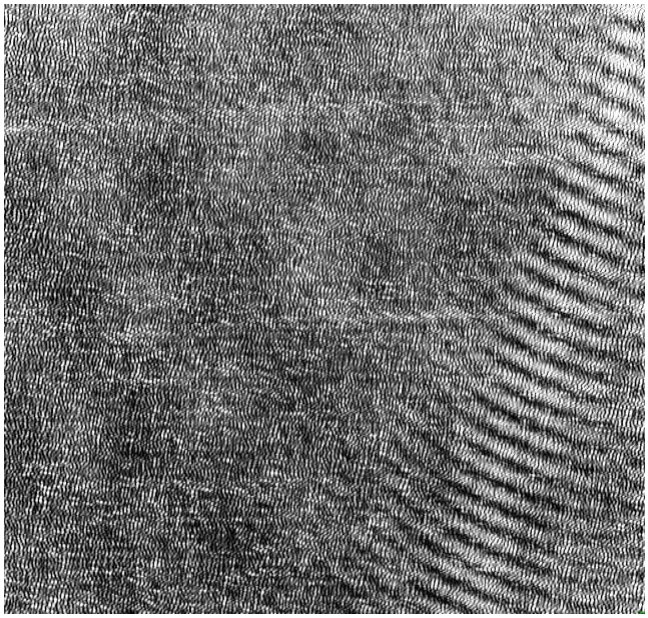

Figure 22a: The interferogram recorded from the aluminium block with 'XUO' inscription without padding.

The results demonstrate that IR digital holography can be a viable method to obtained the phase and amplitude reconstructions. The method proposed for improving the accuracy of the reconstruction, based on a zero padding operation compensates for the loss of resolution at longer wavelengths and low spatial resolution of the pyroelectric camera array.

Digitized by UCC, Library

Figure 22b: The amplitude reconstruction of the letters'XUO'without padding operation

Table 3 shows a summary of the objects (materials), size and the distance from the sensor.

Table 3: The sizes of objects and their distance from the camera

Material/ Object	Object size	Distance from camera
Opaque Aluminium (XUO)	3 mm	250 mm
Opaque Aluminium (UOR)	4 mm	250 mm
A disk	(Radius) 25.4 mm	250 mm
Steel plate	700 μm (diameter)	400 mm

Digitized by UCC, Library

The results of the transmission configuration of the concentric circular shaped tracks inscribed in the Aluminium disc are better resolved as a result of padding operation; as shown in figures 23a and 23b.

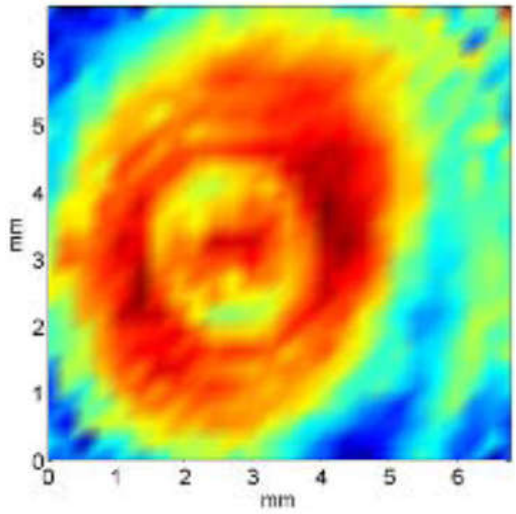

Figure 23a: A 2D reconstruction of the phase images of the concentric circular shaped tracks inscribed on the aluminium disc without padding. (Transmission configuration)

In figure 23b; with zero padding operation, the concentric circular shaped steel disk are visibly clear and fine than in figure 23a. On the other hand, in figures, 23a,24a and 24c, the phase image reconstruction from the disked shaped object displays some amount of roughness of the corresponding reconstruction without padding operation. Figure 23a,23b and 24a,24c,and 24d shows the 2D and 3D reconstructed phase images of the aluminium disc with and without padding in transmission/ reflection configurations.

Digitized by UCC, Library

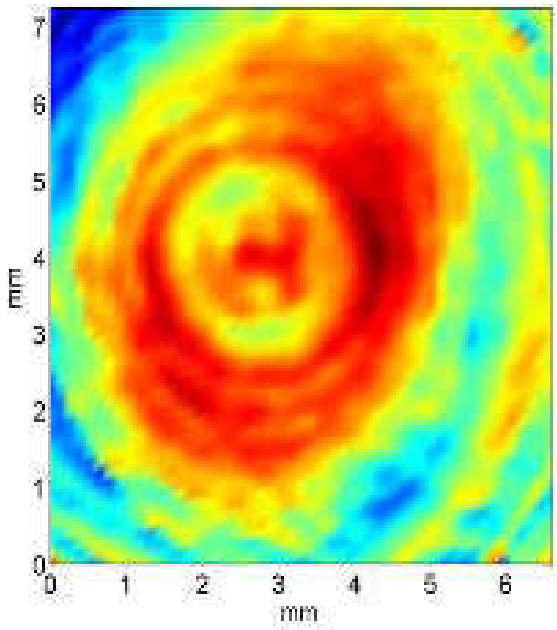

Figure 23b: A 2D reconstruction of the phase images of the concentric circular shaped tracks inscribed on the aluminium disc with zero padding. (Transmission configuration).

However, in the off-axis reflection configuration, the results obtained were in 3D perspectives.

Digitized by UCC, Library

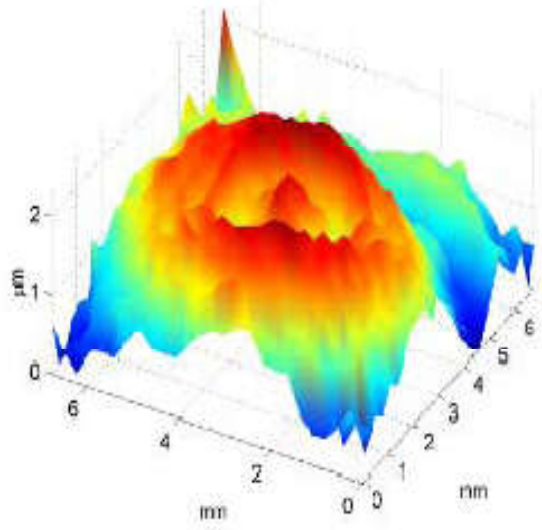

Figure 24a: A 3D perspective of the reconstructed surface profile of the concentric circular shaped tracks inscribed on the aluminium disc without padding.

It will be observed that the circular shaped tracks inscribed in the Aluminium disc are better resolved with zero padding operation as in figure 24b and 24d. This is because of the large angle between the object and reference beams.

Digitized by UCC, Library

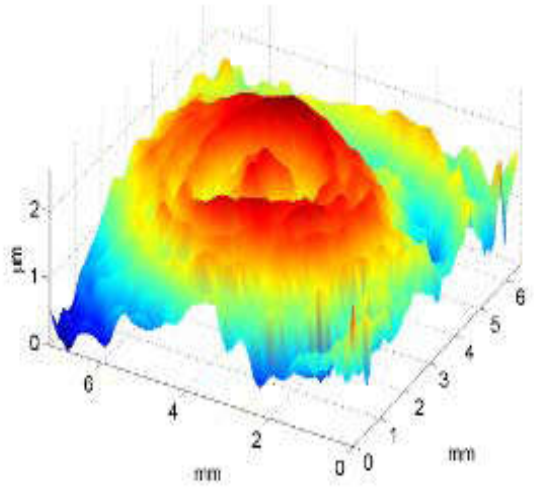

Figure 24b: A 3D perspective of the reconstructed surface profile of the concentric circular shaped tracks inscribed on the aluminium disc with zero padding.

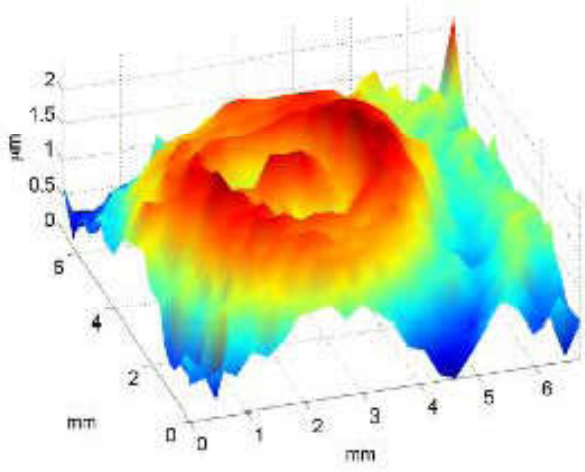

Figure 24c: A 3D perspective of the reconstructed surface profile of the concentric circular shaped tracks inscribed on the aluminium disc without padding.

Digitized by UCC, Library

Also, in figure 24b and 24d shows noticeable smoothness of the corresponding image reconstruction with zero padding operation. This is as a result of the fine interference fringes (interferogram), which are closer to each other.

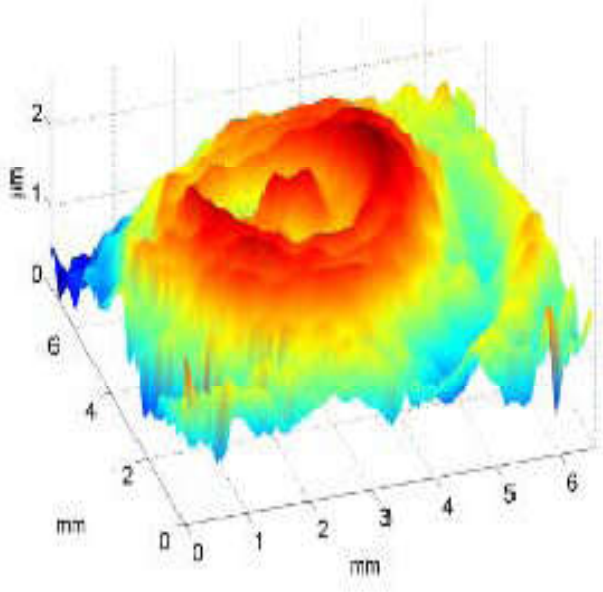

Figure 24d: A 3D perspective of the reconstructed surface profile of the concentric circular shaped tracks inscribed on the aluminium disc with zero padding.

The plane reference wave interferes with the object wave at small angles (≤ 0.5) as required by the sampling theorem. In the experiments, the object plane was at different distances from the recording plane. This was due to the fact that at certain distances, the image will be blurred. So for good fringe contrast, the

Digitized by UCC, Library

reconstruction distances which lead to sharp image formation were varied. In order to compensate for the loss of resolution with increasing reconstruction distance d, zero padding operation was used. Figure 25 and figure 26 shows the reconstruction of one and two euro coins; which displayed some of the 3D feature on the surface of the coin. This was as a result of the 50% reflection from the beam splitter, leading to good fringe contrast.

(a) (b)

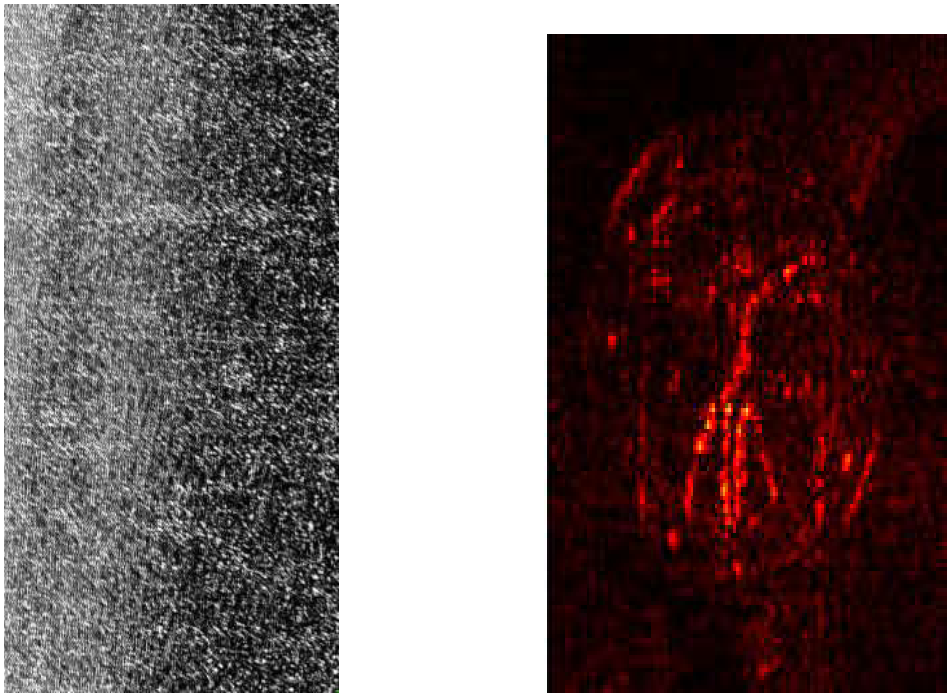

Figure 25: (a) Hologram of the one (1) euro coin using the off-axis reflection configuration and (b) the amplitude reconstruction of one (1) euro coin

Digitized by UCC, Library

(a) (b)

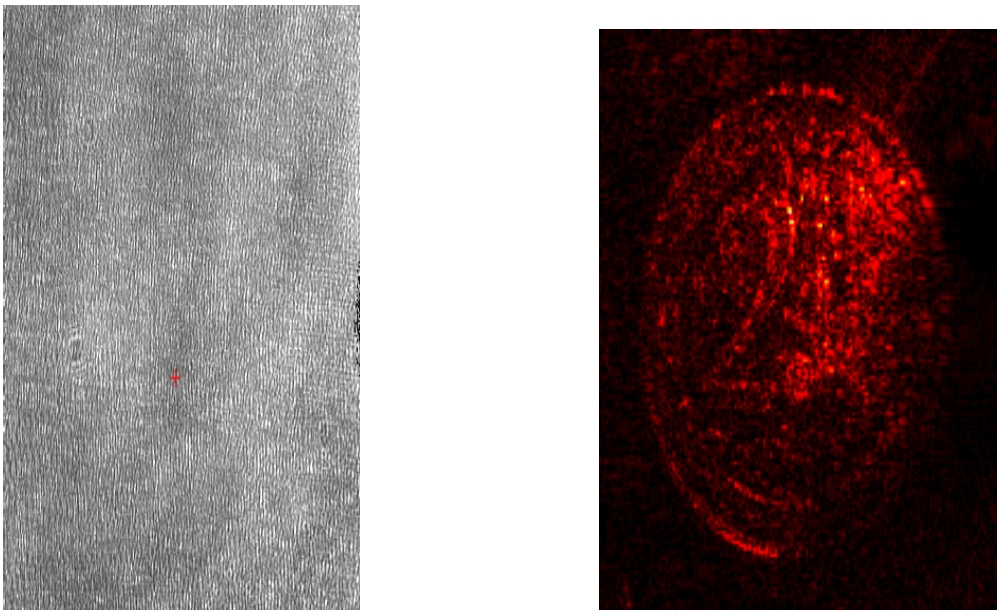

Figure 26: (a) Hologram of the two (2) euro coin using the off-axis reflection configuration and (b) Amplitude reconstruction of the two (2) euro coin.

Similarly, figure 27 shows the reconstruction of a lens mount. A more complex configuration as shown in plate 6 was reconstructed.

Digitized by UCC, Library

(a) (b)

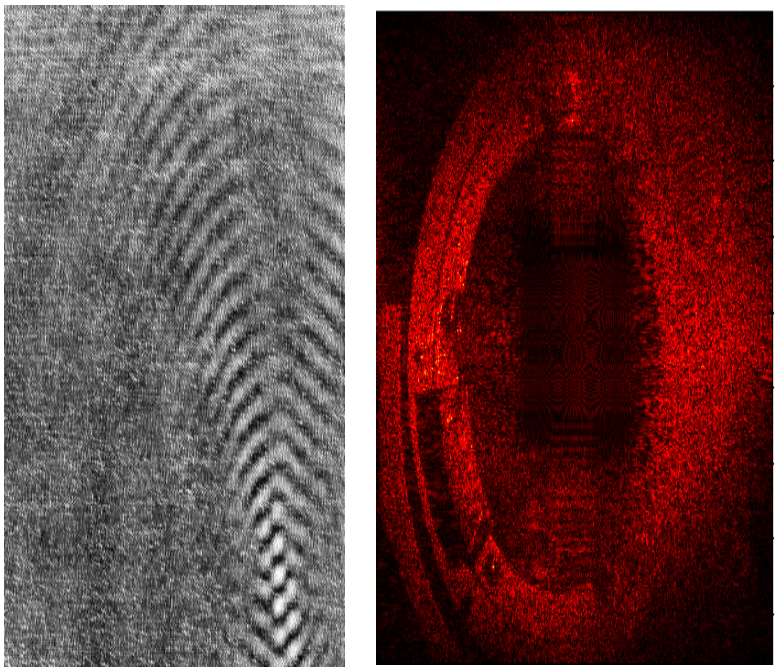

Figure 27: (a) Interferogram recorded for the lens mount using the off-axis configuration and (b)Amplitude reconstruction of the lens mount.

The hologram of the two objects was noticeably different as shown in figure 28 and figure 29. Using appropriate distance in the reconstruction formula, we could focus either of the two.

Digitized by UCC, Library

(a) (b)

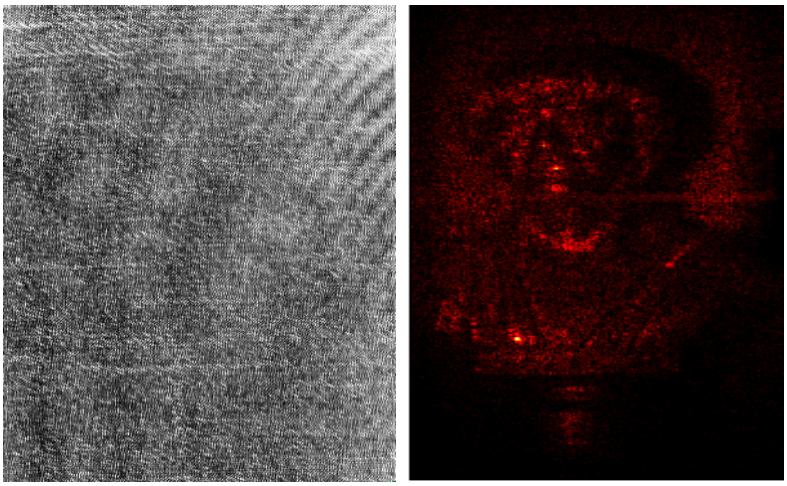

Figure 28:(a) Hologram of Traiano recorded using off-axis reflection configuration and (b)Amplitude reconstruction of Traiano.

The results we had depend on the spatial filter used in the numerical reconstruction. Using the kernel high pass filter, we had quite a degradation of the original signal, since such a filter affects a large set of lower spatial frequencies leading to a reduction in intensity of the inner parts of the hologram. On the other hand, using a band pass filter we could preserve all such levels, affecting only the lowest frequencies and therefore basically only the zero order.

Digitized by UCC, Library

(a) **(b)**

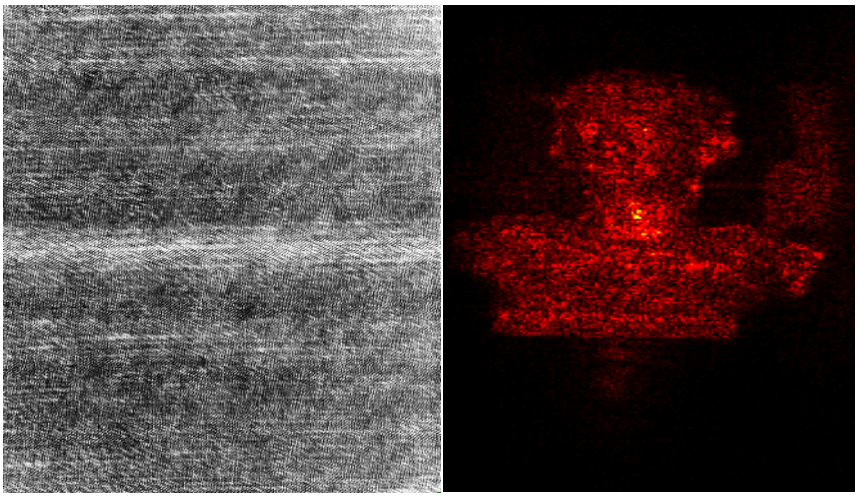

Figure 29: (a) Hologram of Augusto recorded using the off-axis reflection configuration and (b) Amplitude reconstruction of Augusto.

The two metal bronze which represents Augusto and Traiano were reconstructed without padding and using a high pass filter, Augusto was in focus as in figure 29. The metal bronze object on the right side, which is farther from the detector had a scattered surface as illustrated in figure 30b.

Digitized by UCC, Library

(a) (b)

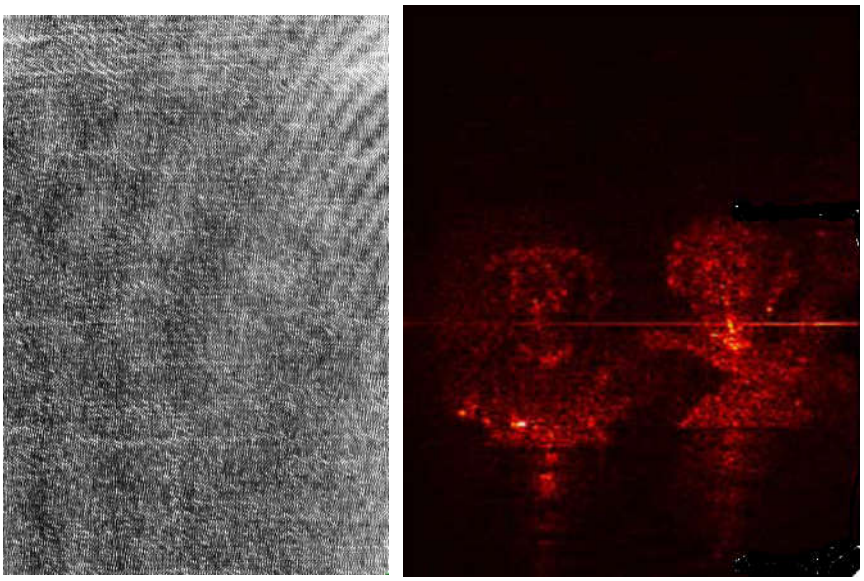

Figure 30: (a) Hologram of the two metal objects recorded using the off-axis reflection configuration and (b) Amplitude reconstruction of two metal objects with Augusto in focus.

Again with padding, using high pass filter, we could focus Augusto, the one on the right side which was farther from the detector had a highly scattered surface as shown in figure 30. The process was repeated using band pass filters and the same results were obtained. The real and unsharp virtual images of the object are separated because of the off-axis geometry. Also, it can be observed that the virtual image is in focus and the real image was blurred. This clearly shows that the reconstructed images suffer particularly from the bright dc-term which affects the quality of the reconstructed image. Furthermore, the image reconstructed wave- front field was aberrated and it appears that a noticeable astigmatism was present, probably due to the collimator lens used in the hologram

Digitized by UCC, Library

recording system. If objects with larger dimensions have to be recorded, the recording distance increases up to several meters and this is not feasible in practice. To overcome this a negative lens in the object arm (between the object and camera), this is to generate a reduced virtual image of the object distance given in the lens equation. The wave field emerging from this virtual image was superimposed with the reference wave and the resulting hologram recorded. This configuration enables us to obtain a larger, about twice, the field of view in relation to the previous set up as shown in figure 30 and figure 31.

(a) (b)

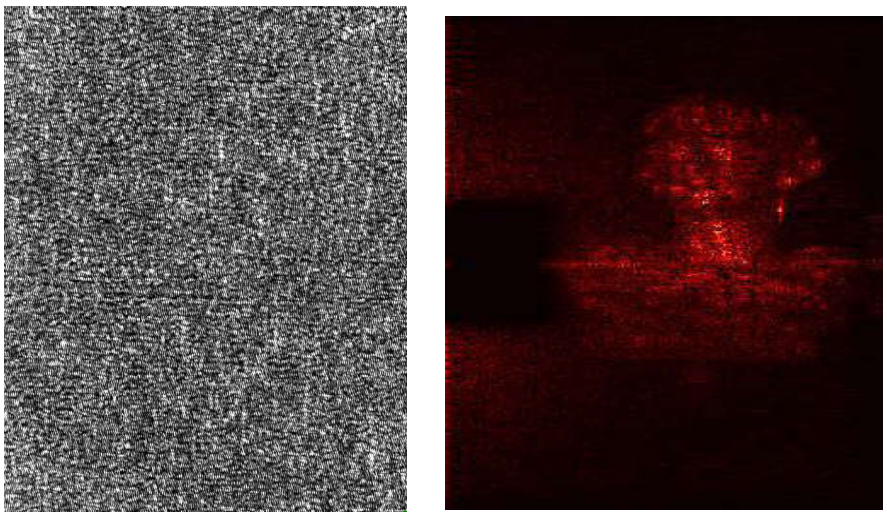

Figure 31:(a) Interferogram recorded using the off-axis reflection configuration and (b) Amplitude reconstruction of August without negative lens

Digitized by UCC, Library

(a) (b)

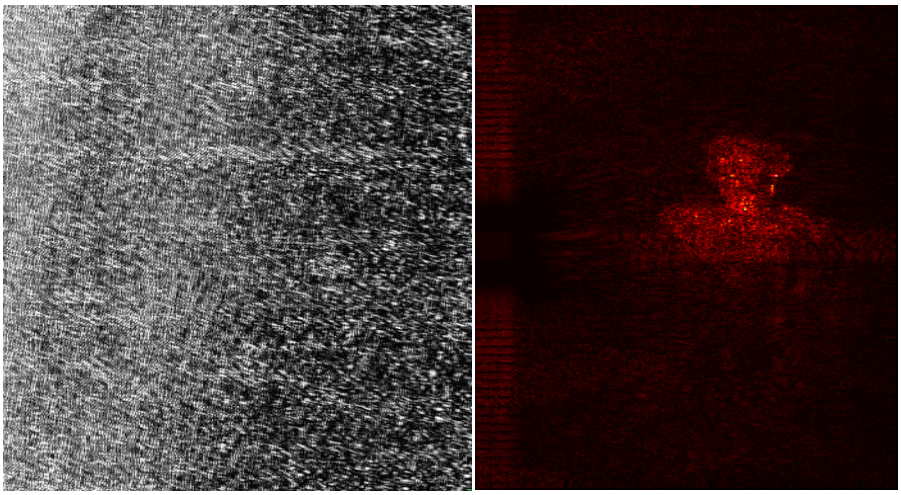

Figure 32: (a) Interferogram recorded using the off-axis configuration and (b) Amplitude reconstruction of Augusto with a negative lens

The results of some materials such as Aluminium plate, marble plate and earthenware tree are shown in figures 33- 35. Plate 8 shows an Aluminium plate drilled with holes and its amplitude reconstruction in figure 35. The length of the Aluminium plate was 100 cm which was reconstructed as shown in figure 33 without padding operation. This further shows that 3D imaging with long infrared wavelength has a larger field of view which is an advantage.

Digitized by UCC, Library

(a) (b)

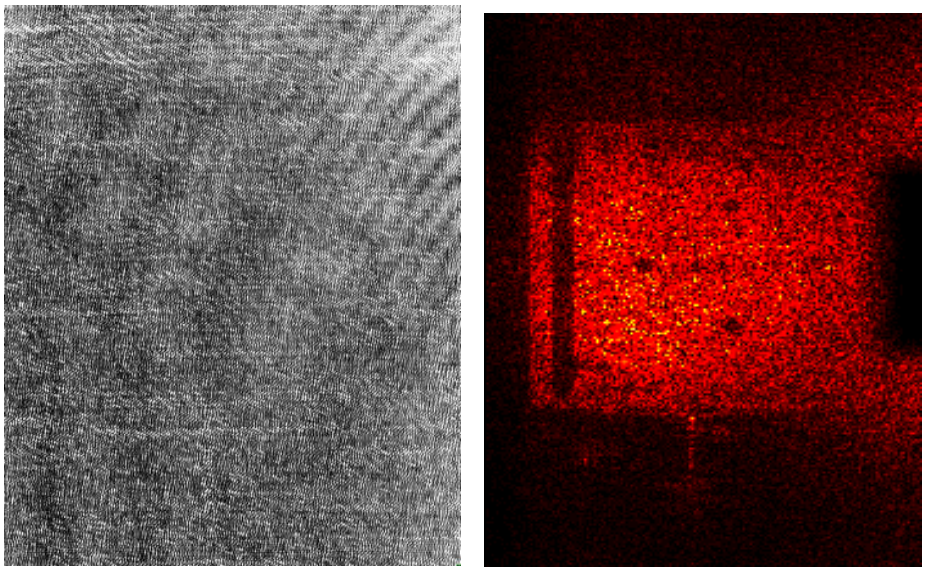

Figure 33: (a) Interferogram recorded using the off-axis reflection configuration and (b) Amplitude reconstruction of Aluminium plate.

(a) (b)

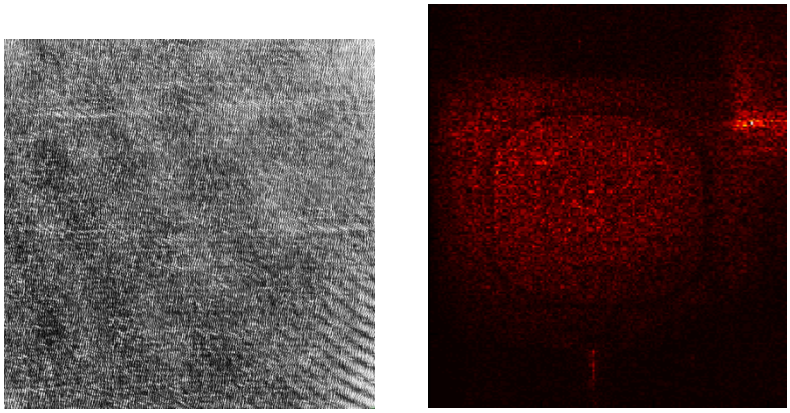

Figure 34: (a) Interferogram recorded using the off-axis reflection configuration and (b) Amplitude reconstruction of a marble plate

Digitized by UCC, Library

(a) (b)

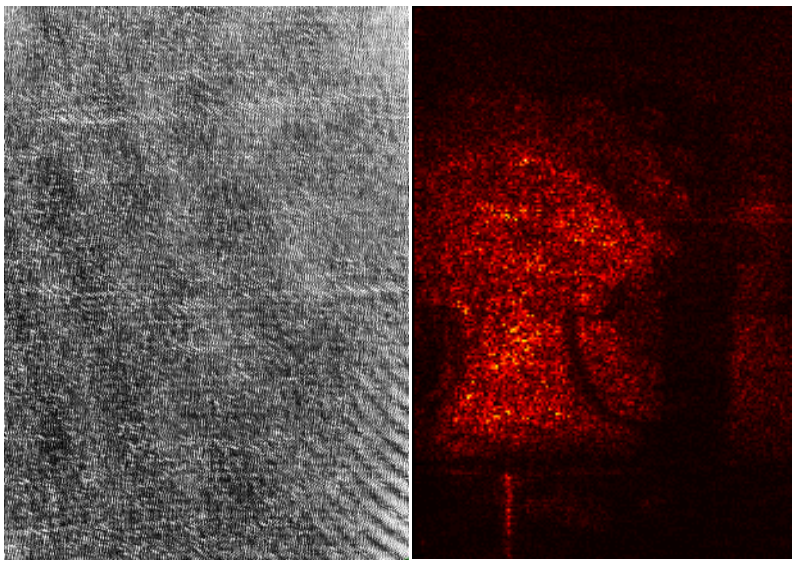

Figure 35: (a) Interferogram recorded using the off-axis reflection configuration and (b) Amplitude reconstruction of earthenware tree

The same configuration was used to record the interferogram of a bronze statue, 30 cm high as shown in plate 7. The results of numerical amplitude reconstruction of a bronze statue are shown in figure 36 and 37.

Digitized by UCC, Library

(a) (b)

Plate 8: (a) Interferogram recorded using the off-axis reflection configuration and (b) Aluminium plates with holes drilled

Digitized by UCC, Library

(a) (b)

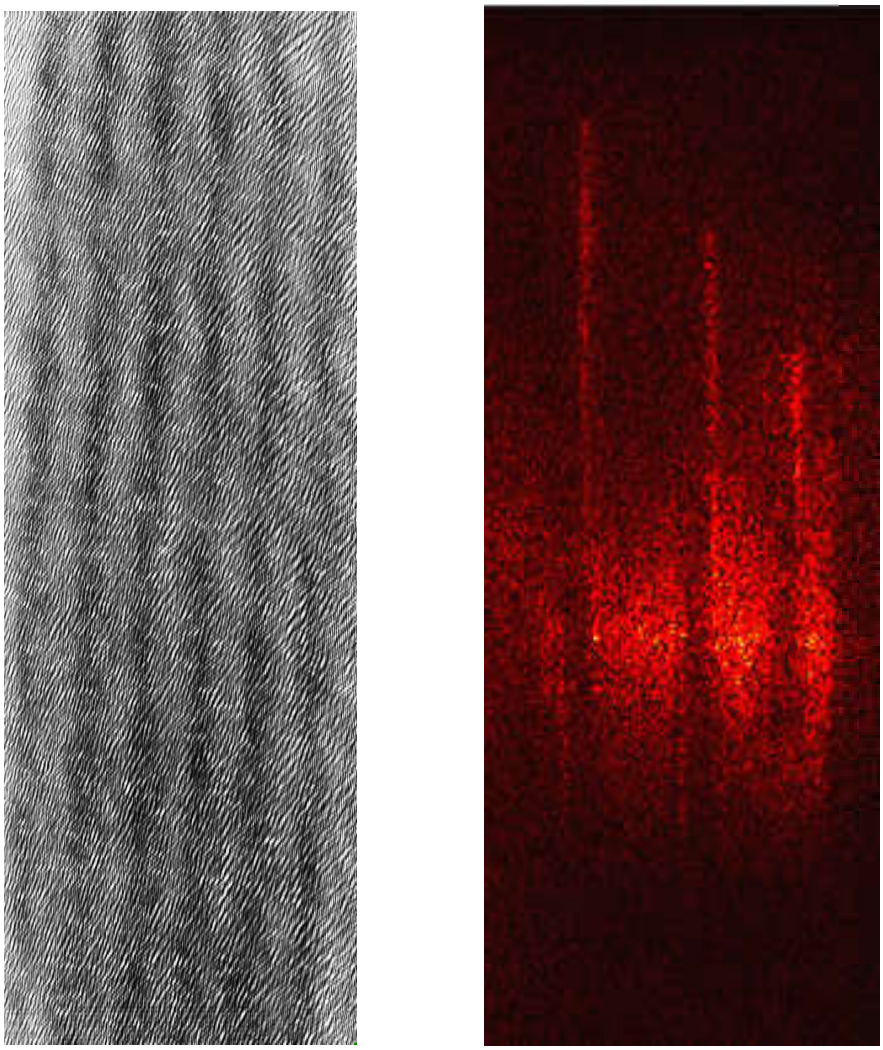

Figure 36: (a) Interferogram recorded in the off-axis reflection configuration and (b) Amplitude reconstruction of the Aluminium plate drilled with holes

Digitized by UCC, Library

(a) (b)

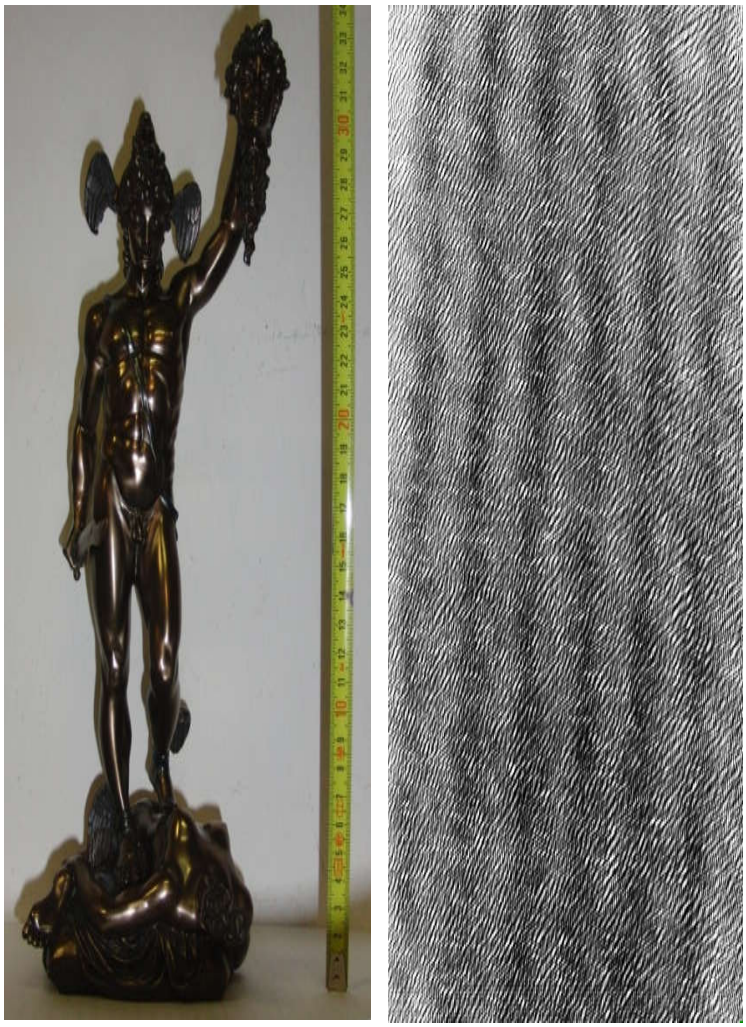

Plate 9: (a) A bronze sculpture and (b) the recorded interferogram.

Digitized by UCC, Library

(a) (b)

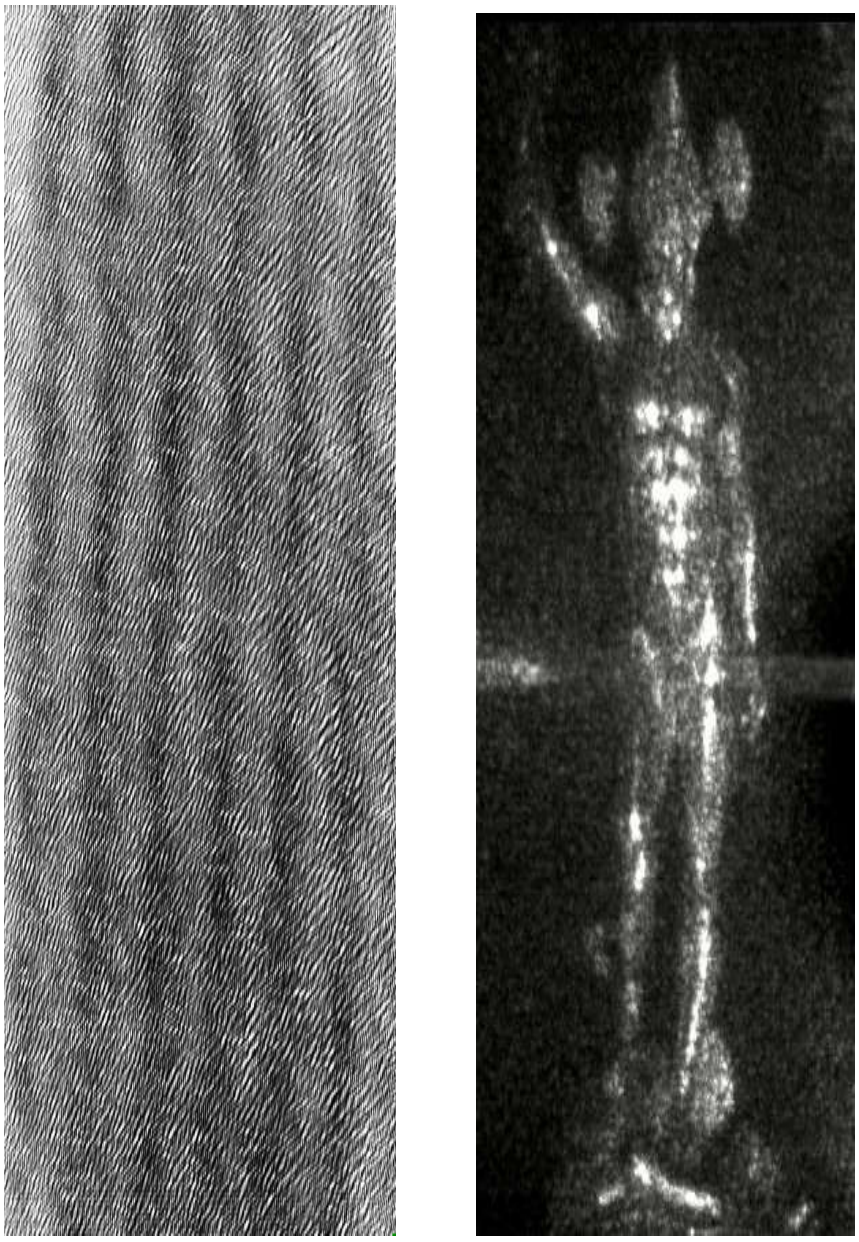

Figure 37: (a) Interferogram recorded of the Bronze sculpture using the off-axis configuration and (b) Amplitude reconstruction of the Bronze sculpture using double beam

Digitized by UCC, Library

(a) (b)

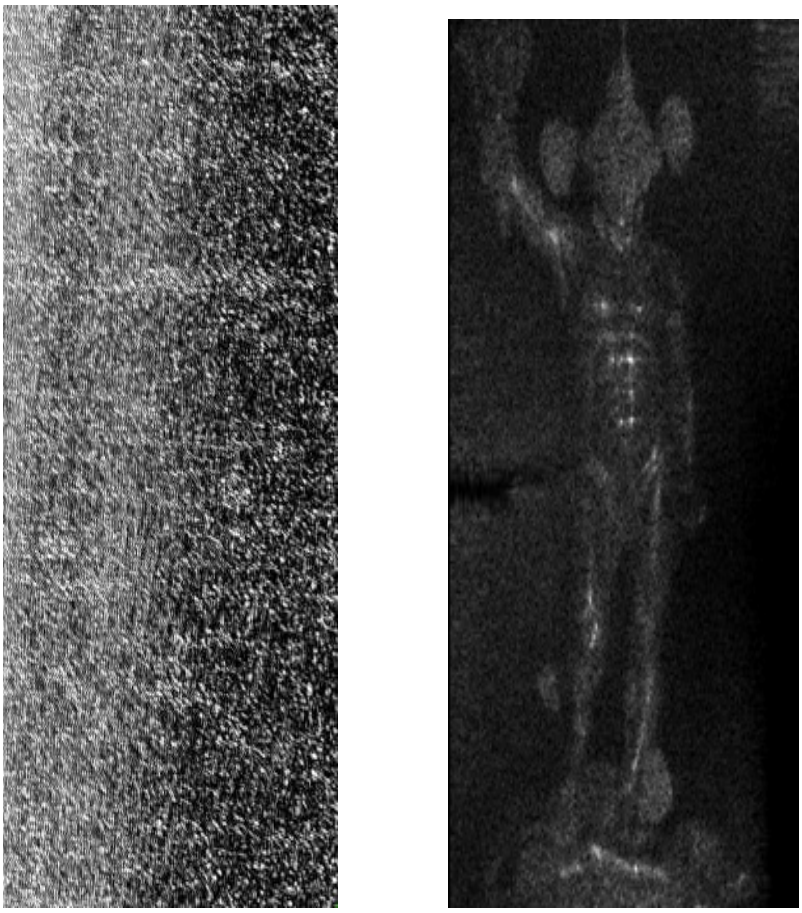

Figure 38: (a) Interferogram recorded of the Bronze sculpture using the off-axis reflection configuration and (b) Amplitude reconstruction of Bronze sculpture using a single beam.

Whenever large object recording and reconstruction is required, digital holography with CO_2 the laser has many advantages, with respect to digital holography invisible region (Allaria et al., 2003).

A long wavelength radiation has a lower sensitivity to sub-micrometric vibrations and this peculiarity provides a higher fringe visibility when large sample are

Digitized by UCC, Library

investigated. Plate 10, the human mannequin and the interferogram recorded using the off-axis reflection configuration.

(a) (b)

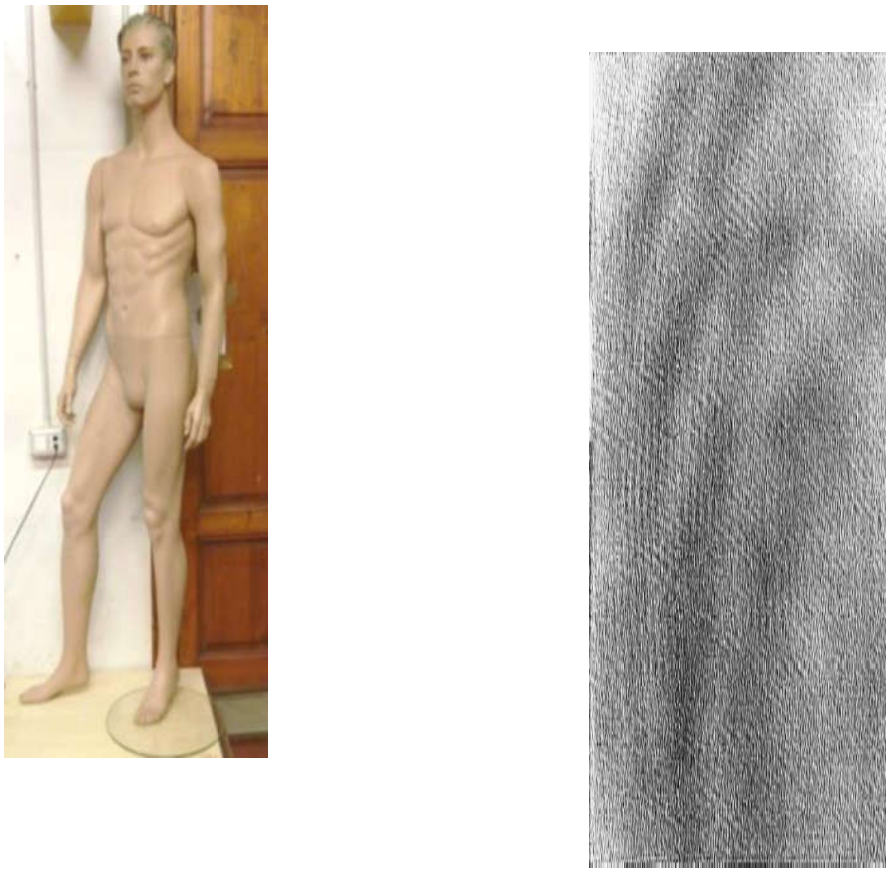

Plate10: (a) The human size mannequin and (b) Interferogram recorded

Furthermore, the high output of CO_2 lasers allowing irradiating more efficiently and uniformly on the surface of large samples (Pedrini et al., 1996). Also, with long wavelength, a human size mannequin was reconstructed, as shown in figure 39. Finally, with longer wavelength, it was possible to use larger

Digitized by UCC, Library

angles and ultimately, smaller distances between the object and the recording device.

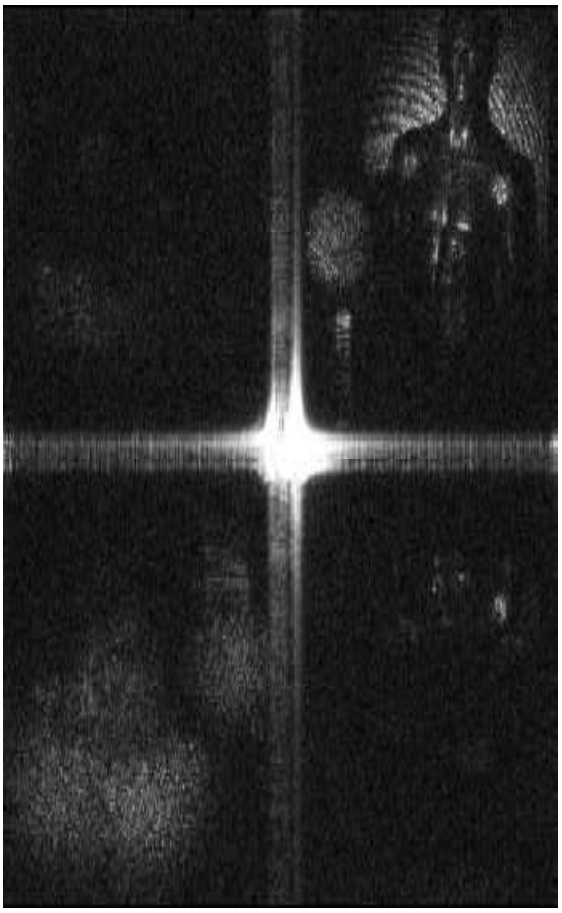

Figure 39: Amplitude reconstruction of the human mannequin using the off-axis reflection configuration.

Digitized by UCC, Library

CHAPTER FIVE

SUMMARY, CONCLUSION AND RECOMMENDATION

This chapter was organised into three main parts namely Summary, Conclusions and Recommendations. However, a summary of the entire thesis would be given first before conclusion and finally recommendations.

SUMMARY

In summary, within the course of the research that formed the thesis, a comprehensive experimental model has been developed to investigate three-dimensional imaging with long infrared digital holography. This model was based on Fresnel's approximation and the convolution approach to numerically reconstructing three-dimensional images of large objects. In addition, applying 3D imaging with long infrared digital holography to microscopy, this technology has a great potential in diverse research areas such as metrology and quality control of micro-components and cell observation in Biology. The maximum size of the objects that can be imaged with long IR wavelength is proportional to the source wavelength at any fixed target-sensor distance. The advantages of 3D imaging with long IR wavelength are;

i. A long wavelength IR radiation has lower sensitivity to sub- micrometric vibrations; this quality provides a higher fringe visibility when large samples are investigated.
ii. The high output power of CO_2 lasers allowing irradiating more effectively and uniformly the surface area of large samples.

Digitized by UCC, Library

iii. It is possible to use larger angles and smaller distance between the object and the recording device.

iv. Infrared digital holography has also been applied for large object investigations.

v. The quantitative results from CO_2 a laser operating at $10.6\ \mu m$ for the reconstruction of objects with accurately known dimensions can be used as a benchmark to evaluate the effects caused by different processing methods and establish a standard to optimize the processing in digital holographic applications.

vi. No wet-chemical or other processing of holograms

vii. Lensless imaging, that is, no aberrations by imaging devices.

Disadvantages of 3D imaging with long IR wavelength are;

i. The lower spatial resolution of the infrared sensor arrays compared to those in the visible region is limiting factor to accurate numerical wave front reconstruction for the digitized interferogram.

ii. Rather large pixel pitch, which would seriously limit the achievable spatial resolution, coupled with very limited number of pixels on the detector.

Digitized by UCC, Library

CONCLUSION

In conclusion, a 3D imaging with long infrared digital holography at 10.6 μm, was tested both in transmission and reflection configurations. The results demonstrate that IR digital holography can be a viable method to obtain phase and amplitude reconstructions at long wavelength. The off-axis reflection configuration was an effective configuration for separating the zero order and twin image; the large angle between the reference beam and the object beam led to this separation of the diffraction orders. Transmission configuration makes use of the full pixel count in forming the holographic image but the zero order and the twin image terms are superimposed on the image. The spatial resolution of the reconstructed image was proportional to the wavelength and to the distance between object and sensor, which varies inversely to the lateral dimensions of the sensor. Large object reconstruction was possible due to the use of negative lenses which generate a reduced virtual image of the object. Speckle noise was unavoidable and very disturbing in digital holography. Long infrared wavelength in the off-axis reflection configuration has the potential to be a promising solution to the problem of large object measurement.

Digitized by UCC, Library

RECOMMENDATIONS

Research work presented in this thesis on the 3D imaging with long infrared digital holography opens up a range of possibilities for further research in this area. Briefly, these possibilities are:

i. This work could be done using optical holographic 3D display for terahertz imaging.
ii. The results obtained in the Mid- IR could be extended to the THz domain.
iii. The CO_2 laser used in the investigation can be replaced with Quantum Cascade laser (QCL) for further investigation.
iv. To investigate the influence of the bit depth of the CCD camera in digital holography.

Digitized by UCC, Library

REFERENCES

Abramson, N. (1976). Holographic contouring by translation. *Applied Optics, 15(4)***,** 1018-1022.

Abramson, N. (1983). Light-in-flight recording: High- speed holographic motion pictures of ultrafast phenomenon. *Applied Optics,* 22(2), 215-232

Abramson, N. (1984a). Light-in-flight recording 2: Compensation for the limited speed of light used for observation. *Applied Optics*, 23(10), 1481-1492

Abramson, N. (1984b). Light-in-flight recording 3: Compensating for optical relativistic effects. *Applied Optics*, 23(22), 4007-4014.

Abramson, N. (1985). Light-in-flight recording 4: Visualizing optical relativistic phenomena. *Applied optics*,24(20), 3323-3329.

Allaria,E.,Brugioni,S.,DeNicola,S.,Ferraro,P.,Grilli,S.,&Meucci,R.(2003).Digital Holography at 10.6 micron. *Optics Communications*, 215(4),257-262.

Amadesi, S., Gori, F., Grella, R., & Guattari, G. (1974). Holographic methods for painting diagnostics. *Applied Optics***,** 13(9)**,** 2009-2013.

Baez, A. V. (1952). Study in diffraction microscopy with special reference to X-rays. *JOSA,* 42(10)**,** 756-762.

Beaulieu,R., Lessard,R.A., Cormier,M., Blanchard,M & Rioux,M(1978). Pulsed IR holography on Takiwax films. *Applied Optics* 17(22), 3619

Beaulieu,R.M & Lessard, R.A.(1997). Review of recording media for holography at 10 μm. In *electronic Imaging '97* (pp.298-305). International Society for Optics and Photonics.

Bragg, W. L. (1939). A new type of 'X-ray microscope. *Nature,* 143**,** 678.

Digitized by UCC, Library

Bragg, W. L. (1942). The X-ray microscope. *Nature,* 149(3782)**,** 470-471.

Bragg, W. L. & Rogers, G. L. (1951). Elimination of the unwanted image in diffraction Microscopy. *Nature,* 167**,** 190-191.

Brooks, R. E., Heflinger, L. O. & Wuerker, R. F. (1965). Interferometry with a holographically reconstructed comparison beam. *Applied Physics Letters,* 7(9)**,** 248-249.

Brown, B. R. & Lohmann, A. W. (1966). Complex spatial filtering with binary masks. *Applied Optics,* 5(6)**,** 967-969.

Burch, J. M., Huggins, E. W., Barell, H., Mckeown, P. A., Lake, H. A., ... & Smith, B.(1965). Report and discussion on: ‘’The application of lasers in production engineering’’. (1965). *The Production Engineer, 9(*44)**,** 431-442 .

Bruck, Y. M., & Sodin, L. G. (1979). On the ambiguity of the image reconstruction problem. *Optics Communications*, *30*(3), 304-308.

Bryngdahl, O. & Wyrowski, F. (1990). Digital holography: computer- generated holograms. *Progress in Optics,*28, 1-86.

Calixto, S. (1988). Infrared recording with gelatin films. *Applied Optics*, 27(10), 1977-1983.

Chen, F., Brown, G. M. & Song, M. (2000). Overview of three-dimensional shape measurement using optical methods. *Optical Engineering,* 39(1)**,** 10-22.

Chen, C. C., Lee, T. K., & Miao, J. (2007). Phase retrieval from exactly oversampled diffraction intensity through deconvolution. *PHYSICAL REVIEW B Phys Rev B*, *75*, 012102.

Digitized by UCC, Library

Chivian,J.S.,Claytor,R. N & Eden,D.D (1969). Infrared holography at 10.6 μm. *Applied Physics Letters,* 15(4), 123-125

Cloud, Gray L.(1995). *Optical methods of engineering analysis*. Cambridge University press. 269-390.

Collier, R. J., Doherty, E. T. & Pennigton, K. S. (1965). Application of Moire techniques to holography. *Applied Physics Letters,* 7(8)**,** 223-225.

Cuche, E., Marquet, P. & Depeursinge, C. (1999). Simultaneous amplitude-contrast and quantitative phase-contrast microscopy by numerical reconstruction of Fresnel off-axis holograms. *Applied Optics,* 38(34)**,** 6994-7001

Cuche, E., Marquet, P. & Depeursinge, C. (2000a). Spatial filtering for zero-order and twin image elimination in digital off-axis holography. *Applied Optics,* 39(23)**,** 4070-4075

Cuche, E., Marquet, P. & Depeursinge, C. (2000b). Aperture apodization using cubic spline interpolation: Application in digital holographic microscopy. *Opt*ics *Communications,* 182(1) ,59-69.

Decker, G., Herold, H., & Röhr, H. (1972). Holography and Holographic Interferometry with Pulsed High-Power Infrared Lasers. *Applied Physics Letters*, *20*(12), 490-492.

Demetrakopoulos, T. H., & Mittra, R.,(1974). Digital and Optical reconstruction of images from suboptical diffraction patterns. *Applied Optics,*13(3), 665-670.

De Nicola, S., Ferraro, P., Grilli, S., Miccio, L., Meucci, R., Buah-Bassuah, P. K., & Arecchi, F. T. (2008). Infrared digital reflective-holographic 3D shape measurements. *Optics Communications*, *281*(6), 1445-1449.

Digitized by UCC, Library

De Nicola, S., Geltrude, A., Arecchi, F. T., Al-Naimee, K., Locatelli, M., & Meucci, R. (2011). *Infrared holography for wavefront reconstruction and interferometric metrology*. INTECH Open Access Publisher.

Denisyuk, Y. N. (1962). Photographic reconstruction of the optical properties of an object in its own scattered radiation field. *Soviet Physics - Doklady, (vol.*7**,** 543-545)

Dresel, T., Hausler, G. & Venzke, H. (1992). Three-dimensional sensing of rough surfaces by coherence radar. *Applied Optics***,** 31(7)**,** 919-925.

Duadi, H., Garcia, J., Rodrigo, J. A., Margalit, O., Alieva, T., Mico, V., & Zalevsky, Z. (2011). *Digital holography and phase retrieval*. INTECH Open Access Publisher.

Dubois, F., Schockaert, C., Callens, N, & Yourassowsky, C., (2006). Focus plane detection criteria in digital holography microscopy by amplitude analysis. *Optics Express 14(13)***.** 5895-5908.

Ferraro,P., Paturzo,M., Memmolo, P., & Finizio,A.(2009). Controlling depth of focus in 3D image reconstructions by flexible and adaptive deformation of digital holograms. *Optics Letters. 34(18)*, 2787-2789.

Ferraro, P., Grilli, S., Alfieri, D., De Nicola, S., Finizio, A., Pierattini, G., & Striano, V. (2005). Extended focused image in microscopy by digital holography. *Optics express*, *13*(18), 6738-6749.

Digitized by UCC, Library

Ferraro, P., De Nicola, S., Finizio, A., Coppola, G., Grilli, S., Magro, C., & Pierattini, G. (2003). Compensation of the inherent wave front curvature in digital holographic coherent microscopy for quantitative phase-contrast imaging. *Applied optics*, *42*(11), 1938-1946.

Fienup, J. R. (1978). Reconstruction of an object from the modulus of its Fourier transform. *Optics letters*, *3*(1), 27-29.

Fienup, J. R. (1982). Phase retrieval algorithms: a comparison. *Applied optics*,*21*(15), 2758-2769.

Füzessy, Z., Gyimesi, F., Kornis, J., Raczkevi, B., Borbely, V., & Gombkötö,B. (2006). Analogue and Digital Holography: Absolute and Comparative Measurements and Measuring Range Extension (Analoge und Digitale Holografie: Absolute und vergleichende Messungen sowie Messbereichserweiterungen). *tm-Technisches Messen*, *73*(3/2006), 132-141.

Gabor, D. (1948). A new microscopic principle. *Nature,* 161(4098)**,** 777-118.

Gabor, D. (1949). Microscopy by reconstructed wave fronts. In *Proceedings of the Royal Society of London A Mathematical, Physical and Engineering Sciences(vol.* 197**,**No.105 454-487).The Royal Society.

Gabor, D. (1951). Microscopy by reconstructed wave fronts: II. *Proceedings of the Physical Society. Section B,* 64(6),449.

George,N.,Khare,K & Chi, W. (2006). Electronic holography at terahertz and infrared frequencies. In *Proceedings of the Seventh International Symposium on Display Holography*. (pp. 117-119) .River Valley.

Digitized by UCC, Library

Goodman, J. W. & Lawrence, R. W. (1967). Digital image formation from Electronically detected holograms. *Applied Physics Letters,* 11(3)**,** 77-79.

Goodman, J. W., & Gustafson, S. C.(1996). Introdution to Fourier Optics.*Optical Engineering,*35(5), 1513-1513.

Goodman, J. W. (2005). *Introduction to Fourier Optics (Third Edition),* Englewood, Colorado, Roberts & Company Publishers.

Grilli,S.,Ferraro,P.,DeNicola,S.,Finizio,F.,Pierattini,G.&Meucci,R(2001). whole optical wavefields reconstruction by digital holography. *Opics Express, 9(6)*, 294-302.

Groh, G. (1968). Multiple imaging by means of point holograms. *Applied Optics,* 7(8)**,** 1643-1644.

Gyímesi, F., Füzessy, Z., Borbély, V., & Ráczkevi, B. (2009). Analogue difference holographic interferometry for two-wavelength contouring. *Optics Communications*, *282*(2), 276-283.

Haddad, W. S., Cullen, D., Solem, J. C., Longworth, J. W., McPherson, A., Haines, K. & Hildebrand, B. P. (1965). Contour generation by wavefront Reconstruction. *Physics Letters,* 19(1)**,** 10 - 11.

Harrison, R. W. (1993). Phase problem in crystallography. *JOSA A*, *10*(5), 1046-1055.

Hayes, M. H. (1982). The reconstruction of a multidimensional sequence from the phase or magnitude of its Fourier transform. *Acoustics, Speech and Signal Processing, IEEE Transactions on*, *30*(2), 140-154.

Hecht, E., & Zajac, A. (1998). Optics Addison- Wesley. *Reading, Mass,* 301-305.

Digitized by UCC, Library

Izawa, T., & Kamiyama, M. (1969). Infrared holography with organic photochromic films. *Applied Physics Letters,* 15(7), 201-203.

Ji, Z. and Leu, M. C. (1989). Design of optical triangulation devices. *Optics & Laser Technol.,* 21(5)**,** 335-338.

Jones, R., & Wykes, C.(1983) *Holographic and Speckle interferometry*. Cambridge University Press, Cambridge. 57.

Juptner, W., Pomarico, J., & Schnars, U. (1996) Light-in-flight measurements by digital holography. In *SPIE's 1996 International Symposium on Optical Science, Engineering, and Instrumentation* (pp.135-141). International Society for Optics and Photonics.

Kang, M. G., & Chaudhuri, S. (2003). Super-resolution image reconstruction.*Signal Processing Magazine, IEEE*, *20*(3), 19-20.

Keferstein, C. P. & Marxer, M. (1998). Testing bench for laser triangulation sensors. *Sensor Review,* 18(3)**,** 183-187.

Kim, M. K., Yu, L. & Mann, C. J. (2006) Interference techniques in digital holography. *Journal of Optics A: Pure and Applied Optics,* 8(7)**,** S518.

Kim, M. K. (2011). *Digital Holographic Microscopy* (pp. 149-190). Springer New York.

Kirkpatrick, P. & El-Sum, H. M. A. (1956) Image formation by reconstructed wave Fronts: In Physical principles and methods of refinement''. *JOSA,* 46(10)**,** 825-831.

Klein, M. V & Furtak, T. E. (1986) *Optics*, (second edition), Wiley, New York.

Digitized by UCC, Library

Kobayashi,S & Kurihara, K. (1971) Infrared Holography with Wax and Gelatin Film. *Applied. Physics Letters 19(11),*482-484

Koek, W. D., Bhattacharya, N., Braat, J. J. M., Ooms, T. A. & Westerwell, J., (2005). Influence of virtual images on the signal-to-noise ratio in digital in-line particle holography. *Optics Express,* 13(7)**,** 2578-2589.

Koester, C. J. and Vanderburgh Jr, A. (Eds.) *Optical & electro-optical information proceeding.* Cambridge: Massachusetts Institute of Technology Press.

Kogelnik, H. (1965) Holographic image projection through inhomogeneous media. *Bell System Technical Journal,* 44(10)**,** 2451-2455.

Kreis, T. M. & Juptner, W.(1997) Suppression of dc term in digital holography. *Optical Engineering; 36(8),* 235-60

Kronrod, M. A., Merzlyakov, N. S. & Yaroslavsky, L. P. (1972) Reconstruction of holograms with a computer. *Soviet Physics-Technical Physics,* 17**,** 333-334.

Kujawinska, M., Salbut, L. & Patroski, K. (1991) Three-channel phase stepped system for moiré interferometry. *Applied Optics,* 30(13)**,** 1633-1635.

Kwon,O., Wyant, J.C, & Hayslett, C.R(1980). Rough surface Interferometry at 10.6 microns..*Appl. Opt,. 19,* 1862-1869.

Lai, S., King, B., & Neifeld, N. A.,(2000). Wavefront reconstruction by means of phase-shifting digital in-line holography. *Optical Engineering,*173, 1829-1839.

Laporta ,P., (2007). Quantitative Phase Microscopy of microstructures with extended measurement range and correction of chromatic aberrations by multiwavelength digital holography. *Opt. Express 15***,** 14591-14600

Digitized by UCC, Library

Lauterborn, W., & Kurz, T. (2013). *Coherent optics: fundamentals and applications*. Springer Science & Business Media.

Le Clerc, F., Gross, M., & Collot, L.(2001). Synthetic aperture experiment in the visible with on-axis digital heterodyne holography. *Optics Letters, 26(20)*. 1550-1552

Lee, W. H., (1978). Computer-generated holograms: techniques and applications. Progress in Optics, 16, 120-232.

Leith, E. N. & Upatnieks, J. (1962) Reconstructed wavefronts and communication Theory. *JOSA,* 52(10)**,** 1123-1128.

Leith, E. N. & Upatnieks, J. (1963) Wavefront reconstruction with continuous-tone Objects. *JOSA,* 53(12)**,** 1377-1381.

Leith, E. N. & Upatnieks, J. (1964) Wavefront reconstruction with diffused illumination and three-dimensional objects. *JOSA,* 54(11)**,** 1295-1301.

Leith, E. N., & Upatnieks, J. (1966). Holographic imagery through diffusing media. *JOSA,* 56(4)**,** 523-523.

Liebling, M., Blu, T. & Unser, M. (2003). Fresnelets: New multiresolution wavelet bases for digital holography. *IEEE Transactions on Image Processing,* 12**,** 29-43.

Liebling, M., Blu, T. & Unser, M. (2004). Complex-wave retrieval from a single off-axis hologram. *Journal of the Optical Society of America A: Optics and Image Science, and Vision,* 21**,** 367-377.

Liu, Z. G., Bo, F., Wang, Y & Zhu, J. Q. (2002). Super-resolution digital holographic imaging method. *Applied Physics Letters. 81(17)*, 3143-3145.

Digitized by UCC, Library

Liu, G. & Scott, P. D. (1987). Phase retrieval and twin-image elimination for in-line Fresnel holograms. *JOSA A,* 4(1), 159-165.

Lohmann, A. W., & Paris, D. P. (1967). Binary Fraunhofer holograms generated by Computer. *Applied Optics,* 6(10)**,** 1739-1748.

Lu, S. (1968). Generating multiple images for integrated circuits by Fourier-transform Holograms. *Proceedings of the IEEE,*56(1), 116-117.

Ma, L., Wang, H., Li, Y., & Jin, H. (2004). Numerical reconstruction of digital holograms for three-dimensional shape measurement. *Journal of optics A: Pure and applied Optics,* 6(4)**,** 396-400.

Martinez-Leon, L., & Javidi, B (2008) Synthetic-aperture single-exposure on-axis digital holography. *Optics Express. 16(1).* 161-169.

Massig, J. H.,(2002) Digital off-axis holography with synthetic aperture. *Optics Letters. 27(24).* 2179-2181.

Meng, X. F., Cai, L. Z., He, M. Z., Dong, G. Y. & Shen, X. X. (2005). Cross-talk-free double-image encryption and watermarking with amplitude-phase separate modulations. *Journal of Optics A: Pure and Applied Optics,* 7(11)**,** 624-631.

Mico, V., Zalevsky, P., Garcia-Martinez, P., & Garcia, L (2006) Superresolved imaging in digital holography by superposition of tilted wavefronts *Applied Optics. 45(5).* 822-828

Nilsson, B., & Carlsson, T. E. (1998). Direct three-dimensional shape measurement by digital light-in-flight holography. *Applied Optics,* 37(34)**,** 7954-7959.

Digitized by UCC, Library

Onural, L., & Ozgen, M. T. (1992). Extraction of three-dimensional object-location information directly from in-line holograms using Wigner analysis. *JOSA A,* 9(2)**,** 252-260.

Onural, L., & Scott, P. D. (1987) Digital decoding of in-line holograms. *Optical Engineering,* 26(11)**,** 1124-1132.

OPHIR Photonics, Newport Company (2014, December 10). Retrieved December, 2014, from http://www.ophiropt.com/photonics

Osten, W., Baumbach, T., & Juptner, W. (2002). Comparative digital holography. *Optics Letters,* 27(20)**,** 1764-1766.

Park, S. C., Park, M. K., & Kang, M. G. (2003). Super-resolution image reconstruction: a technical overview. *Signal Processing Magazine, IEEE*, *20*(3), 21-36.

Paturzo, M., Merola, F., Grilli., S., De Nicola, S., Finizio, A & Ferraro, P (2008) Super-resolution in digital holography by two dimensional dynamic phase grating. *Optics Express 16(21).* 17107-17118.

Pedrini, G., Gusev, M., Schedin S., & Tiziani, H. J. (2003). Pulsed digital holographic interferometry by using a flexible fiber endoscope. *Optics and Lasers in Engineering,* 40(5)**,** 487-499.

Pelagotti, A., Locatelli, M., Geltrude, A. G., Poggi, P., Meucci, R., Paturzo, M., & Ferraro, P. (2010). Reliability of 3D imaging by digital holography at long IR wavelength. *Display Technology, Journal of*, *6*(10), 465-471.

Digitized by UCC, Library

Pierattini, G. (2003). Compensation of the inherent wave front curvature in digital holographic coherent microscopy for quantitative phase-contrast imaging. *Applied optics*, *42*(11), 1938-1946.

Pomarico, J., Schnars, U., Hartmann, H. J & Juptner, W (1996). Digital recording and numerical reconstruction of holograms: a new method for displaying Light-in-flight. *Applied Optics 34*(35). 8095-8099.

Powell, R. L., & Stetson, K. A. (1965). Interferometric vibration analysis by wavefront Reconstruction. *JOSA,* 55(12)**,** 1593-1598.

Prévost,D.,Thibault,G., Galarneau, P.,Denariez-Roberge,M., Tarrats-.

Rastogi, P. K. (Ed.). (1997) *Optical Measurement Techniques and Applications.* Artech House.

Reicherter, M., Zwick, S., Haist, T., Kohler, C., Tiziani, H., & Osten, W. (2006) Fast digital hologram generation and adaptive force measurement in liquid-crystal-display-based holographic tweezers. *Applied Optics,* 45(5)**,** 888-896.

Rioux,M., Blanchard,M.,Cormier,M., & Beaulieu, R(1978) Use of the TEM_{10} laser mode for ir holography at 10.6 μm. *Applied Optics,* 17(24), 3864-3865.

Rioux, M.,Blanchard,M., Cormier, M.,Beaulieu,R., & Bélanger, D(1977) Plastic recording media for holography at 10.6 μm. *Applied Optics,* 16(7)*,* 1876-1879.

Rogers, G. L. (1950) Gabor diffraction microscopy: the hologram as a generalized zone-plate. *Nature,* 166**,** 237.

Digitized by UCC, Library

Rogers, G. L. (1952) Experiments in diffraction microscopy. *Proceedings of the Royal Society of Edinburgh.Section A. Mathematical and Physical Sciences*,63(03)**,** 193-221.

Rukman,G.I., Lisyanskii, B.E.,Morozov,P.A., & Morozova,S.P(1978) *Holography in the IR region of the spectrum, based on scanning image converter.Measurement techniques,* 21(5), 635-636.

Saugnac,A., & De Contencin ,F. X., (1989). Thermal gratings written in glycerol with CO2 laser radiation. *Applied Optics,* 28(17)*,*3751-3753.

Schnars, U., & Juptner, W. (2005) *Digital Holography: Digital Hologram Recording, Numerical Reconstruction, and Related Techniques.* Springer

Schnars, U. & Juptner, W. (1993) Principles of direct holography for interferometry. In *Proceedings of 2nd International Workshop on Automatic Processing of Fringe Patterns* (pp. 115-120).

Schnars, U., & Juptner, W., (1994). Digital reconstruction of holograms interferometry and shearography. *Applied Optics,*33(20). 4373-4377.

Srinivasan, V., Liu, H. C., & Halioua, M. (1984) Automated phase-measuring profilometry of 3-D diffuse objects. *Applied Optics,* 23(18)**,** 3105-3108.

Stadelmaier, A., & Massing, J. A.,(2000). Compensation of lens aberrations in digital holography. *Optics letters*, 25, 1630-1632.

Stroke, G. W., Restrick, R., Funkhouser, A., & Brumm, D. (1965). Resolution-retrieving compensation of source effects by correlation reconstruction in high resolution holography. *Physics Letters,* 18(3)**,** 274-275.

Digitized by UCC, Library

Takaki, Y., Kawai, H., & Ohzu, H.,(1999). Hybrid holographic microscopy free of conjugate and zero-order images. *Applied Optics,*38(23). 4990-4996.

Thermoteknix Systems Ltd, Miricle Powered by Thermoteknix (2014, December 10). Retrieved December 10, 2014, from http://www.thermoteknix.com/index.

Thompson, B. J., Ward, J. H., & Zinky, W. R. (1967). Application of hologram techniques for particle size analysis. *Applied Optics,* 6(3)**,** 519-526.

Tiziani, H. J. (1997). Optical metrology of engineering surfaces--scope and trends. *Optical measurement techniques and applications, 15-49*

Upatnieks, J. U. R. S. I, Lugt, A. V, & Leith, E. (1966). Correction of lens aberrations by means of holograms. *Applied Optics,* 5(4)**,** 589-593.

Van Haasteren, A. J. P., & Frankena, H. J. (1994) Real-time displacement measurement using a multi camera phase-stepping speckle interferometer. *Applied Optics,* 33(19)**,** 4137-4142.

Vanderlugt, A., Rotz, F. B., & Klooster Jr, A. (1965). Character reading by optical spatial filtering. *Optical and Electro-Optical Information Processing*, 3.

Wagner, C., Seebachers, S., Osten, W., & Juptner, W.(1999). Digital recording and numerical reconstruction of lensless Fourier holograms in optical metrology. *Applied Optics*, 38(22).4812-4820

Wilson, T. (1990). Confocal Microscopy. *Academic Press: London,etc*,426,1-64.

Xu, L., Miao, J & Asundi, A(2000) Properties of digital holography based on in-line configuratio. *Optical Engineering, 39(12),* 3214- 3219.

Digitized by UCC, Library

Yamaguchi, I., Ida, T., Yokota, M., & Yamashita, K. (2006) Surface shape measurement by phase-shifting digital holography with a wavelength shift. *Applied Optics,* 45**,** 7610-7616.

Yaroslavsky, L. P., & Merzlyakov, N. S. (1980). Methods of digital holography. Consultants Bureau, New York

Yu, L., An., Y., & Cai, L., (2002). Numerical reconstruction of digital holograms with variable viewing angles. *Optics Express,* 10, 1250-1257.

Yu, L., & Cai, L., (2001). Iterative algorithm with a constraint condition for numerical reconstruction of a three-dimensional object from its hologram. *JOSA,*18(5), 1033-1045.

Zalevsky, Z. (2011). *Digital holography and phase retrieval*. INTECH Open Access Publisher.

Zelenka, J. S., & Varner, J. R. (1969) Multiple-index holography contouring. *Applied Optics,* 8(7)**,**1431-1434.

Zhang, F., Yamaguchi, I. & Yaroslavsky, L. (2005). Systematic approach for the design of reconstruction algorithm in digital holography. In *Photonics Asia* 2004(pp. 261-270). International Society for Optics and Photonics.

Zhang, Y., Pedrini, G., Osten, W. & Tiziani, H. J. (2003). Image reconstruction for in-line holography with the Yang-Gu algorithm. *Applied Optics,* 42(32)**,** 6452-6457.

Zheng, D. X., Zhang, Y., Shen, J. L., Zhang, C. L. & Pedrini, G. (2005). Wave field reconstruction from a hologram sequence. *Optics Communications,* 249(1)**,** 73-7

Digitized by UCC, Library

APPENDICES

APPENDIX A

PHASE TRANSFORMATION OF ASPHERICAL LENS

The effect of an optical component with refractive index n and thickness d on complex amplitude of a wave is described by the transmission function

$$\tau = |\tau| \exp\left[\quad i\frac{2\pi}{\lambda}(n \quad 1)d \right] \qquad \text{(A1)}$$

This function is calculated in the following for a thin biconvex lens. Such lens consists of two spherical surfaces. Let the radius of curvature of the left half R_1, while that of the right half be designated R_2. We apply the following sign convention: As ray travel from left to right, each convex surface has a positive radius of curvature, while each concave surface has a negative radius of curvature. Due to this convention R_2 has a negative value. Losses due to reflection at the surfaces and due to absorption inside the lens are neglected; that is $|\tau| = 1$ and the refractive index is also constant for the entire lens.

The lens thickness is a function of the spatial coordinates x and y;

$$\mathrm{d}(\mathrm{x},\mathrm{y}) = \mathrm{d}_1(\mathrm{x},\mathrm{y}) + \mathrm{d}_2(\mathrm{x},\mathrm{y}) = \mathrm{d}_{01} \quad \zeta_1 + (\mathrm{d}_{02} \quad \zeta_2) \qquad \text{(A2)}$$

$$\mathrm{R}_1^2 = \mathrm{r}^2 + \left(\mathrm{R}_1 \quad \zeta_1\right)^2 = \mathrm{x}^2 + \mathrm{y}^2 + \mathrm{R}_1^2 \quad 2\mathrm{R}_1\zeta_1 + \zeta_1^2 \qquad \text{(A3)}$$

And

$$\mathrm{R}_2^2 = \mathrm{r}^2 + \left(\quad \mathrm{R}_2 \quad \zeta_2\right)^2 = \mathrm{x}^2 + \mathrm{y}^2 + \mathrm{R}_2^2 \; + 2\mathrm{R}_2\zeta_2 + \zeta_2^2 \qquad \text{(A4)}$$

Digitized by UCC, Library

Neglecting the quadratic terms of $\zeta_{1/2}$ leads to:

$$\zeta_1 = \frac{x^2 + y^2}{2R_1} \qquad (A5)$$

$$\zeta_2 = \frac{x^2 + y^2}{2R_2} \qquad (A6)$$

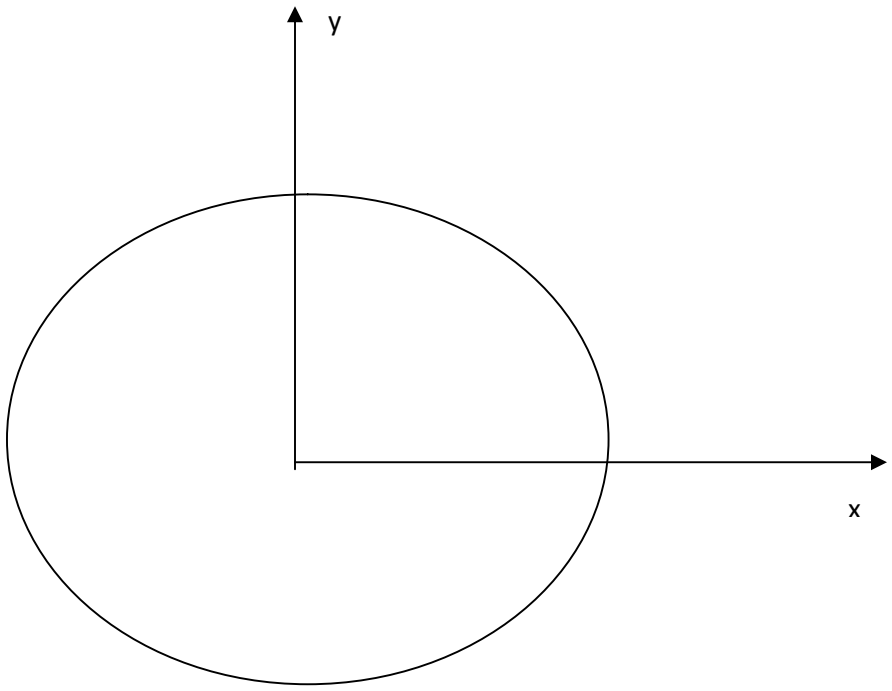

Figure A1: Top view of a biconvex lens

Digitized by UCC, Library

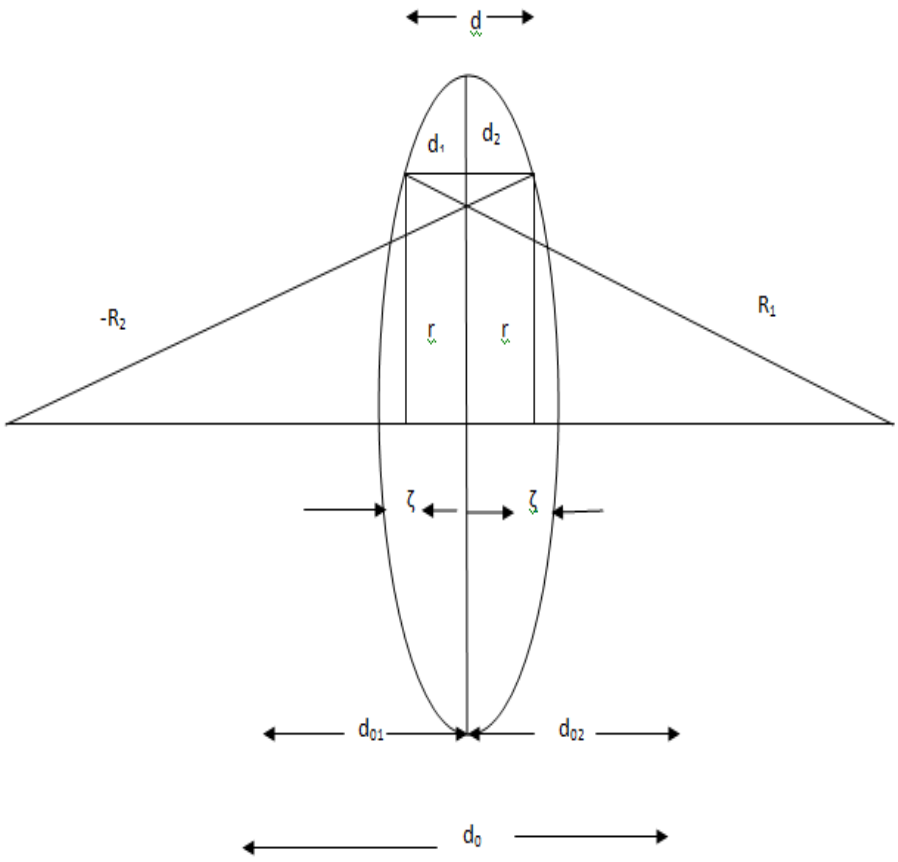

Figure A1: A Cross-sectional view of a biconvex lens.

This level of approximation is consistent with the parabolic approximation used in the Fresnel transformation. The thickness is now:

$$d(x,y) = d_0 \quad \frac{x^2+y^2}{2R_1} + \frac{x^2+y^2}{2R_2} \qquad (A7)$$

Digitized by UCC, Library

Appendix A continued

With the lens makers equation

$$\frac{1}{f} = (n \quad 1)\left[\frac{1}{R_1} \quad \frac{1}{R_2}\right] \qquad \text{(A8)}$$

of geometrical optics following lens transmission function is derived:

$$L(x,y) = \exp\left[i\frac{\pi}{\lambda f}(x^2 + y^2)\right] \qquad \text{(A9)}$$

The constant factor $\exp\left(\frac{-i2\pi}{\lambda}(n \quad 1)d_0\right)$, which only affects the overall phase, has been neglected.

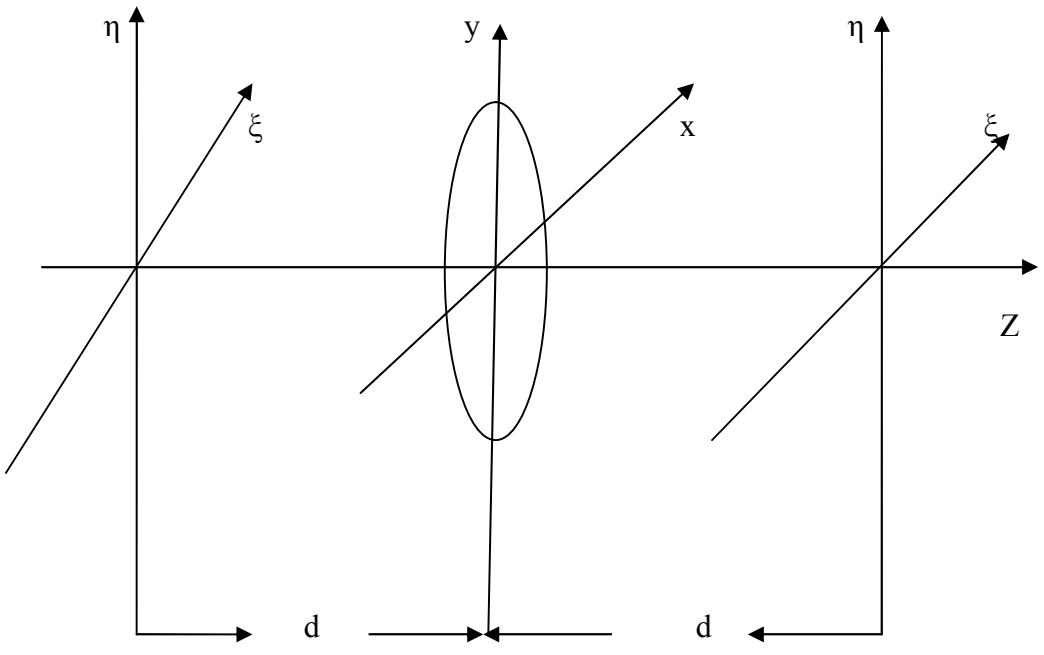

Figure A1: Coordinate system for image formation.

Digitized by UCC, Library

APPENDIX B

Correction of Aberrations

The complex amplitude of an object, which is imaged by a lens can be evaluated. Consider an object lying in the (ξ, η) the coordinate system, the lens is located in the (x, y) system and the image arise in the (ξ', η') a system as shown in figure A1. The object is described by the complex amplitude $E_0(\xi, \eta)$. The complex amplitude in front of the lens is given by:

$$E_0'(x,y) = \exp\left[\ i\frac{\pi}{\lambda d}(x^2+y^2)\right]\int_{-\infty}^{\infty}\int_{-\infty}^{\infty} E_0(\xi,\eta)\exp\left[\ i\frac{\pi}{\lambda d}(\xi^2+\eta^2)\right]\times$$

$$\exp\left[i\frac{2\pi}{\lambda d}(x\xi+y\eta)\right]d\xi d\eta \qquad \text{(B1)}$$

Where the Fresnel approximation was used, the complex amplitude in the image plane is given by:

$$E_0''(\xi',\eta') = \exp\left[\ i\frac{\pi}{\lambda d}(\xi'^2,\eta'^2)\right]\int_{-\infty}^{\infty}\int_{-\infty}^{\infty} E'_0(x,y)L(x,y)\exp\left[\ i\frac{\pi}{\lambda d}(x^2+y^2)\right]\times$$

$$\exp\left[i\frac{2\pi}{\lambda d}(x\xi'+y\eta')dxdy\right] =$$

$$\exp\left[\ i\frac{\pi}{\lambda d}(x\xi^2+y\eta^{\,2})\right]\int_{-\infty}^{\infty}\int_{-\infty}^{\infty}\int_{-\infty}^{\infty}\int_{-\infty}^{\infty} E_0(\xi,\eta)\exp\left[\ i\frac{\pi}{\lambda d}(x^2+y^2)\right]\times$$

$$\exp\left[\ i\frac{\pi}{\lambda d}(\xi^2+\eta^2)\right]\exp\left[i\frac{2\pi}{\lambda d}(x\xi+y\eta)\right]\exp\left[i\frac{2\pi}{\lambda d}(x^2+y^2)\right]\times\exp\left[\ i\frac{\pi}{\lambda d}(x^2+$$

$$y^2)\right]\exp\left[i\frac{2\pi}{\lambda d}(x\xi+y\eta)\right]d\xi d\eta\,dx\,dy \qquad \text{(B2)}$$

Digitized by UCC, Library

Appendix B continued

A magnification of 1 and a focal distance of $f = \frac{d}{2}$ are used for the lens transmission function $L(x,y)$. The image coordinates can be expressed in terms of the object coordinates:

$$\xi = \quad \xi \text{ and } \eta = \quad \eta \qquad \text{(B3)}$$

The minus signs results because according to the laws of geometrical optics the image is upside down. The complex amplitude of the image is now

$$E''_0(\xi,\eta) = \exp\left[\quad i\frac{2\pi}{\lambda d}(\xi^2+\eta^2)\right] E_0(\quad \xi, \quad \eta) =$$

$$\exp\left[\quad i\frac{\pi}{\lambda f}(\xi^2+\eta^2)\right] E_0(\quad \xi, \quad \eta) \qquad \text{(B4)}$$

The wave field in the image plane has to be multiplied by a factor, therefore;

$$P(\xi,\eta) = \exp\left[i\frac{\pi}{\lambda f}(\xi^2+\eta^2)\right] \qquad \text{(B5)}$$

In order to generate the correct phase distribution, the correction factor depends on the wavelength and the coordinates of the image plane. If the intensity of a wave field is to be calculated after reconstruction, then we can neglect the correction factor ($I \propto P \quad P = 1$) .This is also valid, if the phase difference of two wavefields, which are recorded with the same wavelength, is computed:

$$\varphi = \varphi_1 \quad \varphi_2 = {i\pi}/{\lambda f}(\xi^2+\eta^2) + \varphi_1 \quad \left[{i\pi}/{\lambda f}(\xi^2+\eta^2) + \varphi'_2\right] = \varphi'_1$$

φ'_2 (B6)

Digitized by UCC, Library

APPENDIX C

C. The Fourier Transform

C1. Definitions

The one-dimensional Fourier transform of the function f(x) is defined as:

$$\{f(x)\} = F(u) = \int_{-\infty}^{\infty} f(x)\exp[i2\pi ux]dx \qquad (C1)$$

The inverse one-dimensional Fourier Transformation is defined as:

$$^{-1}\{F(u)\} = f(x) = \int_{-\infty}^{\infty} F(u)\exp[i2\pi ux]dx \qquad (C2)$$

The functions $f(x)$ and $F(u)$ are called Fourier transform pair.

The two-dimensional Fourier transform of the function $f(x, y)$ is defined as

$$\{f(x,y)\} = F(u,v) = \int_{-\infty}^{\infty}\int_{-\infty}^{\infty} f(x,y)\exp[\ \ i2\pi(ux+vy)]dxdy \qquad (C3)$$

The corresponding inverse two- dimensional Fourier transformations are defined as:

$$^{-1}\{F(u,v)\} = f(x,y) = \int_{-\infty}^{\infty}\int_{-\infty}^{\infty} F(u,v)\exp[i2\pi(ux+vy)]dudv \qquad (C4)$$

C2. Properties

Some useful theorems about Fourier transform. These formulas are written for two-dimensional case.

Digitized by UCC, Library

Appendix C continued

1. Linearity theorem

$$\{af(x,y) + bg(x,y)\} = aF(u,v) + bG(u,v) \qquad (C5)$$

Where a and b are constants, $F(u,v) = \big(f(x,y)\big)$ and $G(u,v) = \big(g(x,y)\big)$.

2. Similarity theorem

$$\{f(ax,by)\} = \frac{1}{|ab|}F\left(\frac{u}{a},\frac{v}{b}\right) \qquad (C6)$$

3. Shift theorem

$$\{f(x \quad a, y \quad b)\}F(u,v)\exp[\ \ i2\pi(ua+vb)] \qquad (C7)$$

4. Rayleigh's (Parseval's) theorem

$$\int_{-\infty}^{\infty}\int_{-\infty}^{\infty}|f(x,y)|^2dxdy = \int_{-\infty}^{\infty}\int_{-\infty}^{\infty}|f(u,v)|^2dudv \qquad (C8)$$

5. Convolution theorem

The two-dimensional convolution of two functions $f(x,y)$ and $g(x,y)$ is defined as:

$$(f \quad g)(x,y) = \int_{-\infty}^{\infty}\int_{-\infty}^{\infty} f(x',y')g(x \quad x', y \quad y')dx'dy' \qquad (C9)$$

Where the operation denote the convolution. The convolution theorem states that the Fourier transform of the convolution of two functions is equal to the product of the Fourier transforms of the individual functions:

$$\{f(x,y) \quad g(x,y)\} = F(u,v)G(u,v) \qquad (C10)$$

Digitized by UCC, Library

Appendix C continued

6. Autocorrelation theorem

$$\left\{\int_{-\infty}^{\infty}\int_{-\infty}^{\infty} f\ (x', y')f(x + x', y + y')dx'dy'\right\} = |F(u, v)|^2 \qquad (C11)$$

7. Fourier integral theorem

$$^{-1}\{f(x, y)\} = \ ^{-1}\ \{f(x, y)\} = f(x, y) \qquad (C12)$$

8. Differentiation

Differentiation in spatial domain corresponds to a multiplication with a linear factor in the spatial frequency domain:

$$\left\{\left(\frac{\partial}{\partial x}\right)\ \left(\frac{\partial}{\partial y}\right)^n f(x, y)\right\} = (i2\pi u)\ (i2v)^n F(u, v) \qquad (C13)$$

Digitized by UCC, Library

APPENDIX D

The Discrete Fourier Transform

For numerical computations the function to be transformed is given in a discrete form, that is $f(x, y)$ in equation(A1) has to be replaced by the finite series f_k , with integer numbers $k = 0,1, \ldots, N \quad 1$. The continuous variable is now described as integer multiple of a sampling interval x :

$$x = k \ \ x \qquad \text{(D1)}$$

The frequency variable u is converted into discrete variable, as:

$$u = m \ \ u \qquad \text{(D2)}$$

The discrete representation of equation (A1) is then given by:

$$F_m = \ \ x \sum_{k=0}^{N-1} f_k \exp[\ \ i2\pi km \ \ x \ \ u] \ \text{ for } m = 0,1, \ldots, N \quad 1 \qquad \text{(D3)}$$

The maximum frequency is determined by the sampling interval in the spatial domain:

$$u_{max} = N \ \ u = \frac{1}{x} \qquad \text{(D4)}$$

The following expression:

$$F_m = \frac{1}{N} \sum_{k=0}^{N-1} f_k \exp\left[\ \ i2\pi \frac{km}{N}\right] \qquad \text{(D5)}$$

Digitized by UCC, Library

Is therefore defined as one-dimensional discrete Fourier transform (DFT). The inverse transformation is given by:

$$f_k = \sum_{m=0}^{N-1} F_m \exp\left[i2\pi \frac{km}{N}\right] \qquad \text{(D6)}$$

Similar considerations lead to discrete two-dimensional Fourier transform pair:

$$f_{mn} = \sum_{k=0}^{N-1} \sum_{l=0}^{N-1} f_{kl} \exp\left[\ i2\pi\left(\frac{km+ln}{N}\right)\right] \qquad \text{(D7)}$$

For $m = 0,1,\ldots,N \quad 1$. Here a quadratic field sampling points is used, that is the number of points in each row is equal to that in each column. The computation time for discrete Fourier transform is mainly determined by the number of complex multiplications. A two- dimensional DFT can be factorised into two one-dimensional DFT's:

$$f_{mn} = \frac{1}{N^2} \sum_{k=0}^{N-1} \left[\sum_{l=0}^{N-1} f_{kl} \exp\left(\ i2\pi \frac{nl}{N}\right)\right] \exp\left(\ i2\pi \frac{km}{N}\right) \qquad \text{(D8)}$$

The one-dimensional DFT can be programmed most effectively using the fast Fourier transform (FFT) algorithms. These algorithms make use of redundancies and reduce the number of multiplications for a one-dimensional DFT from N^2 to $2N \log_2 N$.

Digitized by UCC, Library

APPENDIX E

Programme for the MATLAB codes for the reconstruction of the holograms.

```
% imagesc(real(a)); clear all;

close all;

%%%INSERIMENTO PARAMETRI

LAM = 10.6;%lunghezza d'onda

Nx = 640;%numero di pixel da elaborare

Ny = 480;%numero di pixel da elaborare

Px = 25;%dimensione x pixel della telecamera

Py = 25;%dimensione y pixel della telecamera

d = -600000;%distanza di ricostruzione

r = 450000;%curvatura del fascio di riferimento se sferico

pad = 3;%ordine di padding

%%%ACQUISIZIONE INTERFEROGRAMMI, PADDING E FILTRAGGIO

%%Carica dati da formato immagine

H0 = imread('augusto&traianoshift','bmp');

H1 = double(H0(1:Ny,1:Nx));

%%Padding

padsize = [(pad*Ny-Ny)/2,(pad*Nx-Nx)/2];

H2 = padarray(H1,padsize);

% %%Nessun filtro

% H = H2;

% %%Sottrazione media
```


Digitized by UCC, Library

```
% Hm = mean2(H2);
% H = H2-Hm*ones(pad*Ny,pad*Nx);
% %%Filtro passa alto
% s = -(1/9)*[1 1 1; 1 -8 1; 1 1 1];
% H = conv2(double(H2),double(s),'same');
%%Filtro finestra Hamming
Hd = zeros(41,41);
Hd(1:40,1:40) = 1;
Hd(17:25,17:25) = 0;
% s = fsamp2(Hd);
s = fwind1(Hd,hamming(41));
H = conv2(double(H2),double(s),'same');
%%%VARIABILI INTEGRANDE
[X,Y] = meshgrid(-pad*Nx/2+1:pad*Nx/2,-pad*Ny/2+1:pad*Ny/2);
% R = 1;%fascio di riferimento piano
R = exp(1i*pi/(LAM*r)*(X.^2*Px^2+ Y.^2*Py^2));%fascio di riferimento
sferico
W=exp(1i*pi/(LAM*d)*(X.^2*Px^2+Y.^2*Py^2));Z=1/(1i*LAM*d)*exp(1i*2*p
i*d/LAM)*exp(1i*pi*LAM*d*(X.^2/((pad*Nx)^2*Px^2)+Y.^2/((pad*Ny)^2*Py
^2)));
%%%RICOSTRUZIONE CAMPO COMPLESSO A DISTANZA d
C = Z.*fftshift(fft2(R.*H.*W));
Amp = abs(C);
```


Digitized by UCC, Library

```
% Fase = atan(imag(C)./real(C));
%%%GRAFICI
figure(1);
imagesc(Amp);
shading interp;
colormap('hot');
title('Ampiezza');
% figure(2);
% imagesc(Fase);
% shading interp;
% colormap('hot');
% title('Fase');
% figure(3);
% subplot(1,2,1);
% a = fftshift(fft2(H2));
% shading interp;
% colormap(gray);
% title('fft ologramma');
% subplot(1,2,2);
% b = fftshift(fft2(H));
% imagesc(real(b));
% shading interp;
% colormap(gray);
```


Digitized by UCC, Library

APPENDIX F

Figure F: Holographic video recording

Digitized by UCC, Library

APPENDIX G

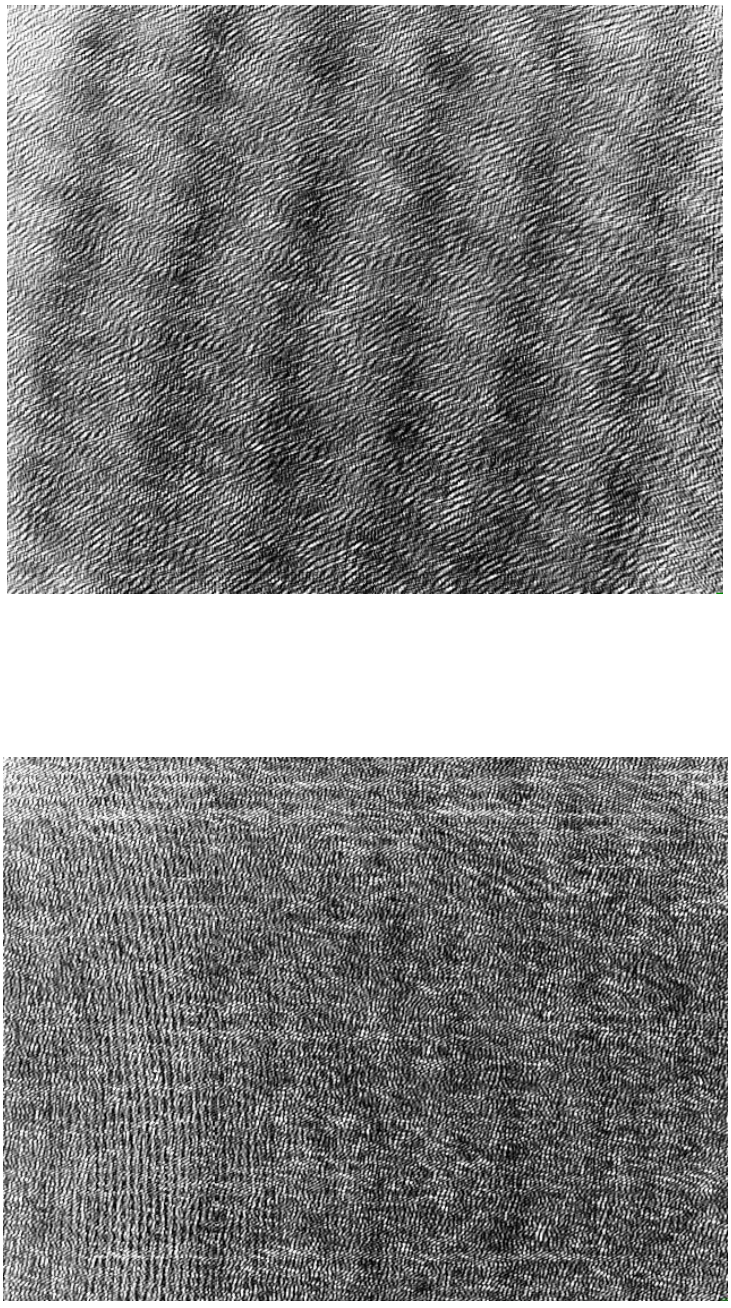

Figure G: The off-axis reflection configuration of the recorded interferogram of the bronze sculpture.

Digitized by UCC, Library

Appendix G continued

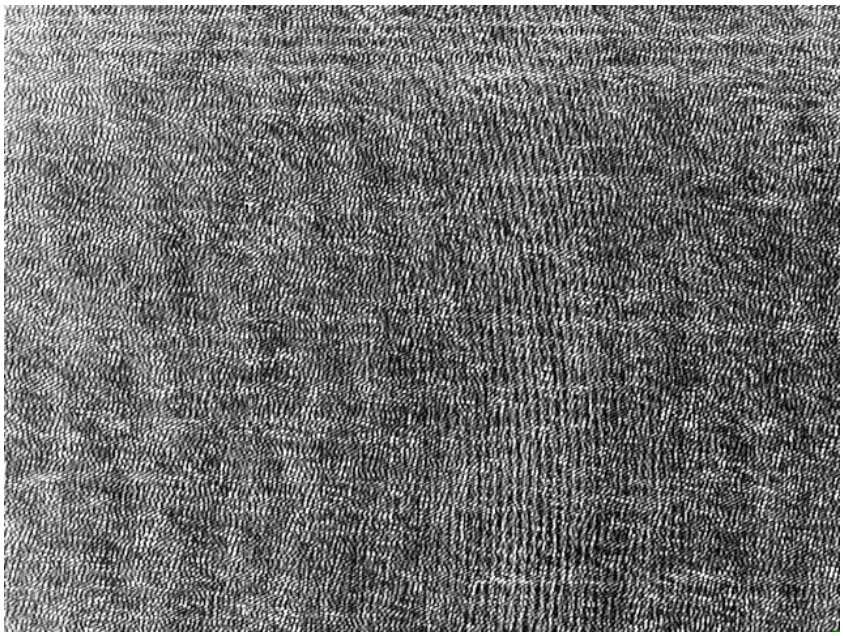

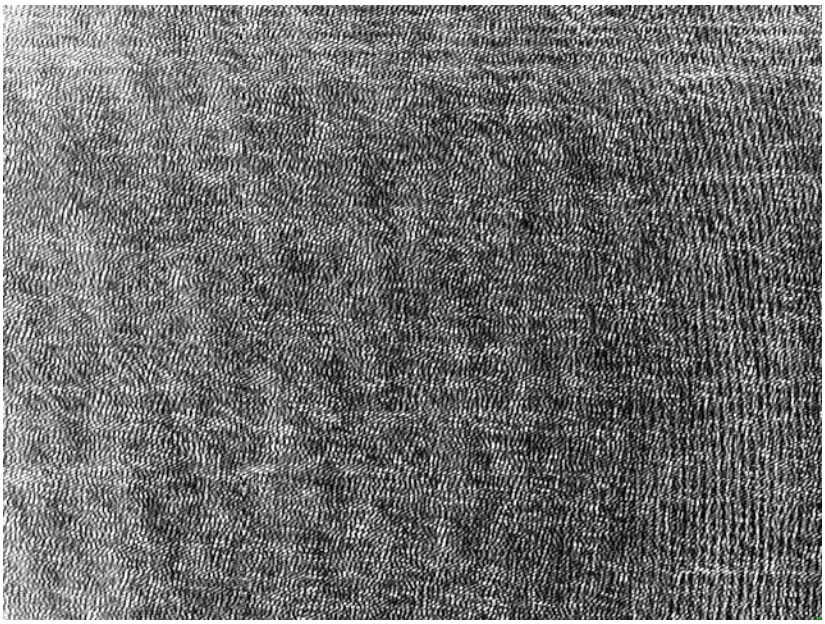

Figure G: The off-axis reflection configuration of the recorded interferogram of the bronze sculpture.

Digitized by UCC, Library

Appendix G continued

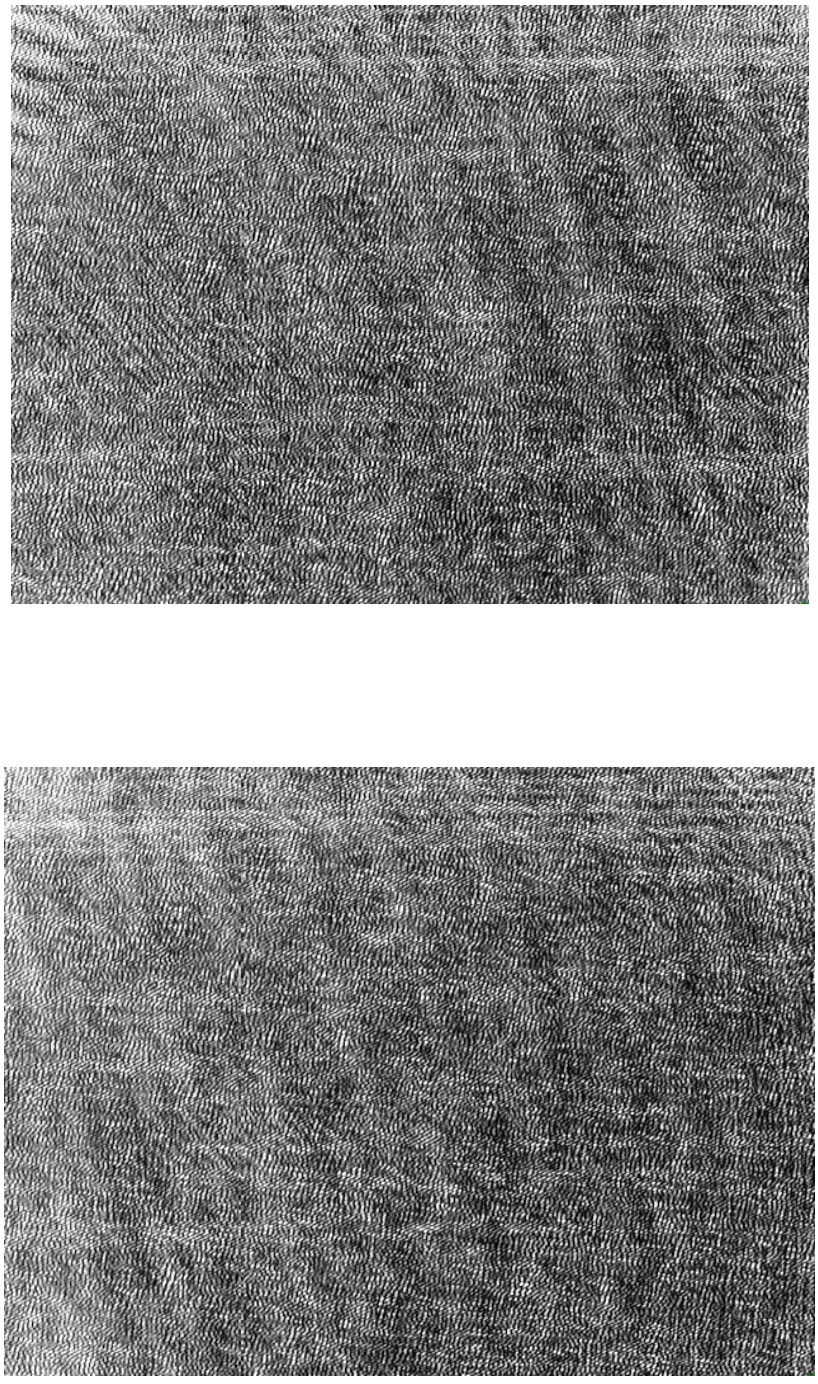

Figure G: The off-axis reflection configuration of the recorded interferogram of Traiano and Augusto.

Digitized by UCC, Library

Appendix G continued

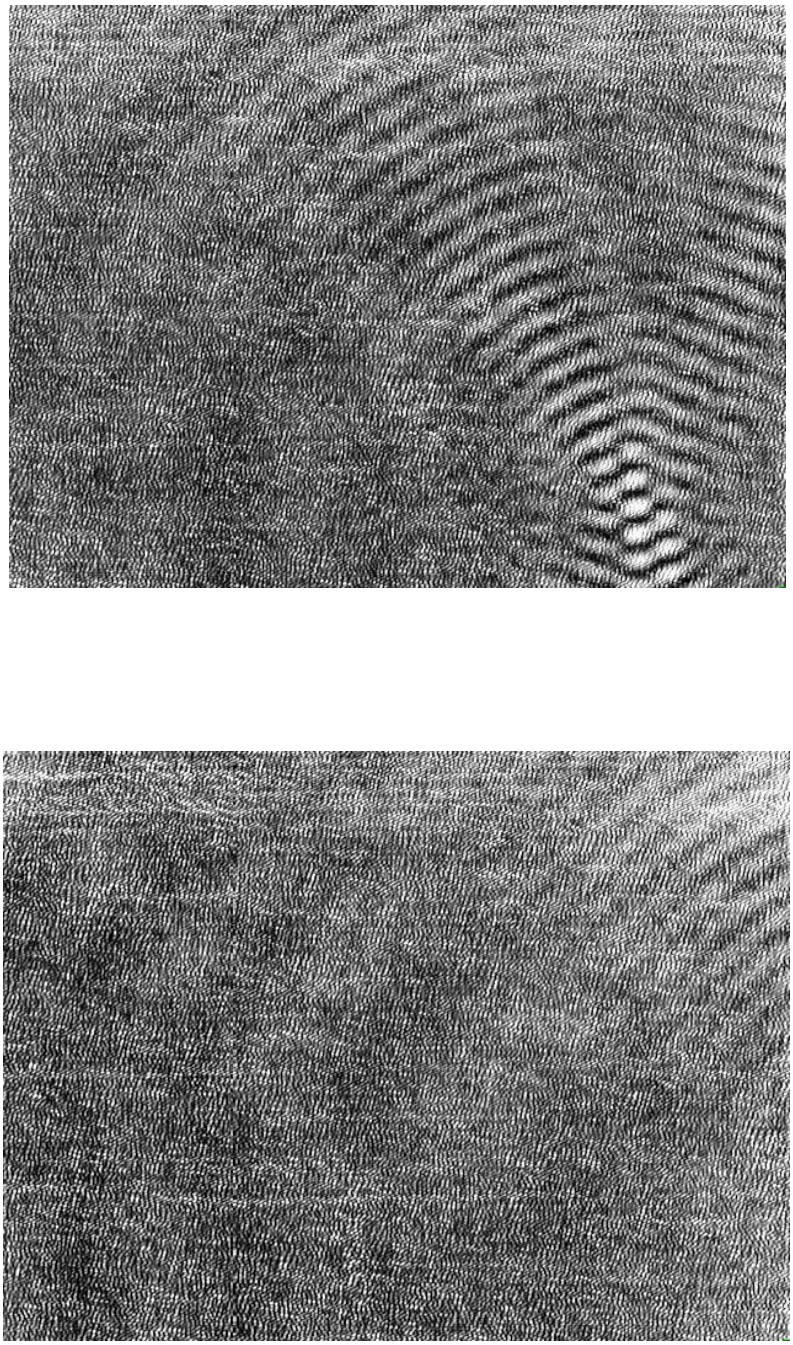

FigureG: The off-axis reflection configuration of the recorded interferogram of Traiano and Augusto.

Digitized by UCC, Library

Appendix G continued

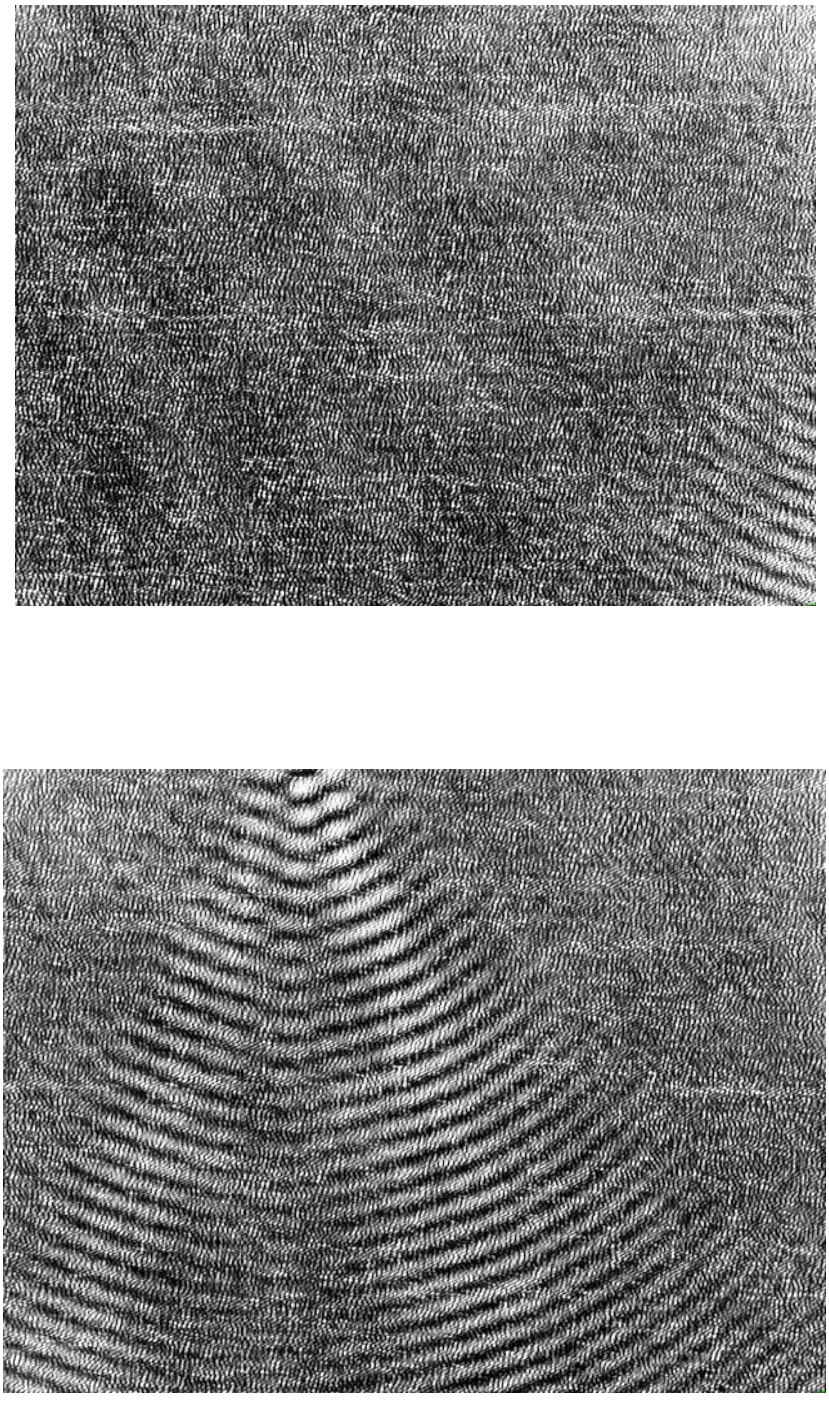

Figure G: The off-axis reflection configuration of the recorded interferogram of the marble plate.

Digitized by UCC, Library

Appendix G continued

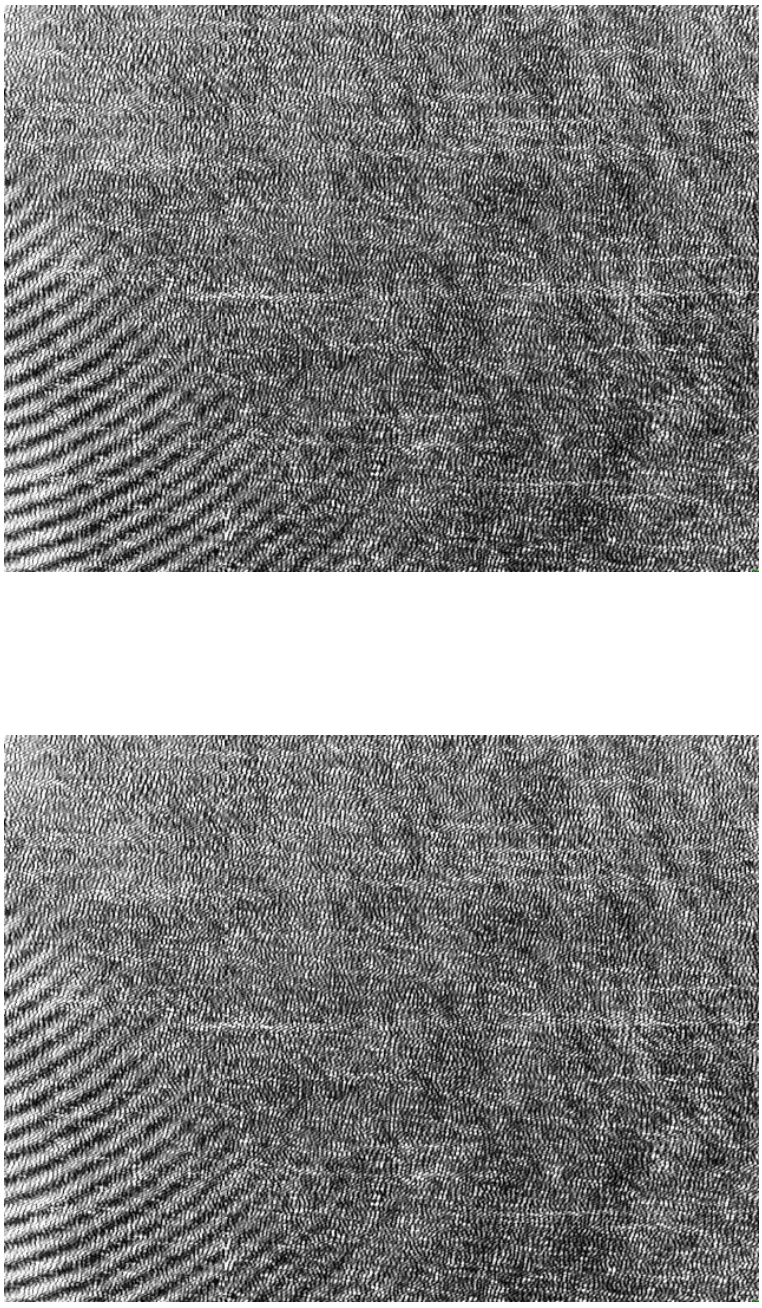

Figure G: The off-axis reflection configuration of the recorded interferogram of the marble plate.

Digitized by UCC, Library

Appendix G continued

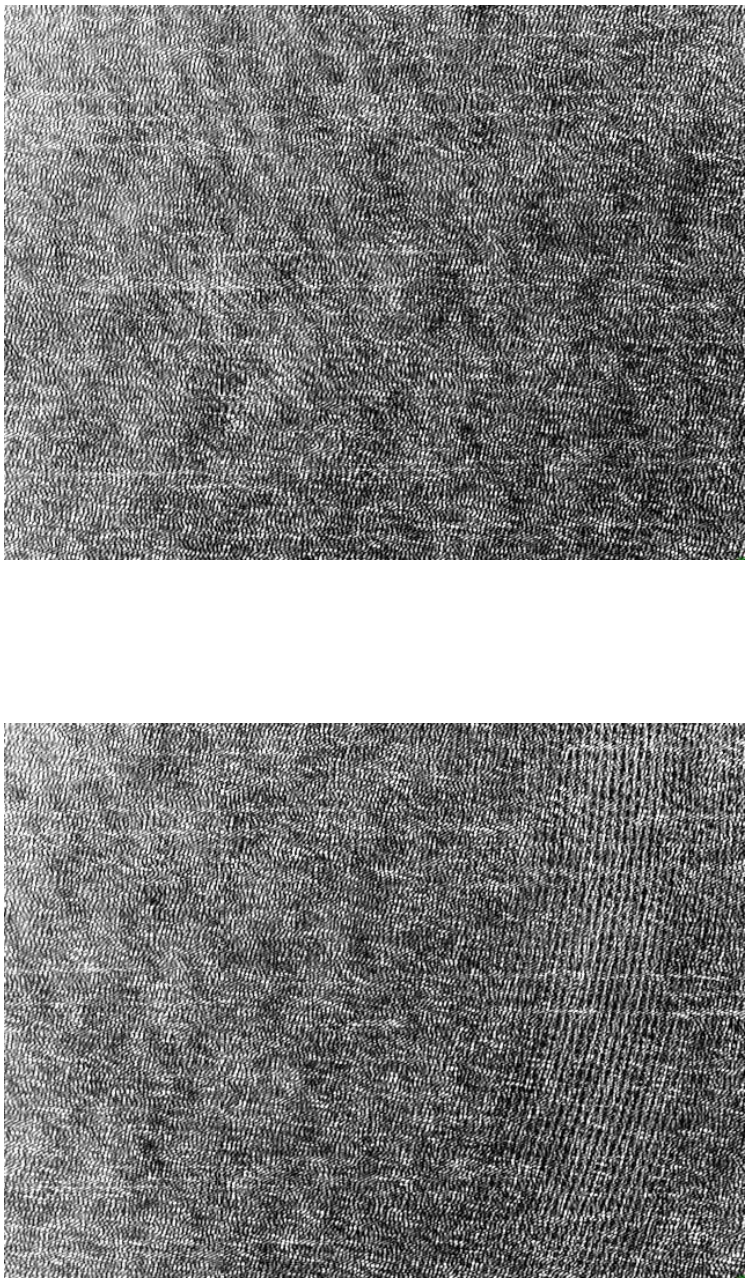

Figure G: The off-axis reflection configuration of the recorded interferogram of the earthenware tree.

Digitized by UCC, Library

Appendix G continued

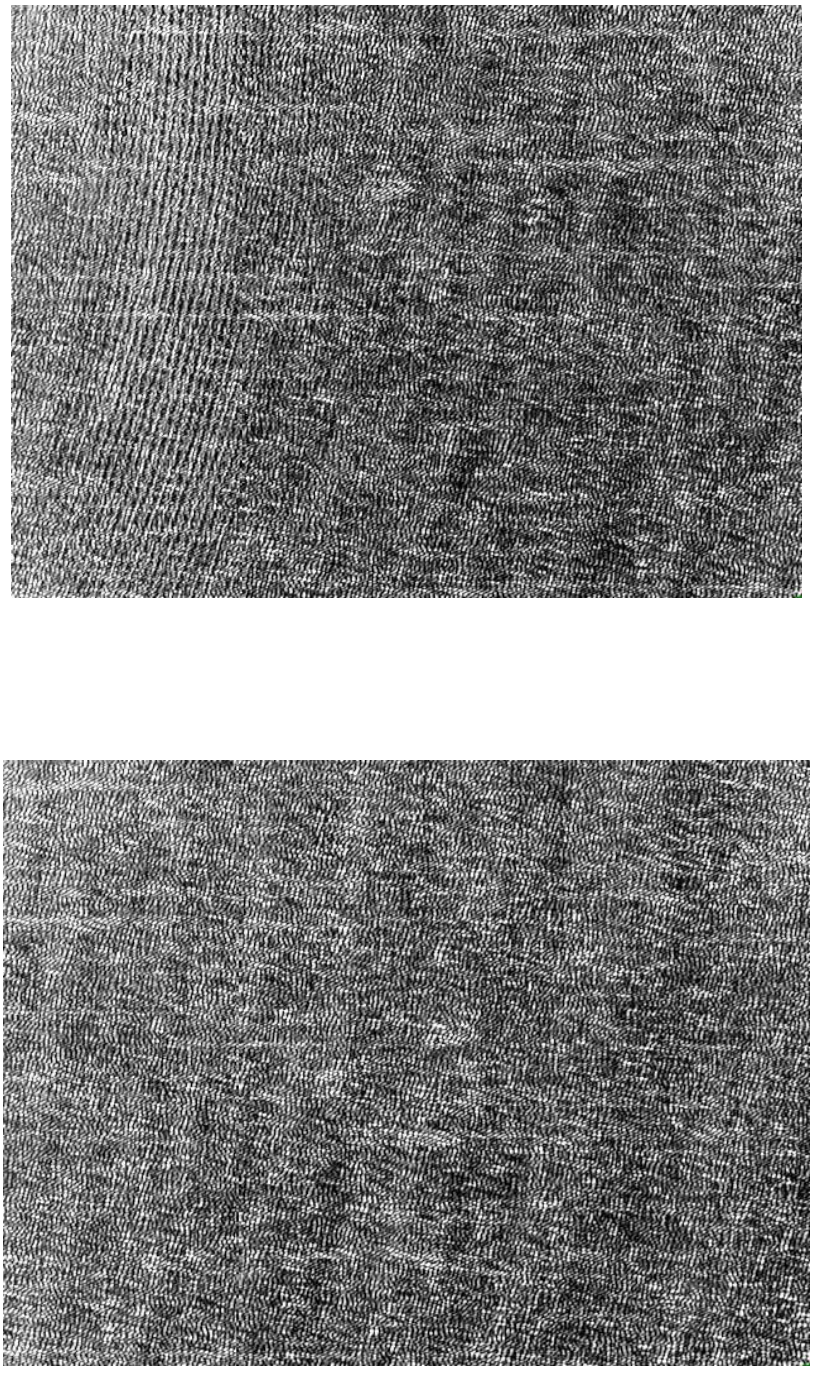

Figure G: The off-axis reflection configuration of the recorded interferogram of the earthenware tree.

Digitized by UCC, Library

Appendix G continued

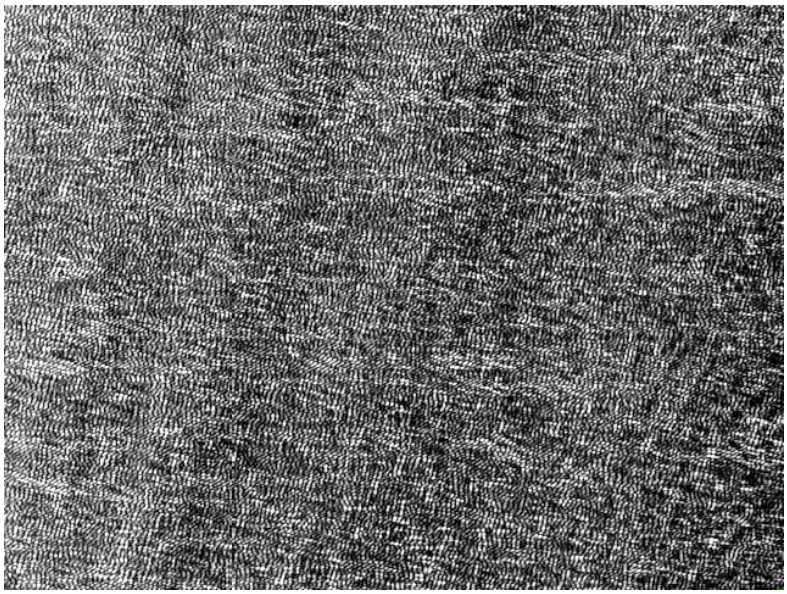

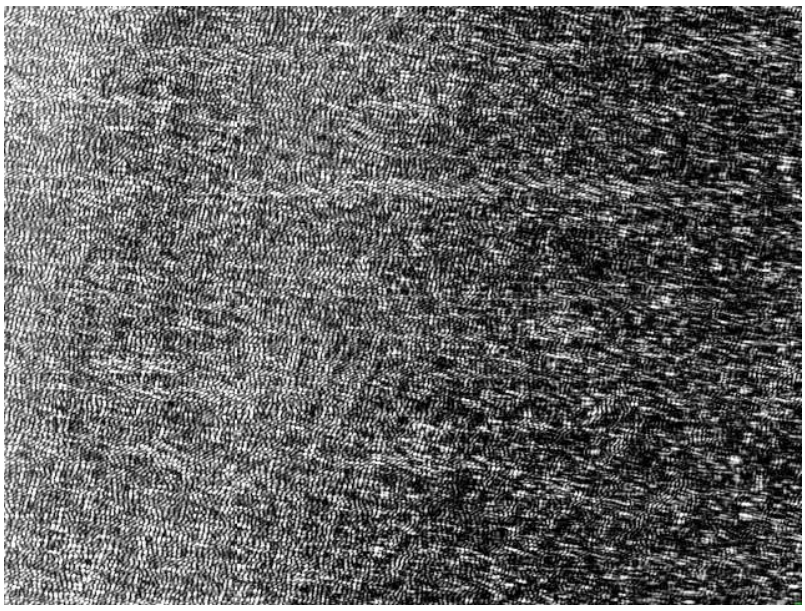

FigureG:The off-axis reflection configuration of the recorded interferogram of the Aluminium plate with drilled holes.

Digitized by UCC, Library

Appendix G continued

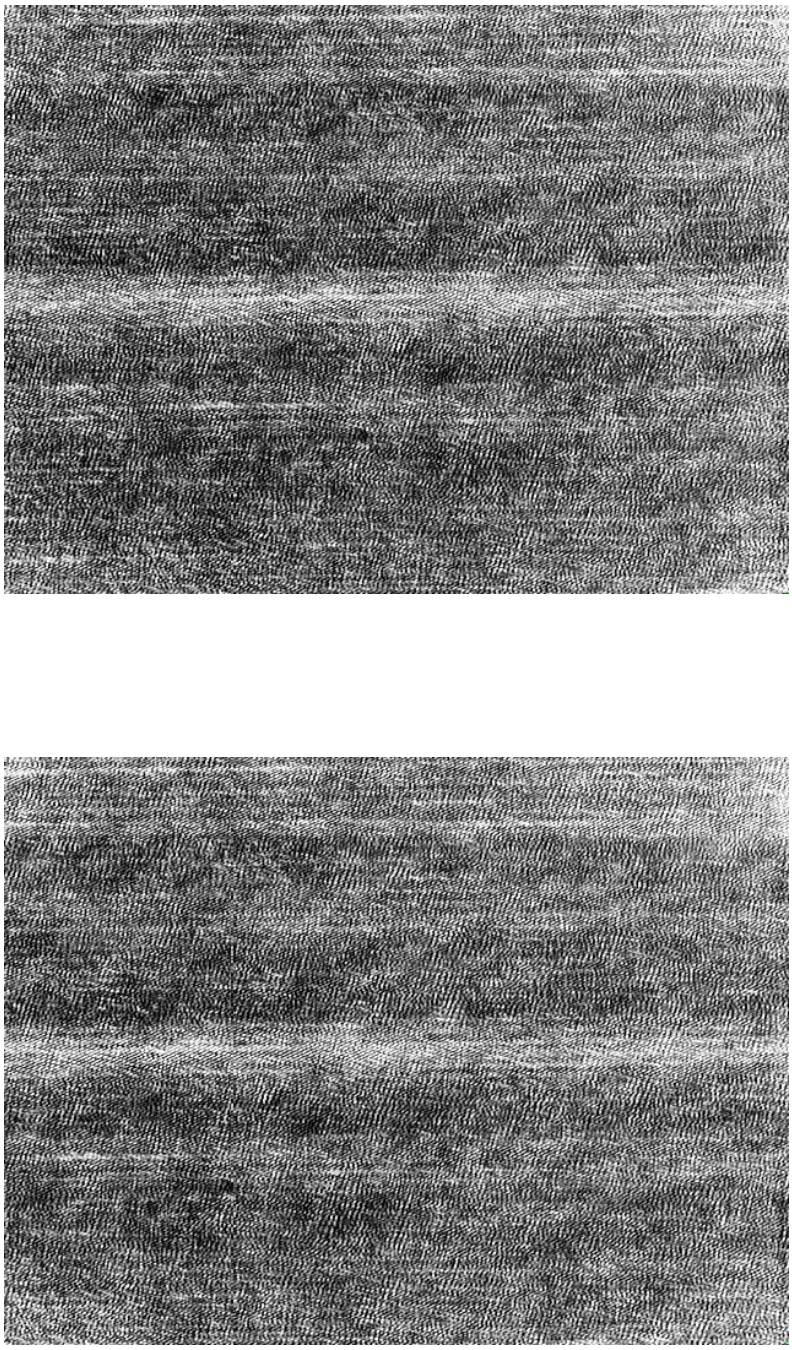

Figure G:The off-axis reflection cofiguration of the recorded interferogram of the Aluminium plate with drilled holes.

Digitized by UCC, Library

Appendix G continued

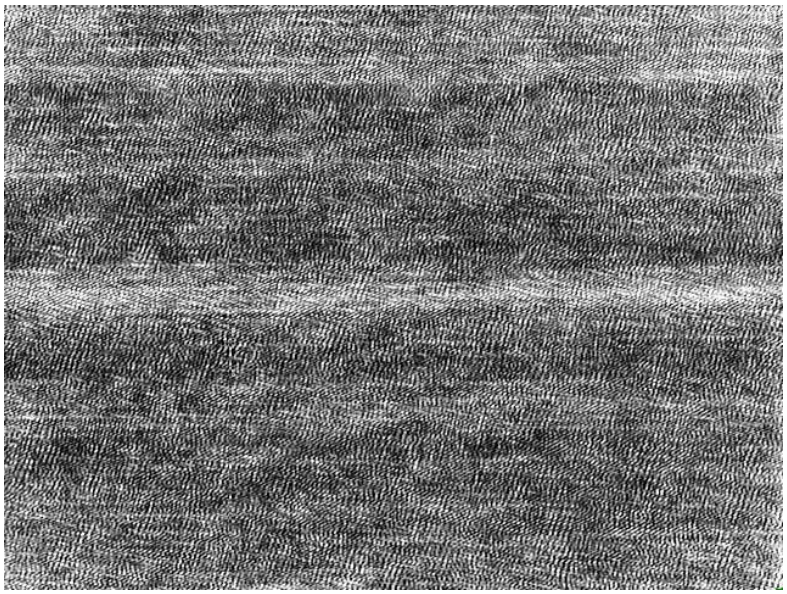

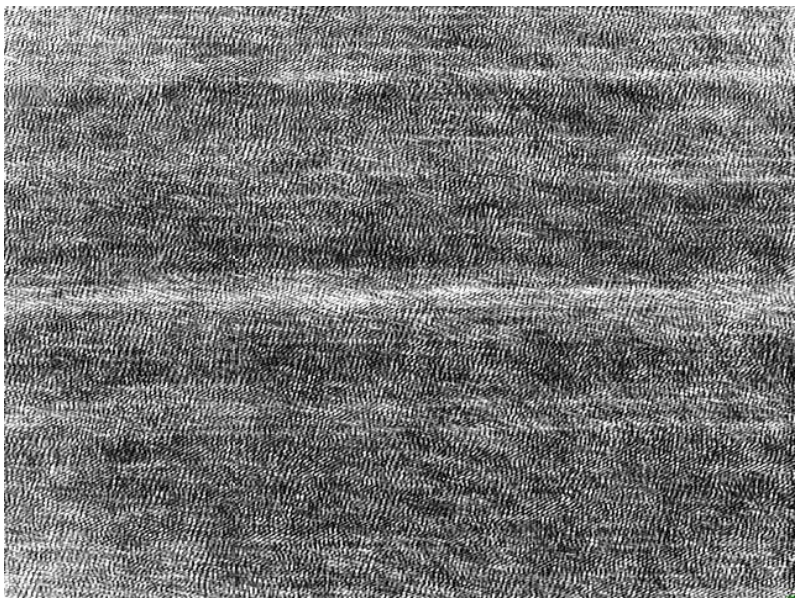

Figure G:The in-line transmission configuration of the recorded interferogram of the letters'XOU'.

Digitized by UCC, Library

Appendix G continued

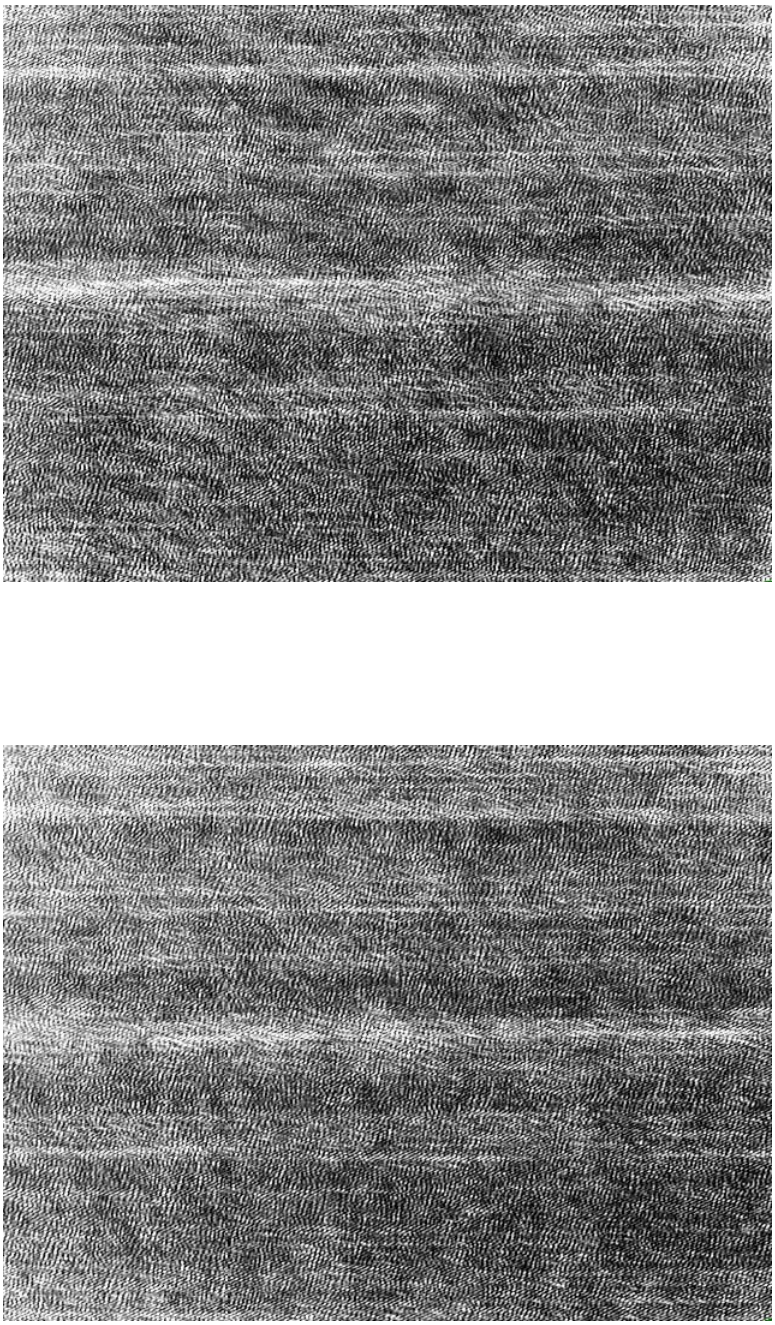

Figure G:The in-line transmission configuration of the recorded interferogram of the letters'XOU'.

Digitized by UCC, Library

Appendix G continued

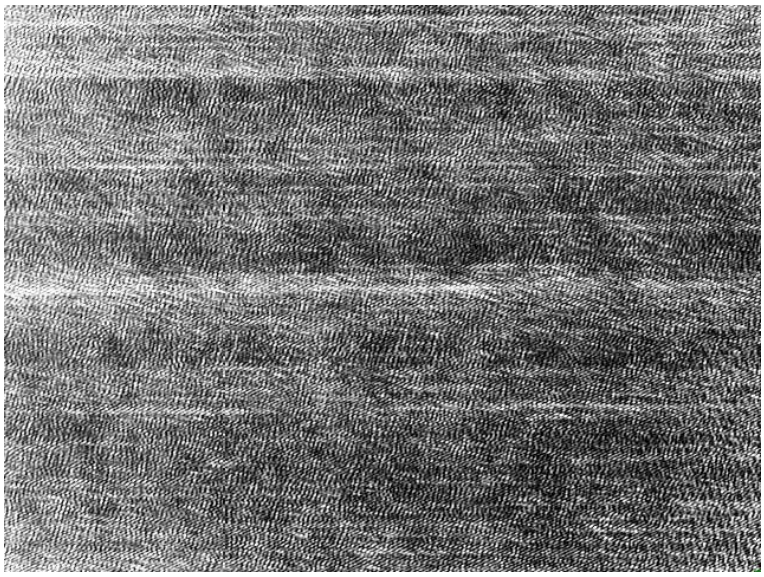

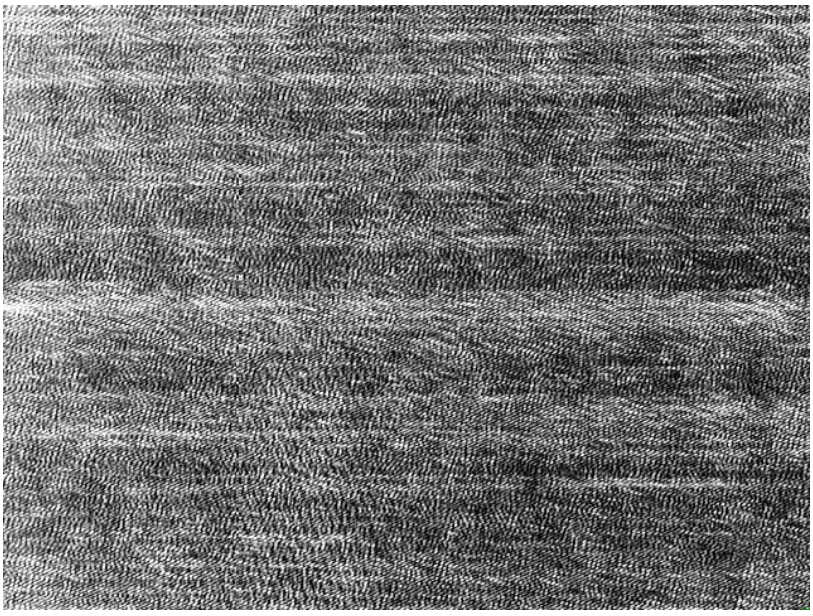

Figure G:The in-line transmission configuration of the recorded interferogram of the letters'XOU'.

Digitized by UCC, Library

Appendix G continued

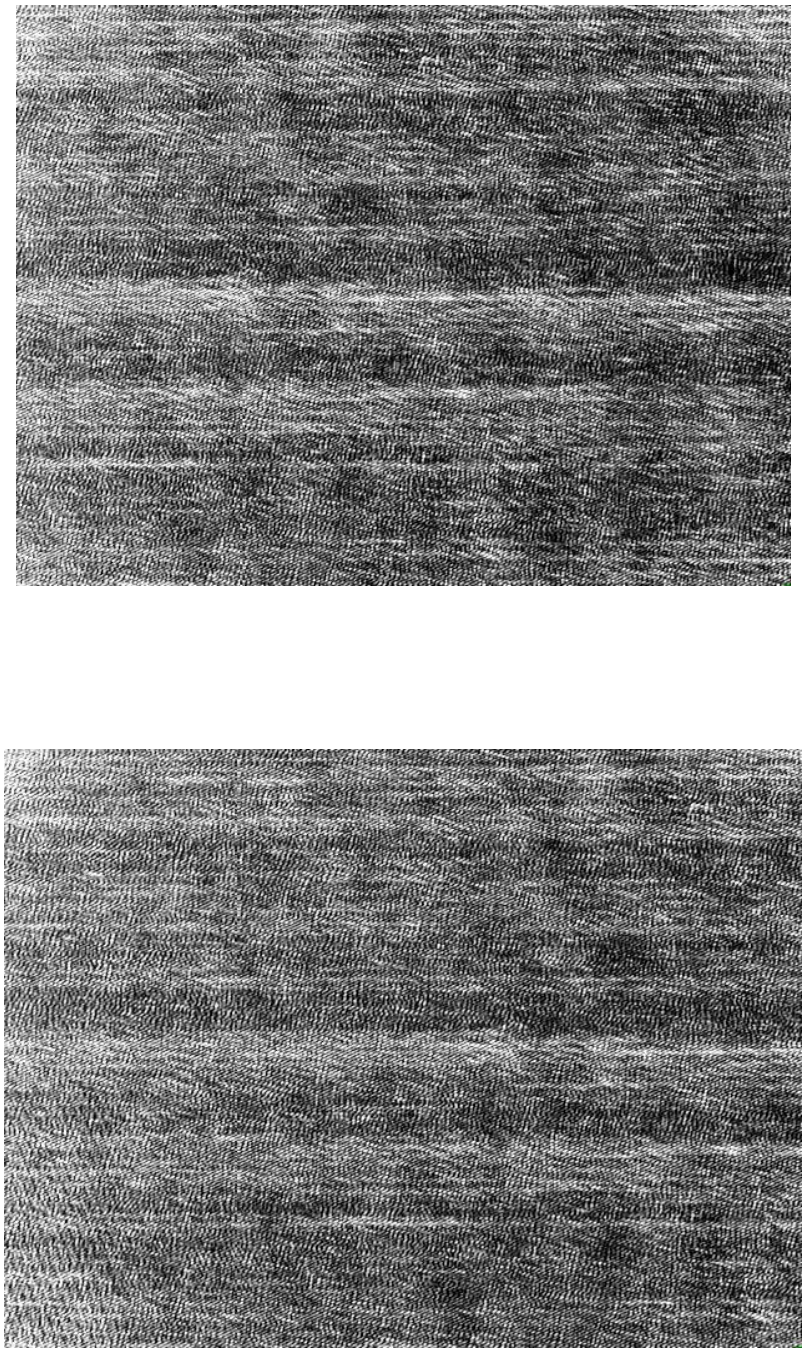

Figure G:The in-line transmission configuration of the recorded interferogram of the letters'ROU'.

Digitized by UCC, Library

Appendix G continued

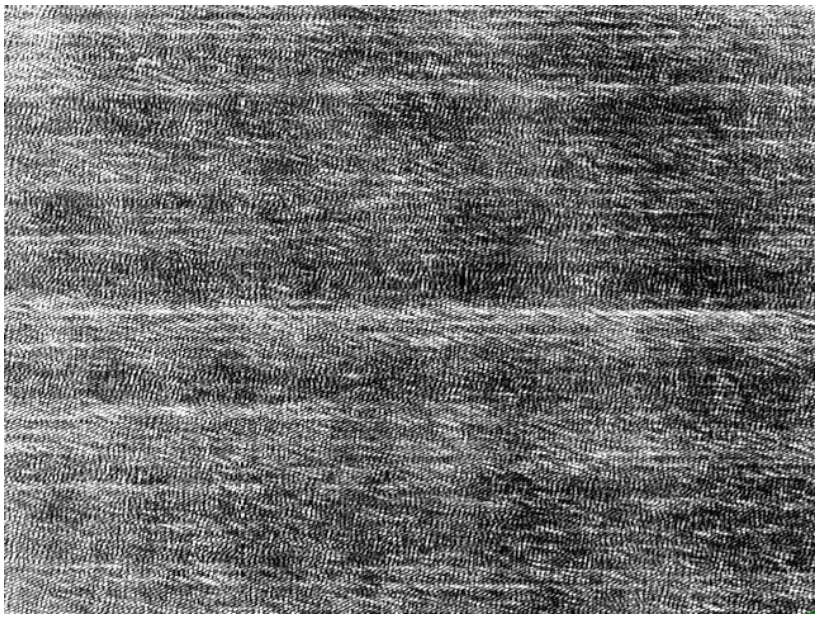

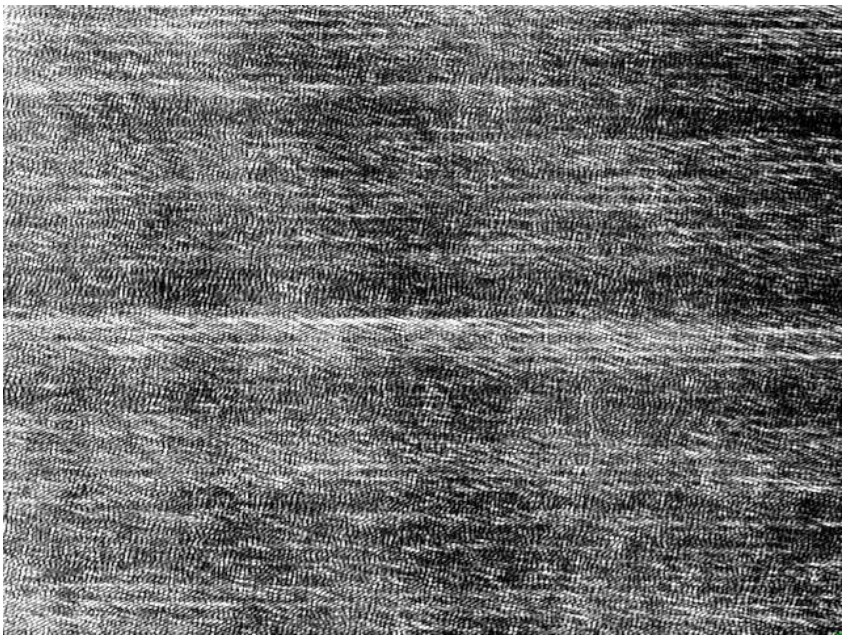

Figure G:The in-line transmission configuration of the recorded interferogram of the letters'ROU'.

Digitized by UCC, Library

Appendix G continued

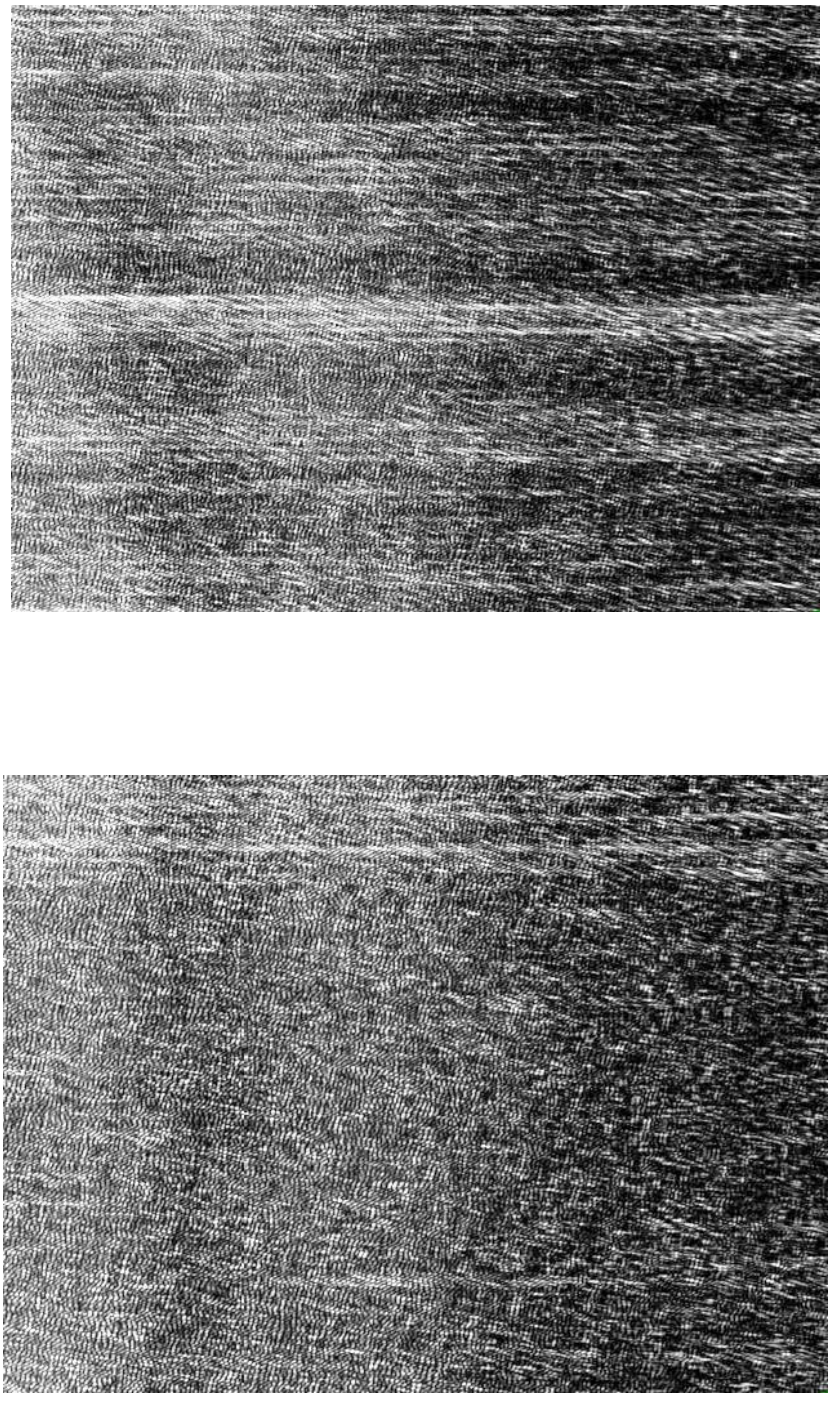

Figure G:The in-line transmission configuration of the recorded interferogram of the letters'XOU'.

Digitized by UCC, Library

Appendix G continued

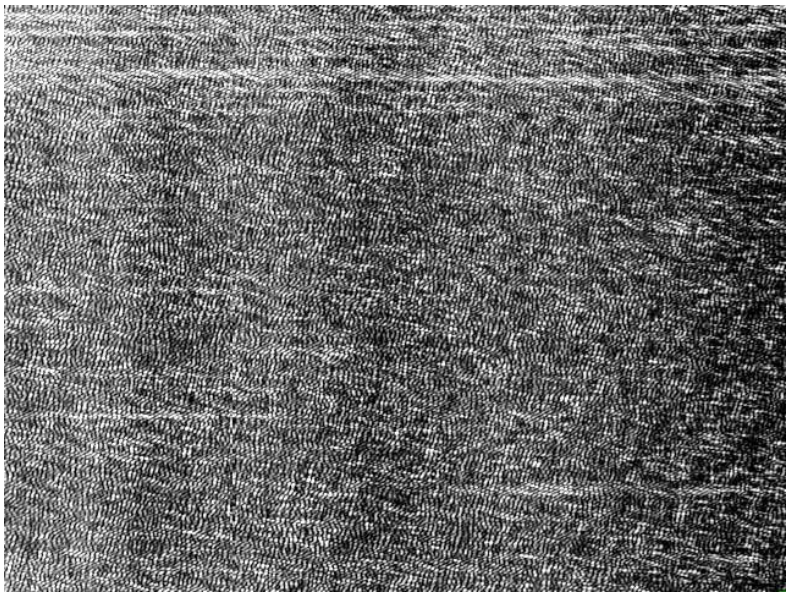

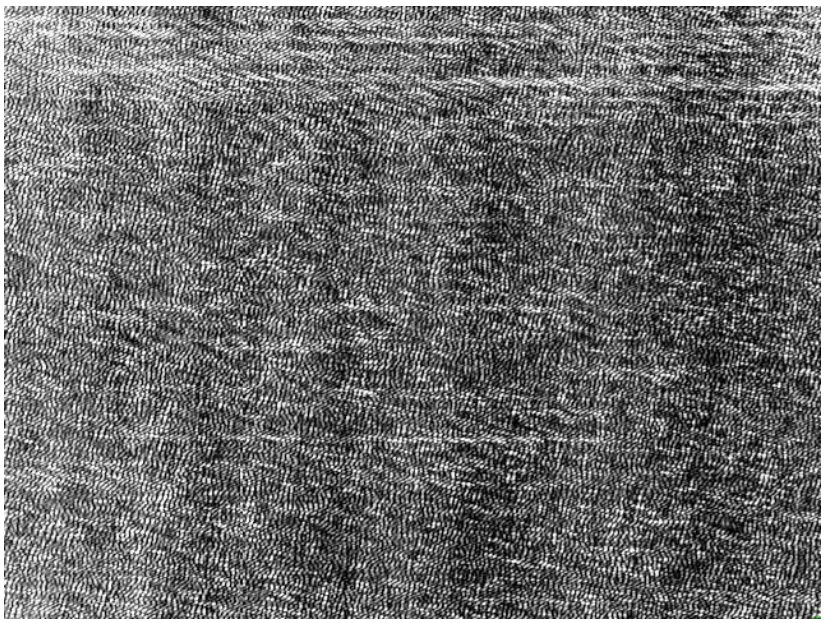

Figure G:The in-line transmission configuration of the recorded interferogram of the USAF test target.

Digitized by UCC, Library

Appendix G continued

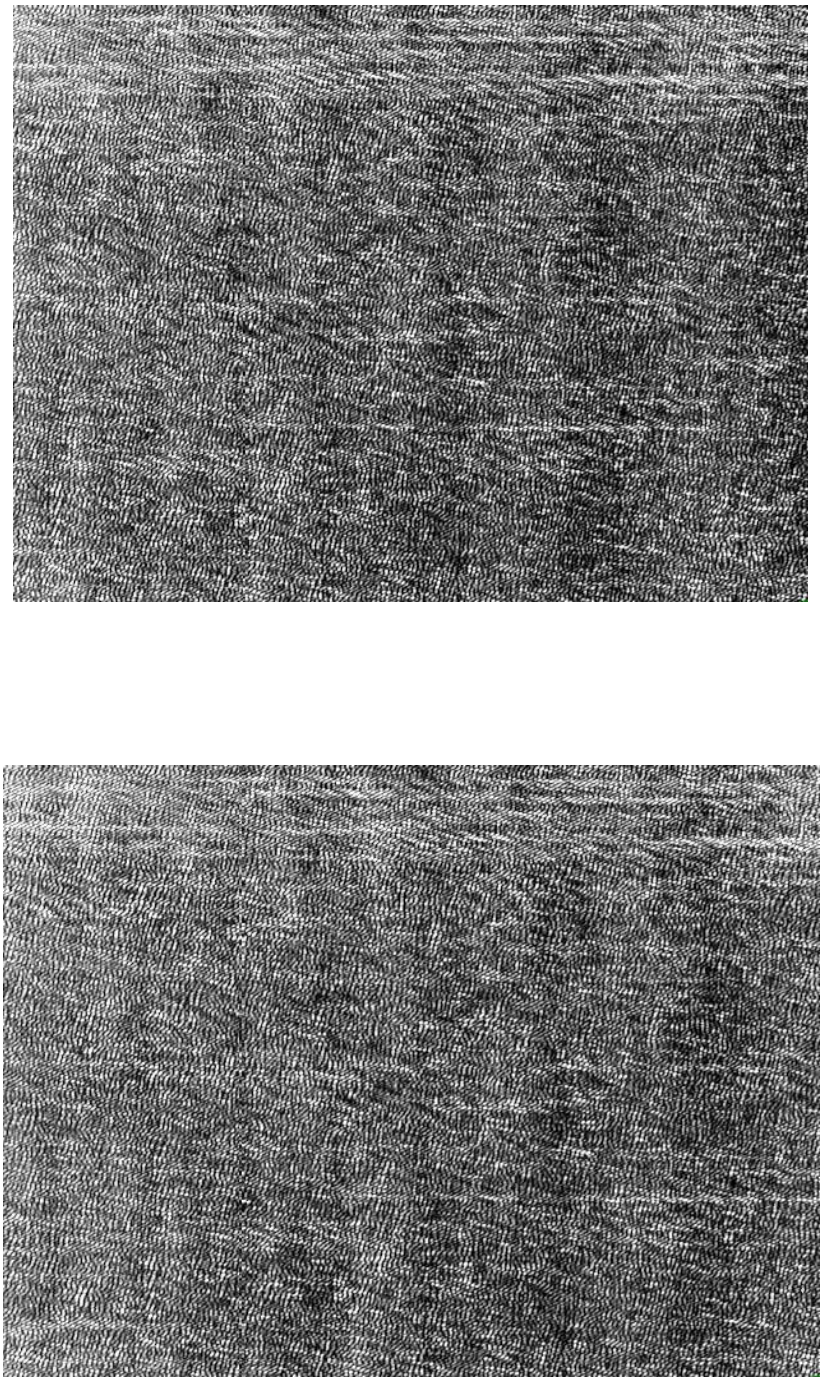

Figure G:The in-line transmission configuration of the recorded interferogram of the USAF test target.

Digitized by UCC, Library

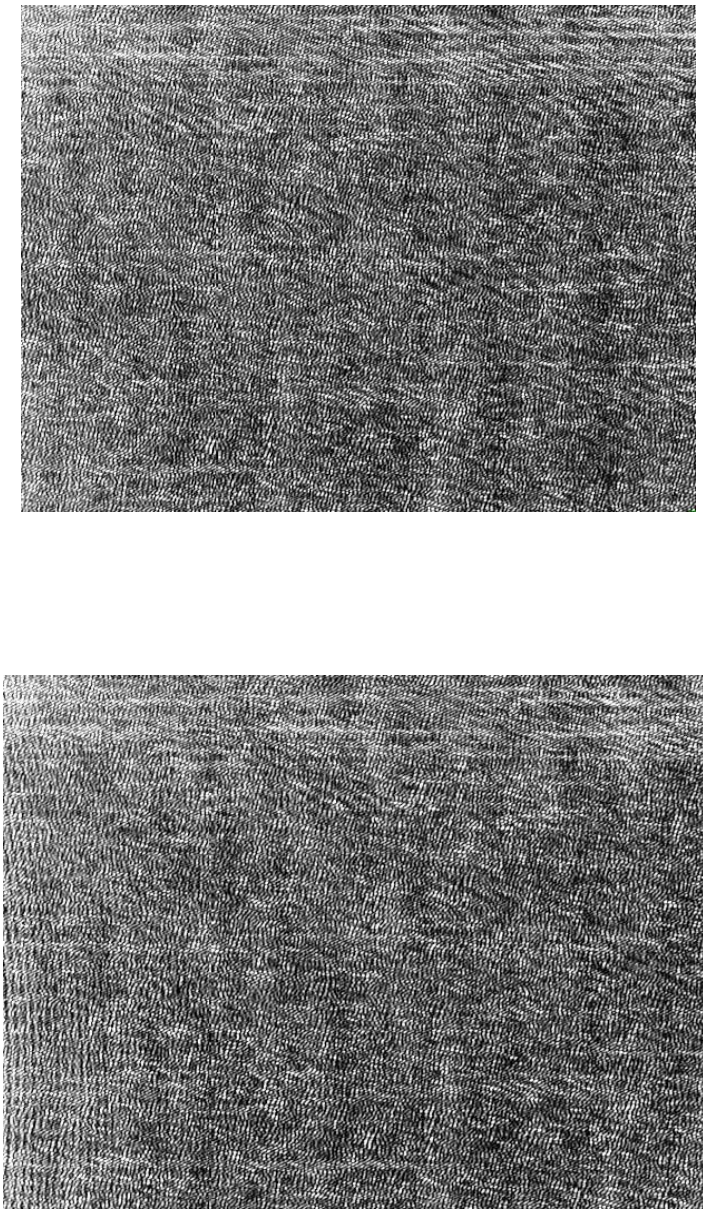

Figure G:The in-line transmission configuration of the recorded interferogram of the USAF test target.

Digitized by UCC, Library

Appendix G continued

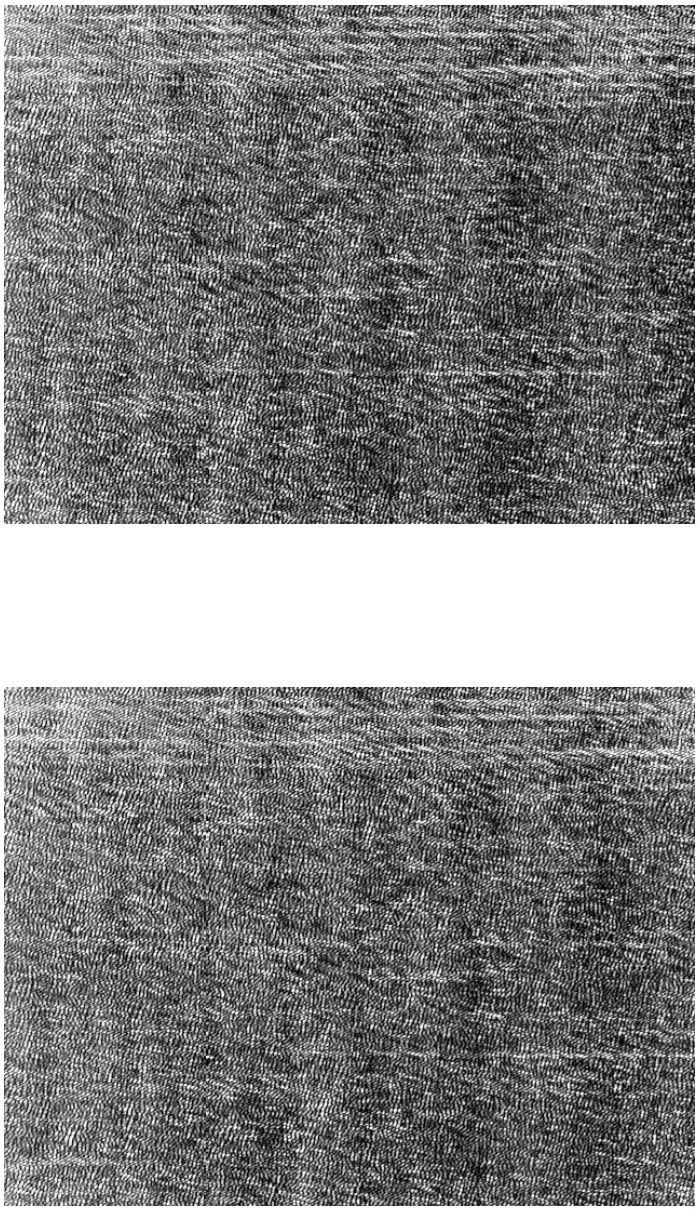

Figure G:The in-line transmission configuration of the recorded interferogram of the USAF test target

Digitized by UCC, Library

Appendix G continued

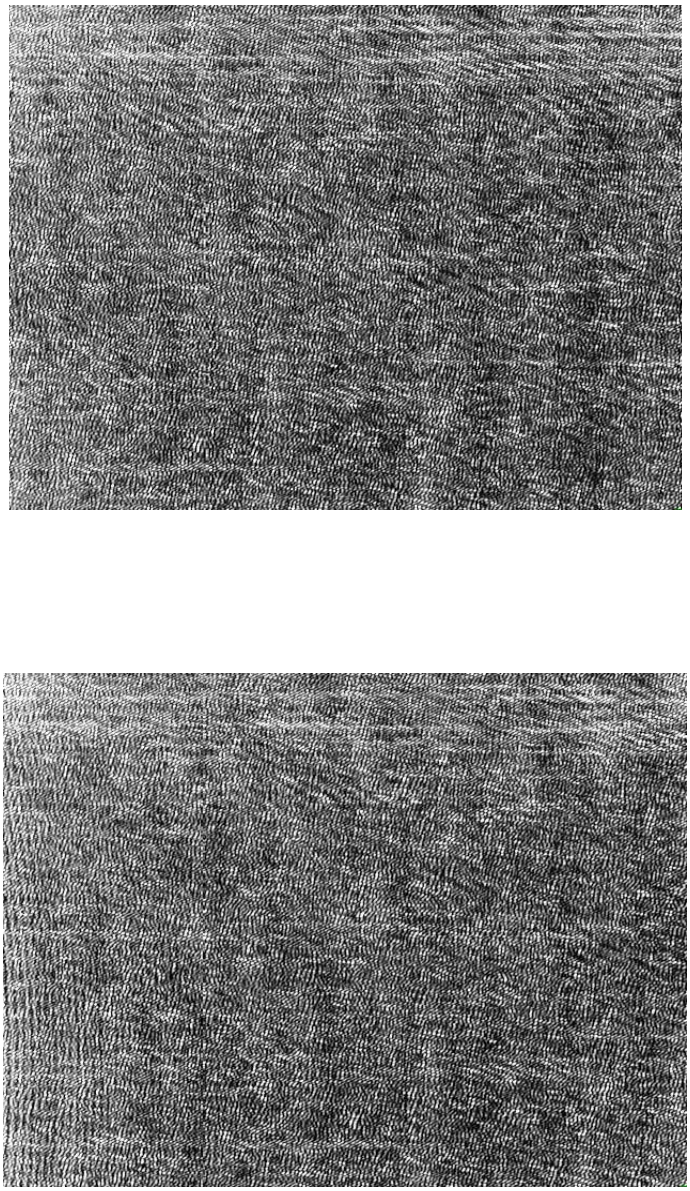

Figure G:The off-axis reflection configuration of the recorded interferogram of the Aluminium disk.

Digitized by UCC, Library

Appendix G continued

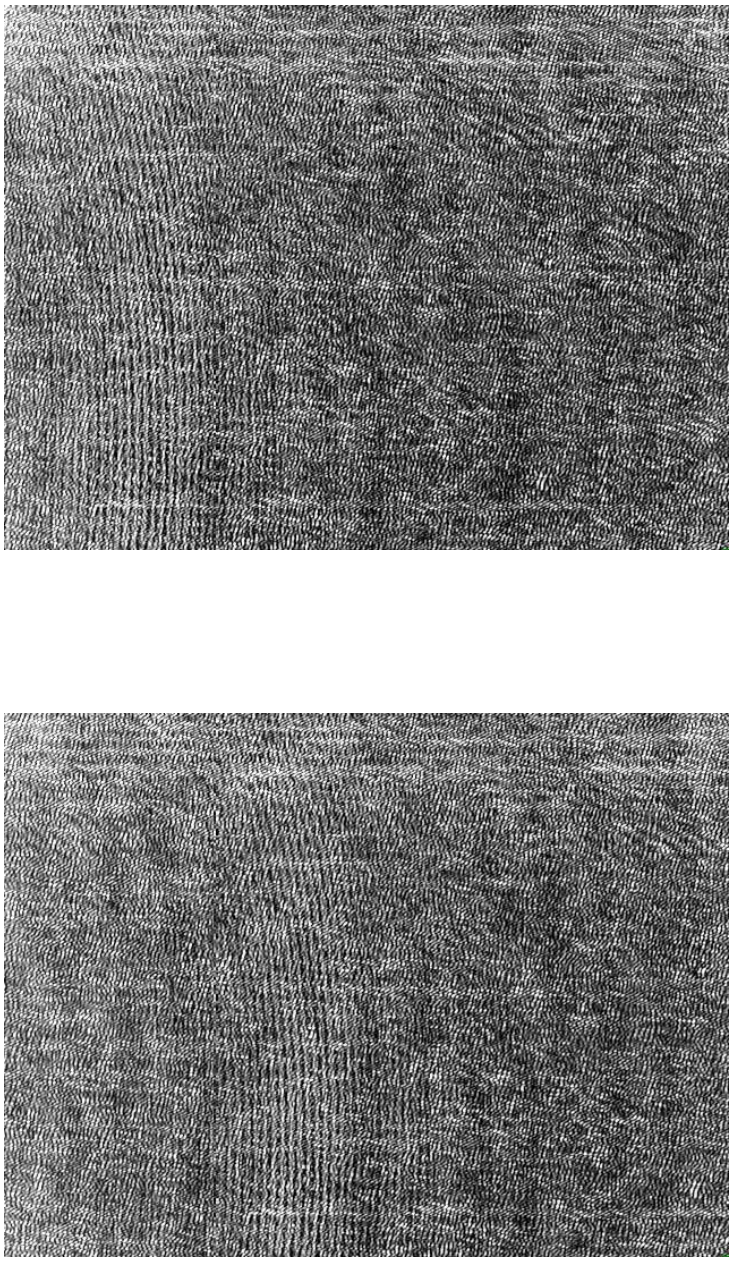

Figure G:The off-axis reflection configuration of the recorded interferogram of the Aluminium disk.

Digitized by UCC, Library

Appendix G continued

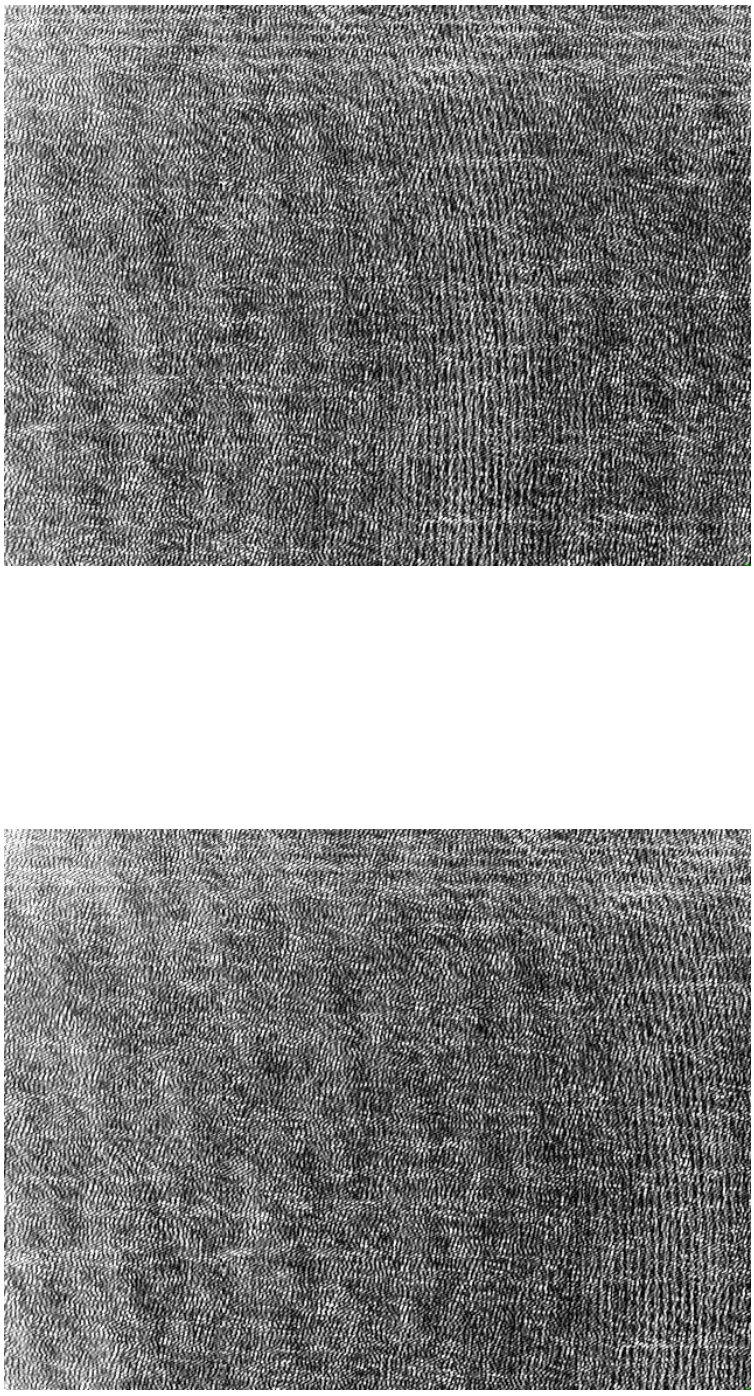

Figure G:The off-axis reflection configuration of the recorded interferogram of the Aluminium disk.

Digitized by UCC, Library

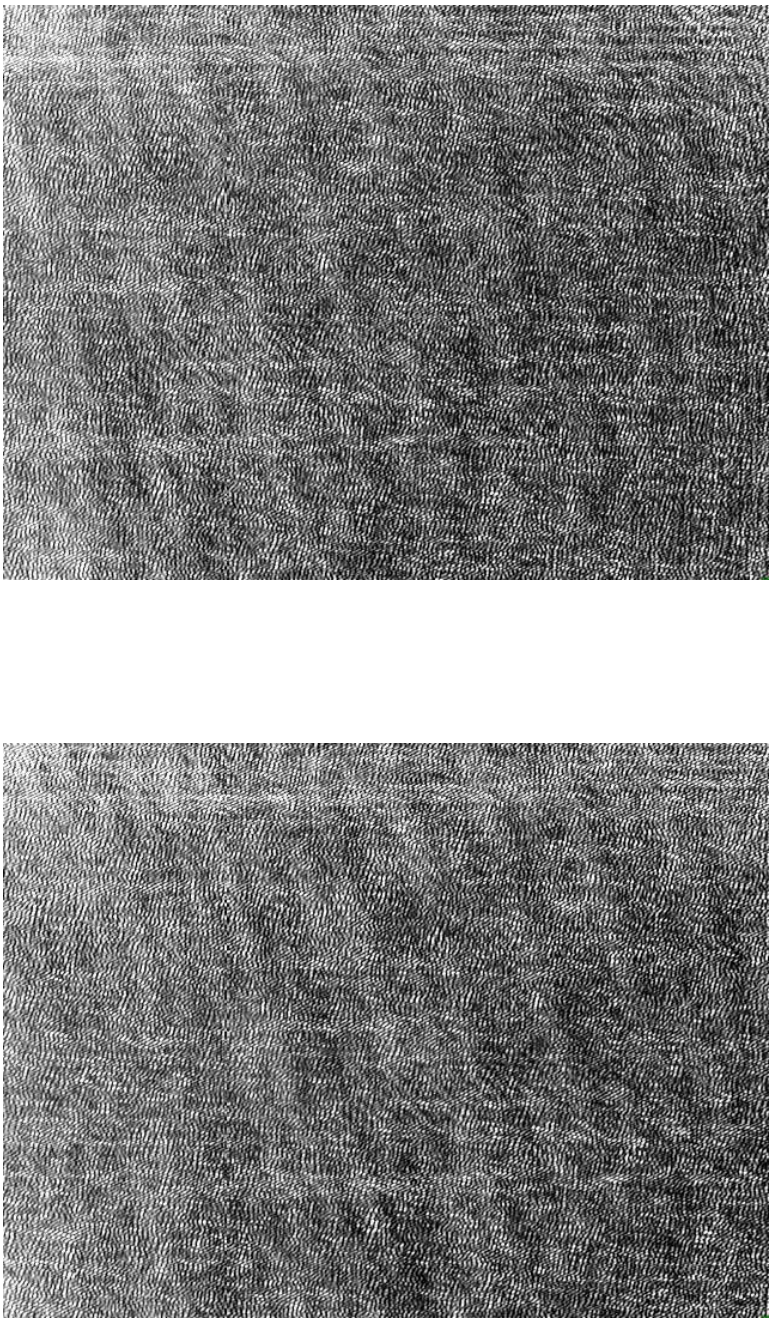

Figure G:The off-axis reflection configuration of the recorded interferogram of the one Euro coin.

Digitized by UCC, Library

Appendix G continued

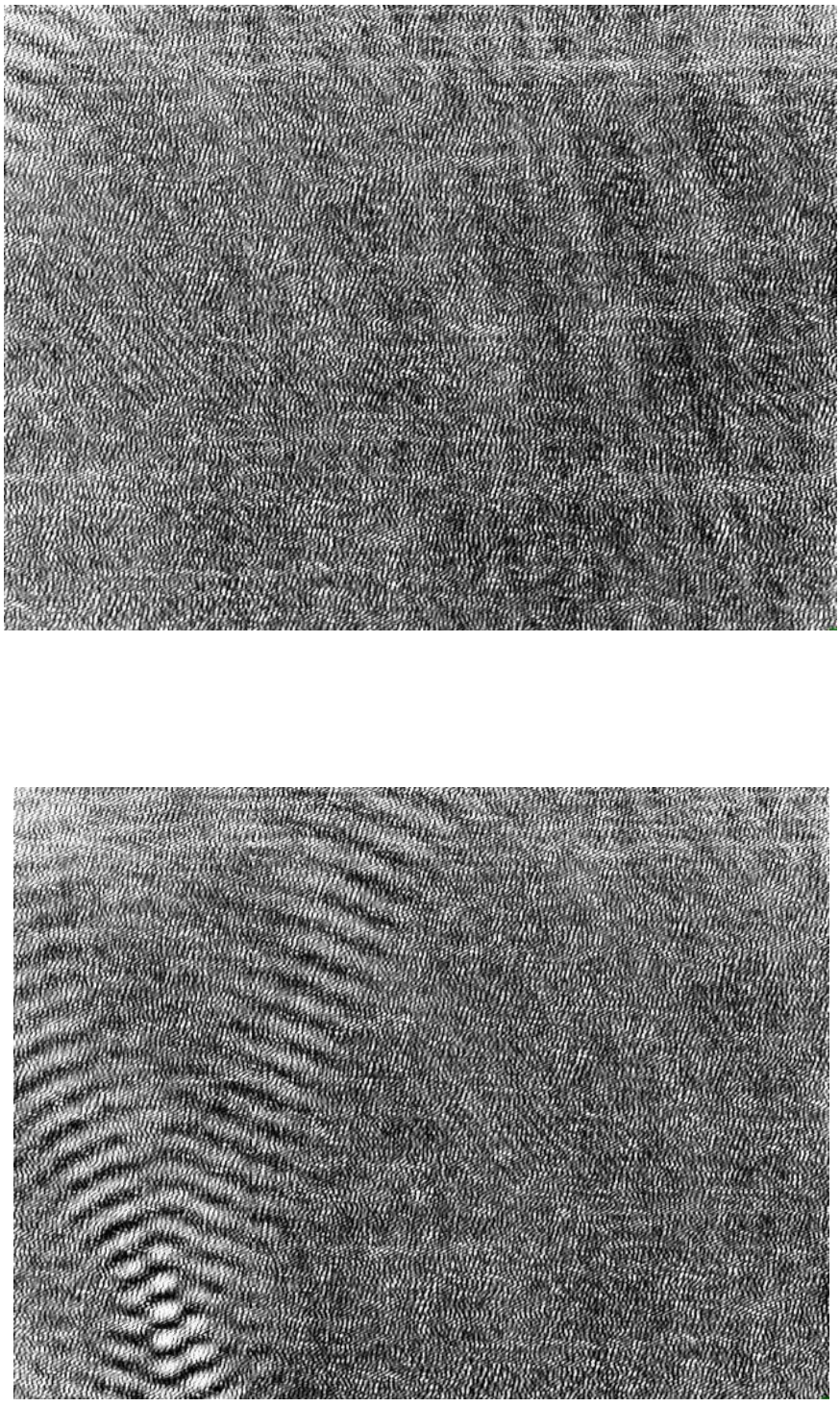

Figure G:The off-axis reflection configuration of the recordedinterferogram of the one Euro coin.

Digitized by UCC, Library

Appendix G continued

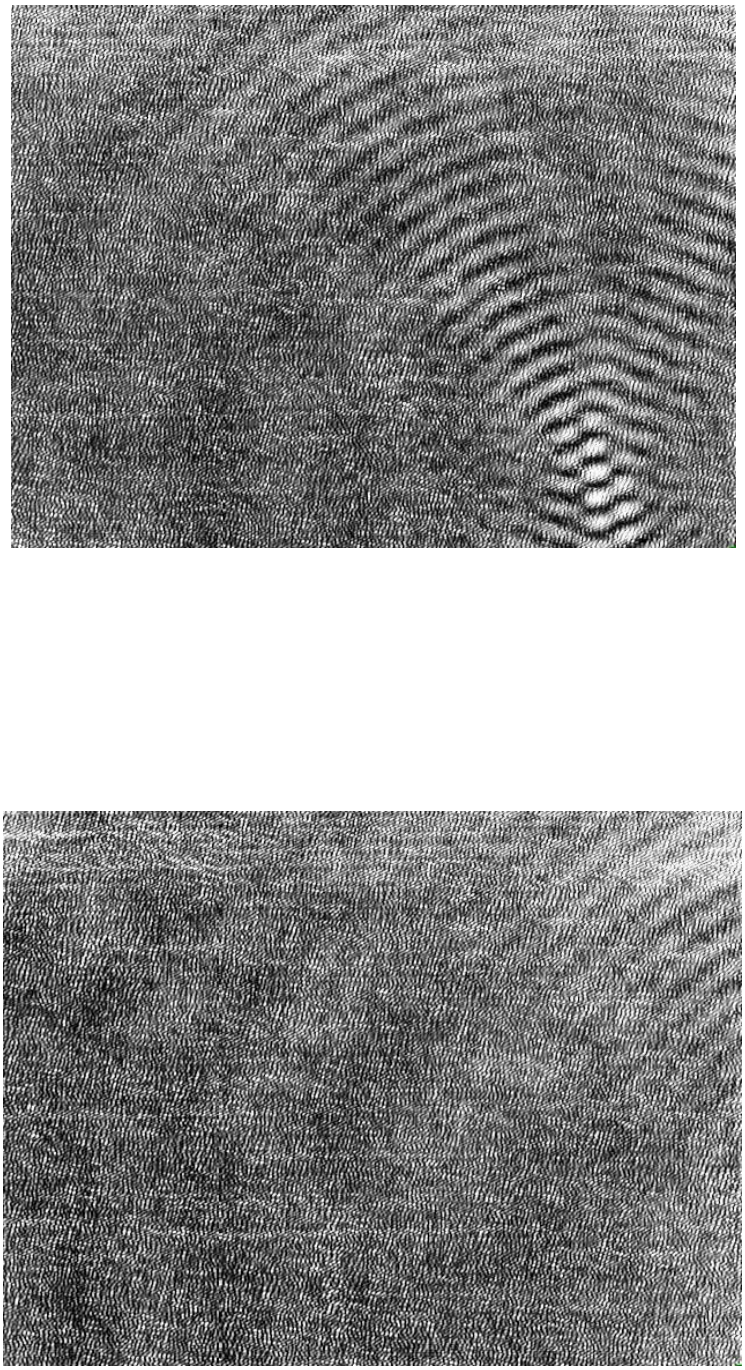

Figure G:The off-axis reflection configuration of the recorded interferogram of the two Euro coin.

Digitized by UCC, Library

Appendix G continued

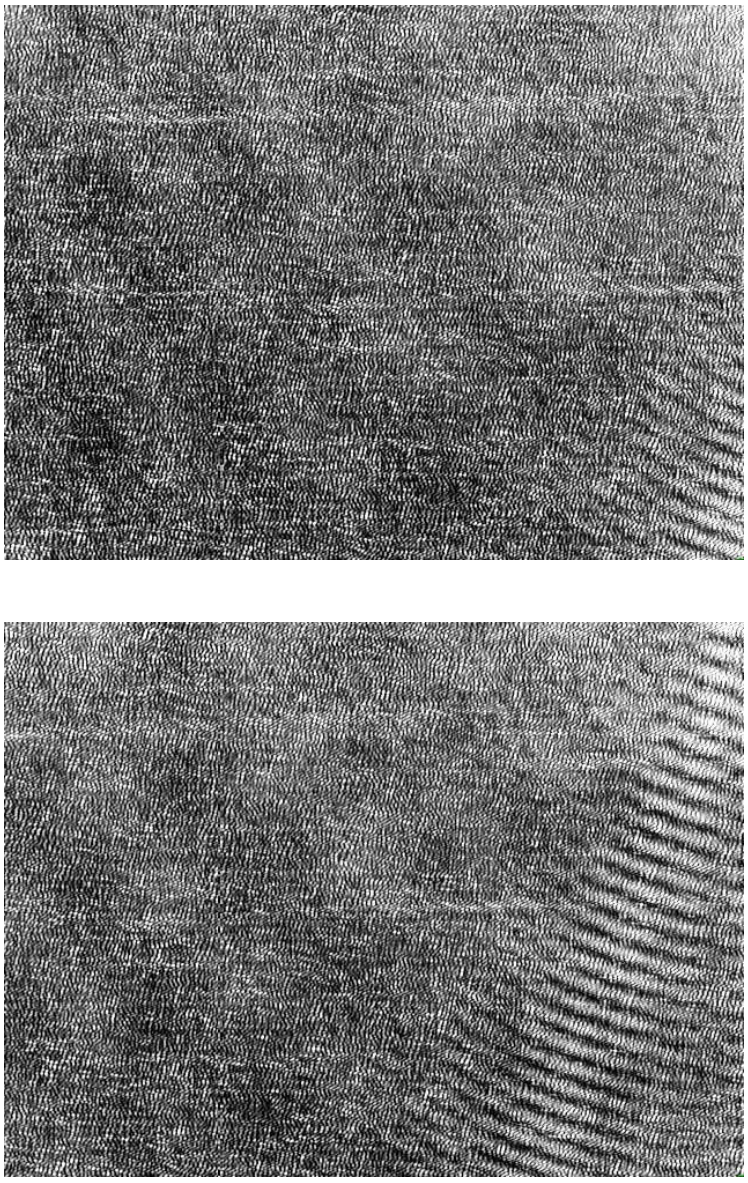

Figure G:The off-axis reflection configuration of the recorded interferogram of the two Euro coin.

Digitized by UCC, Library

Appendix G continued

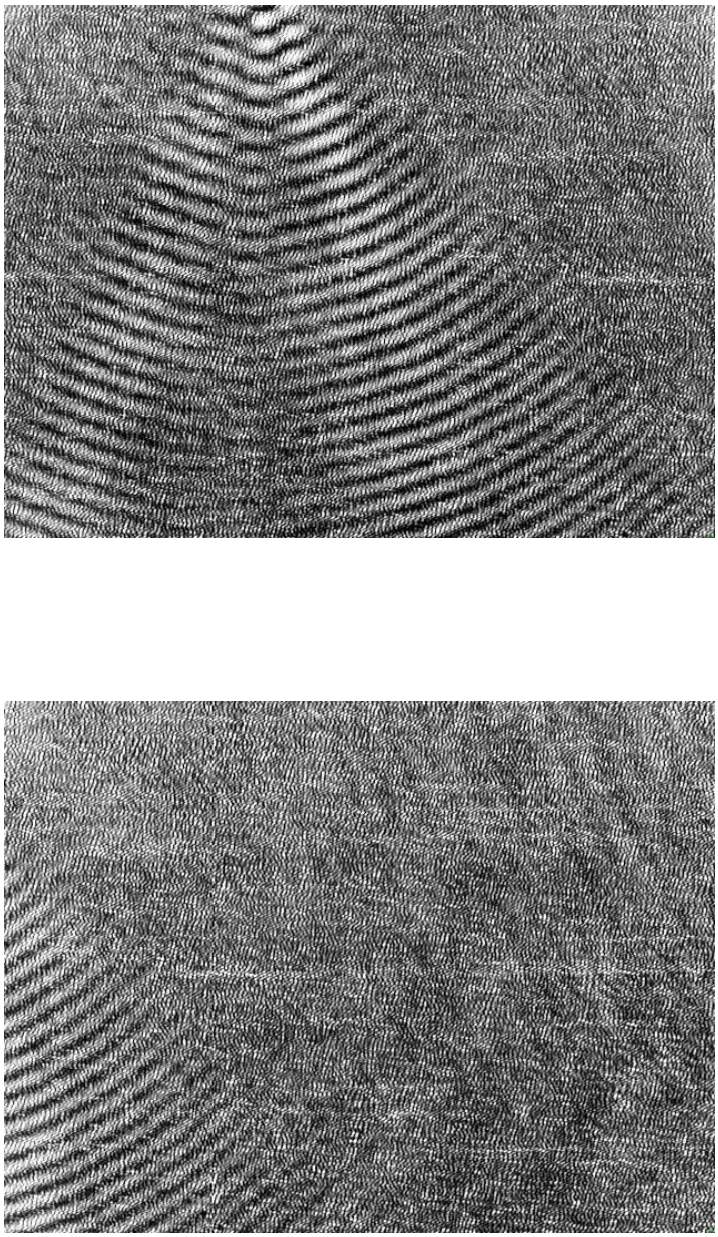

Figure G:The off-axis reflection configuration of the recorded interferogram of the two Euro coin.

Digitized by UCC, Library

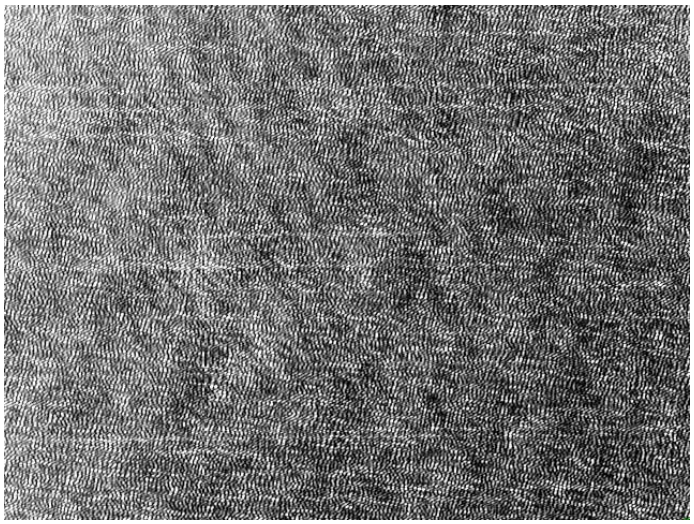

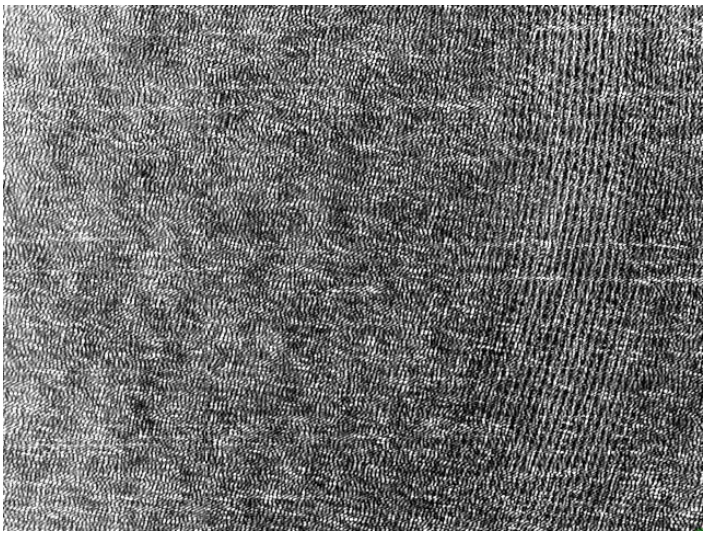

Figure G:The off-axis reflection configuration of the recorded interferogram of the two Euro coin.

Digitized by UCC, Library

Appendix G continued

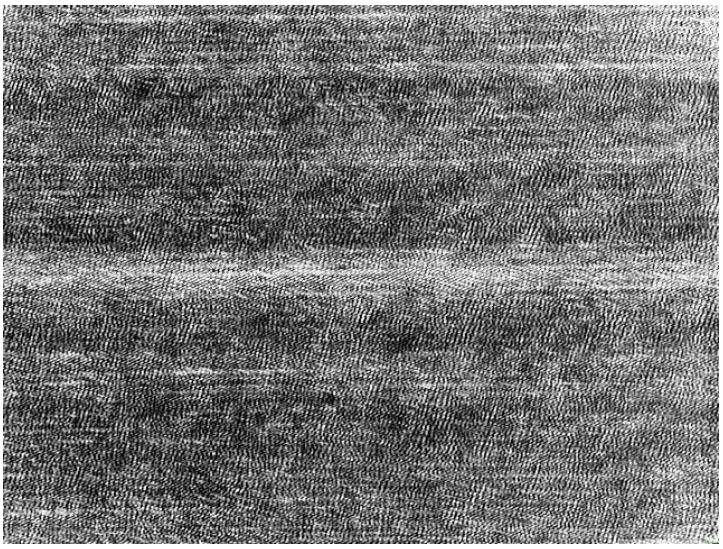

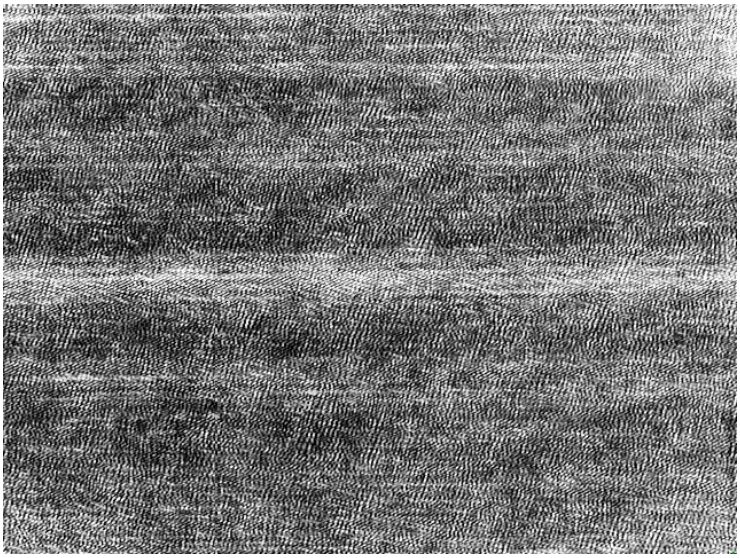

Figure G:The off-axis reflection configuration of the recorded interferogram of the lens mount.

Digitized by UCC, Library

Appendix G continued

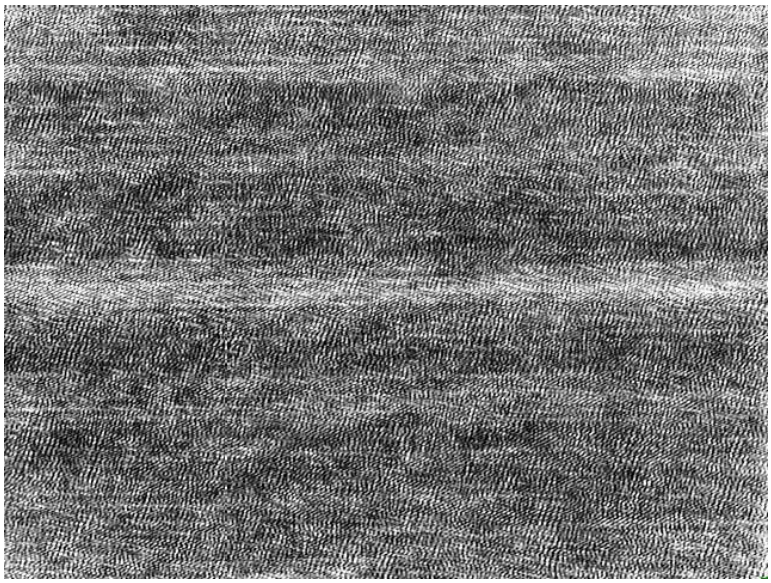

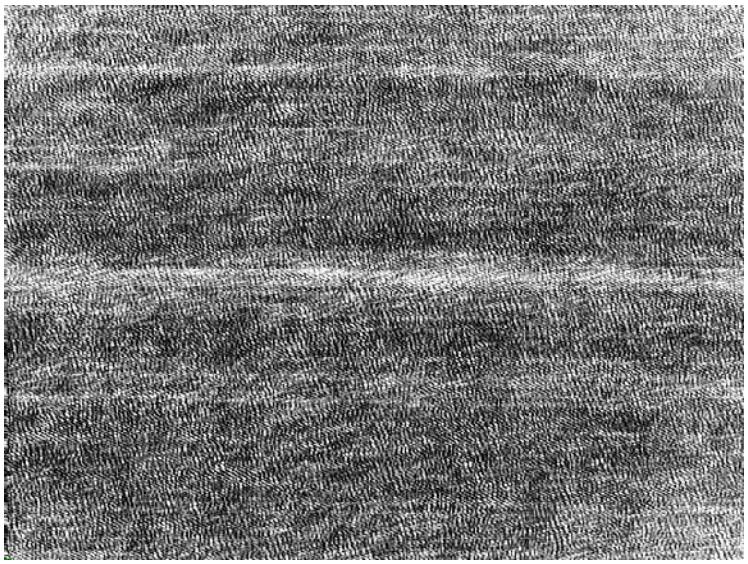

Figure G:The off-axis reflection configuration of the recorded interferogram of the lens mount.

Digitized by UCC, Library

Appendix G continued

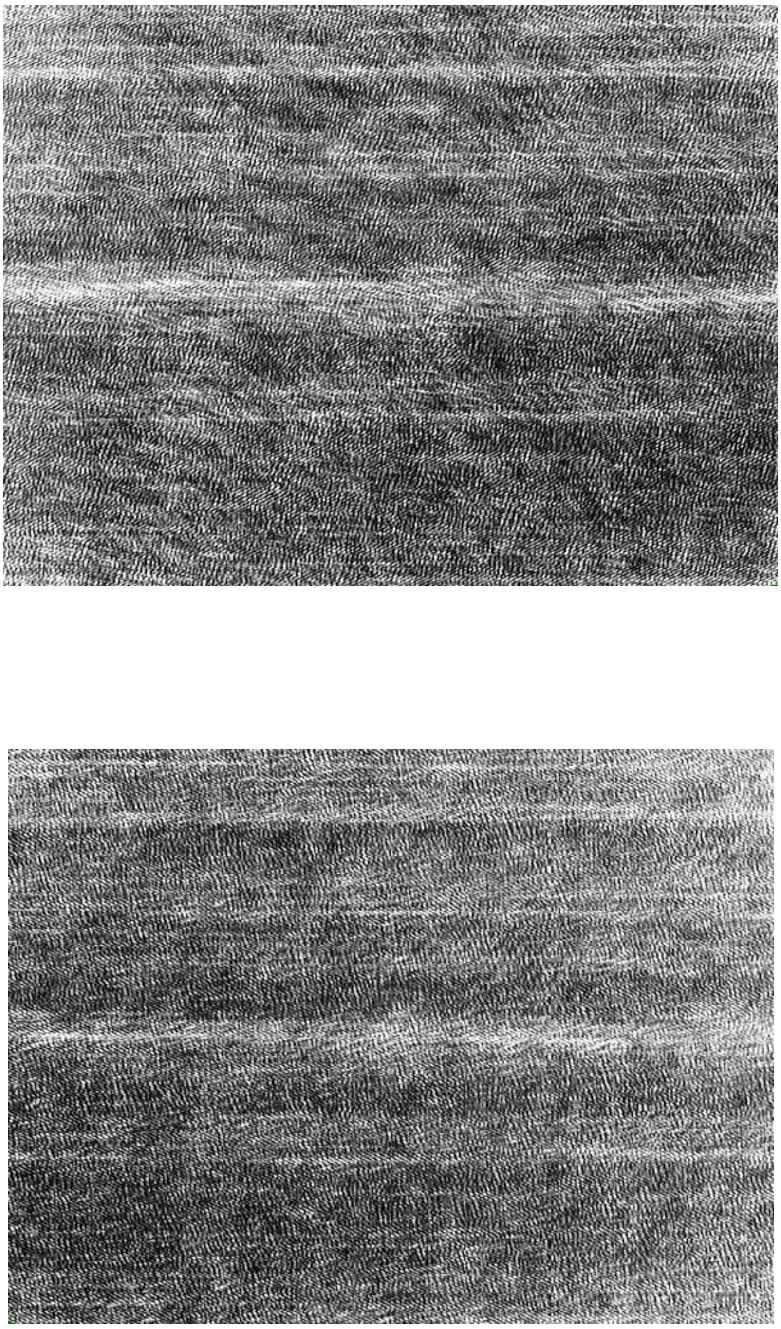

Figure G:The off-axis reflection configuration of the recorded interferogram of the lens mount.

Digitized by UCC, Library

Appendix G continued

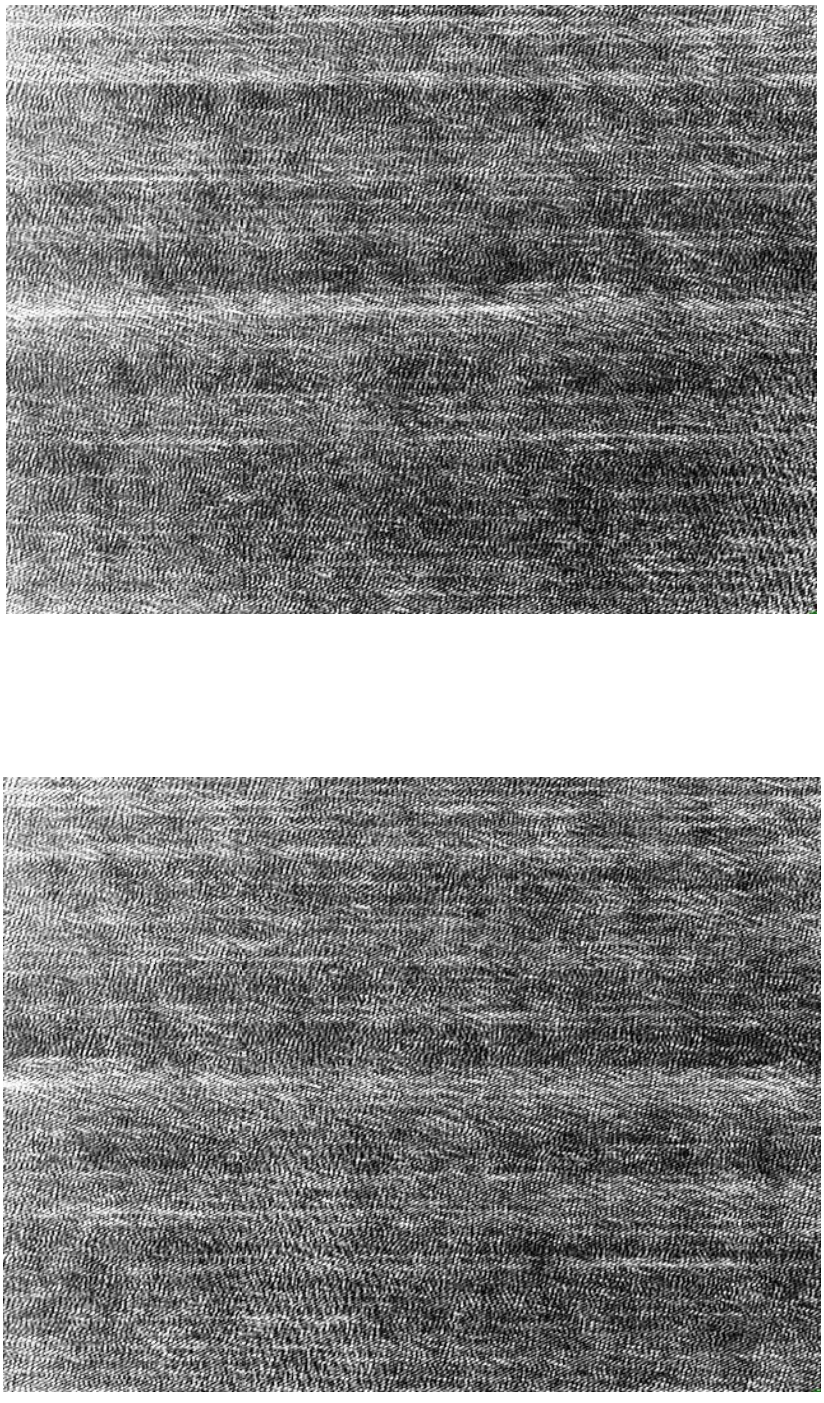

Figure G:The off-axis reflection configuration of the recorded interferogram of the lens mount.

Digitized by UCC, Library

Appendix G continued

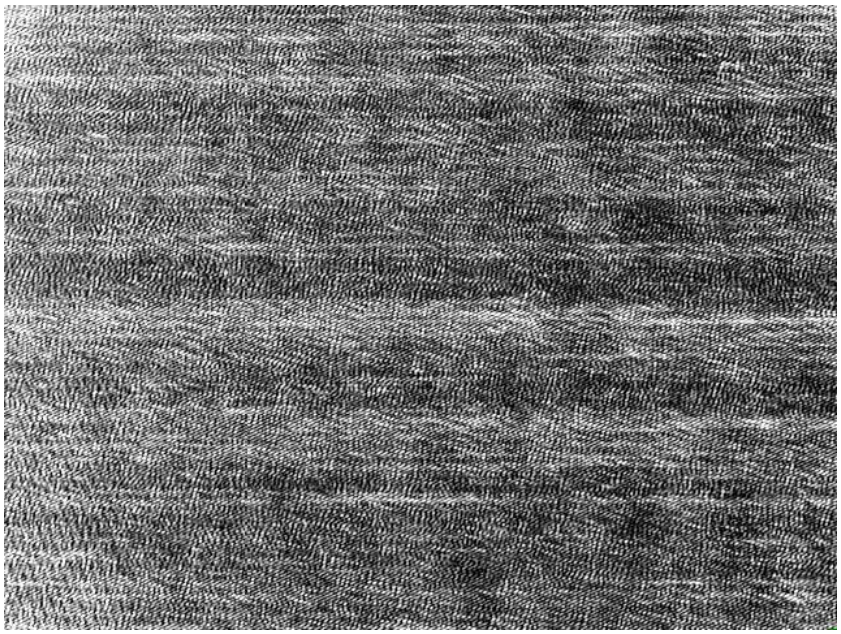

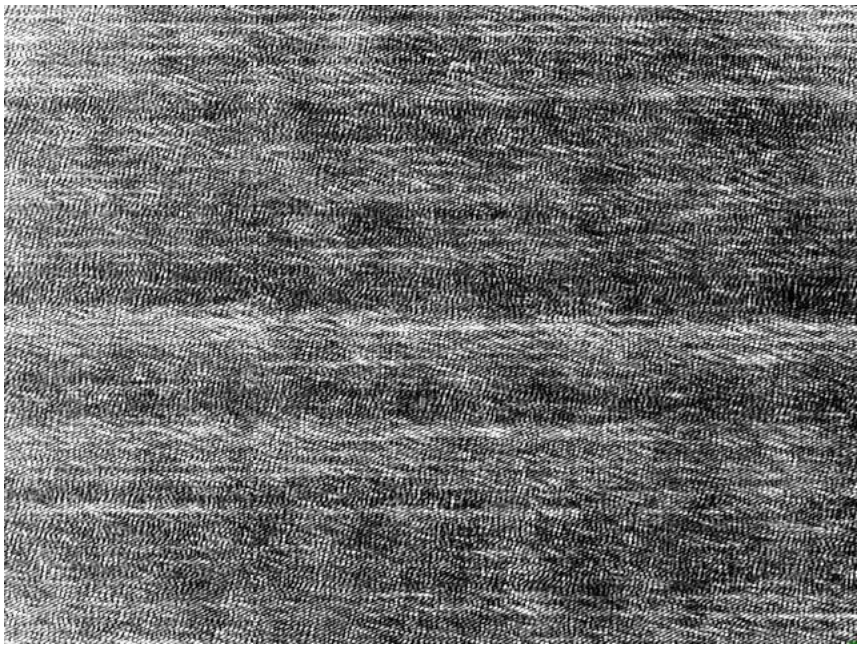

Figure G:The off-axis reflection configuration of the recorded interferogram of the lens mount.

Digitized by UCC, Library

Appendix G continued

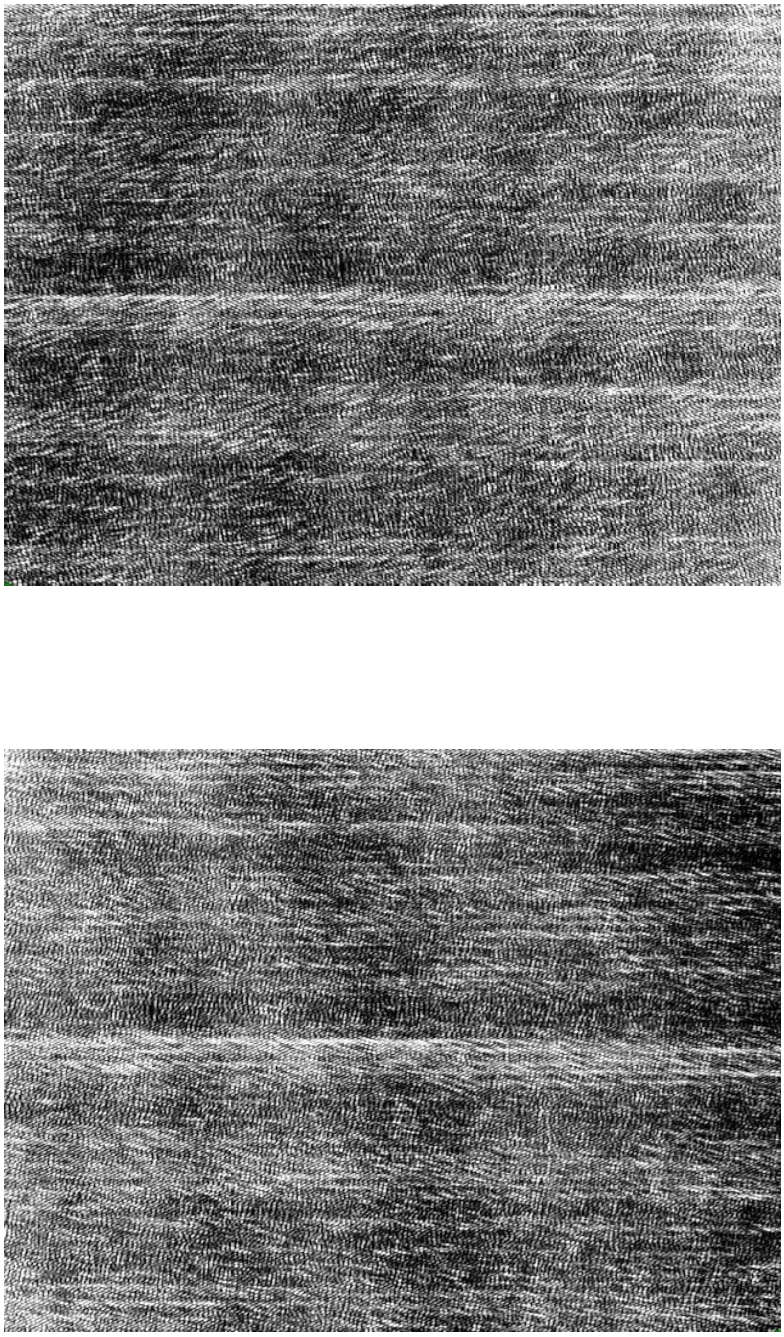

Figure G:The off-axis reflection configuration of the recorded interferogram of the lens mount.

Digitized by UCC, Library

Appendix G continued

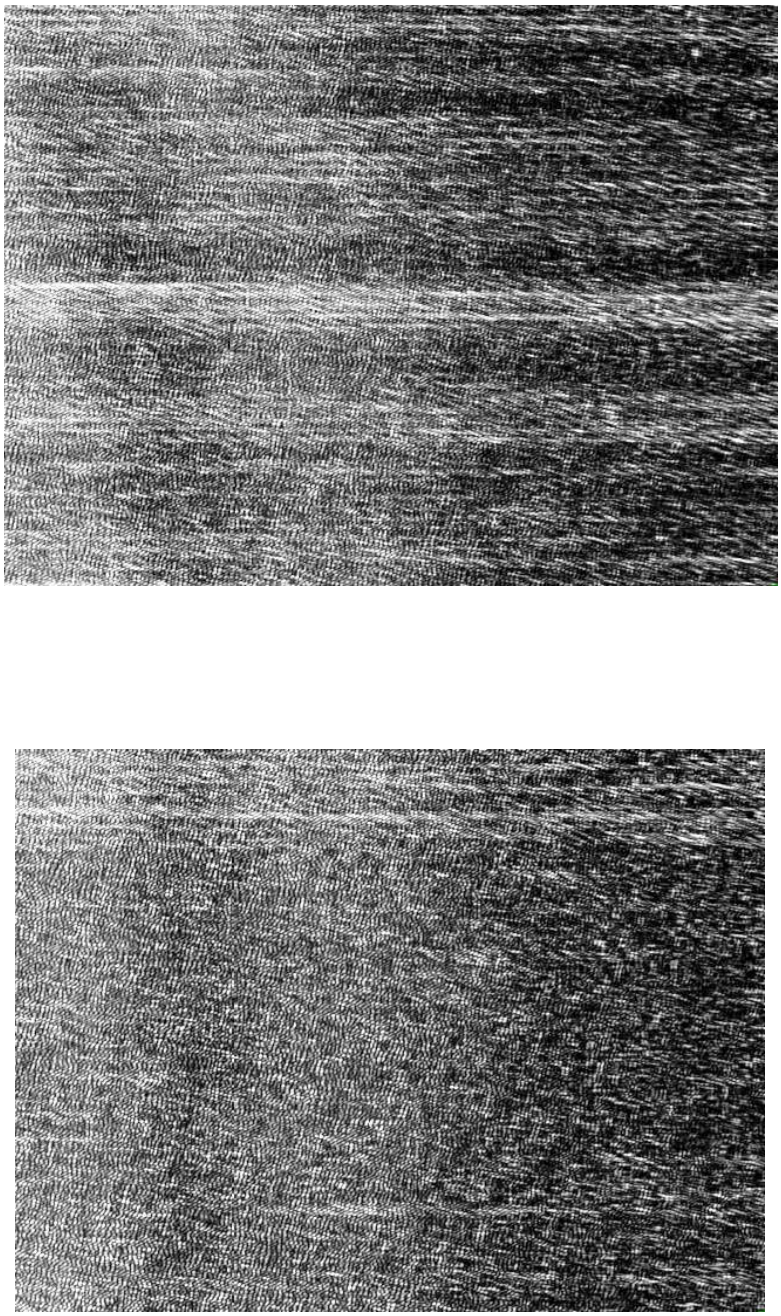

Figure G:The off-axis reflection configuration of the recorded interferogram of the lens mount.

Digitized by UCC, Library

Appendix G continued

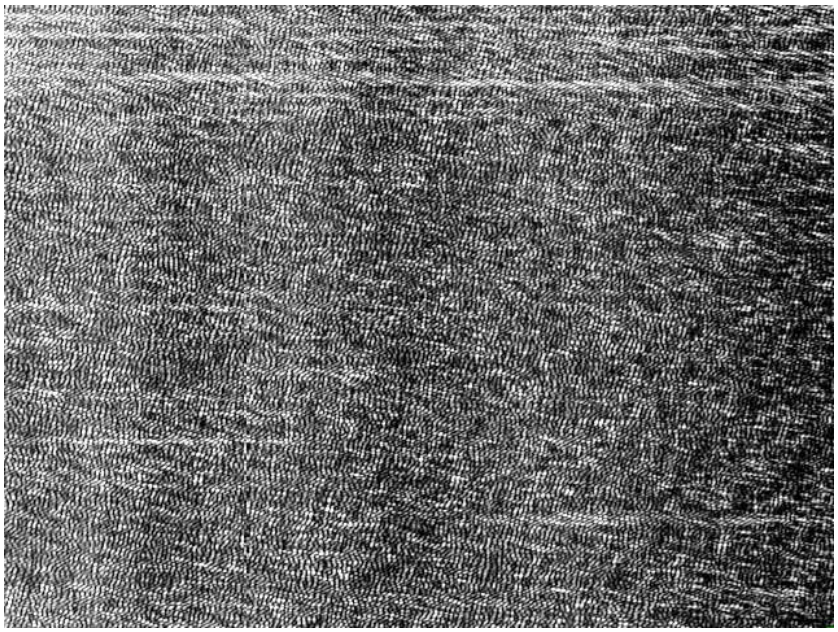

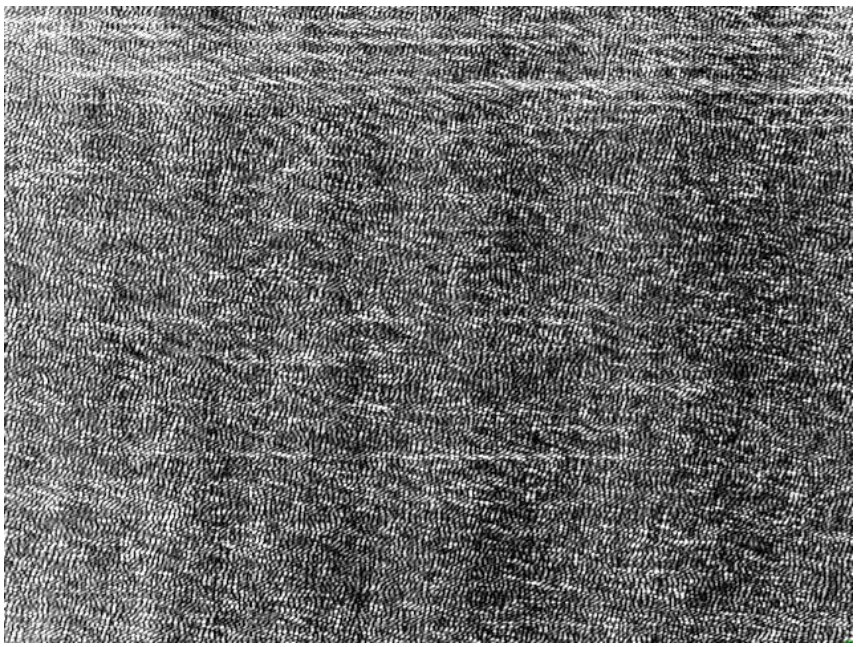

Figure G:The off-axis reflection configuration of the recorded interferogram of Augusto using negative lens.

Digitized by UCC, Library

Appendix G continued

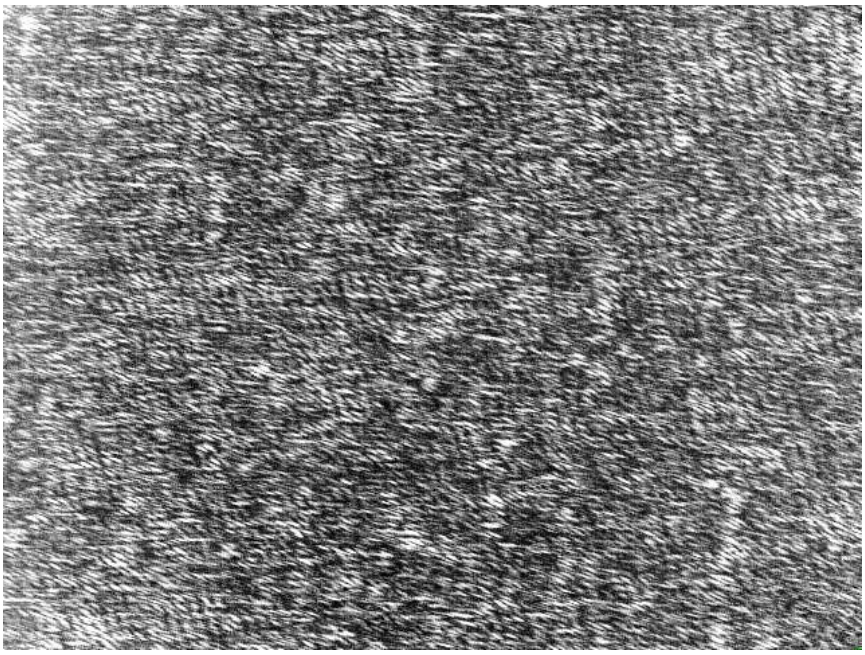

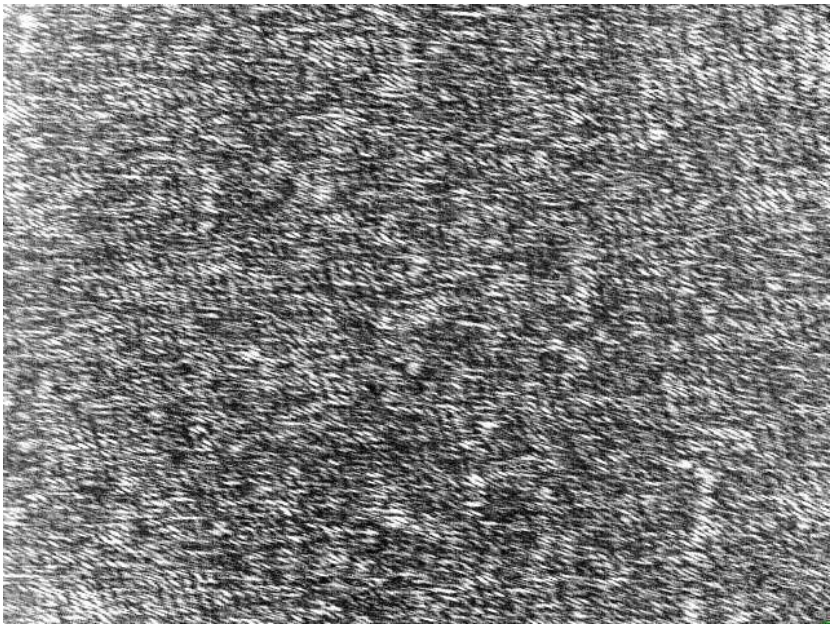

Figure G:The off-axis reflection configuration of the rcorded interferogram of Augusto using negative lens.

Digitized by UCC, Library

Appendix G continued

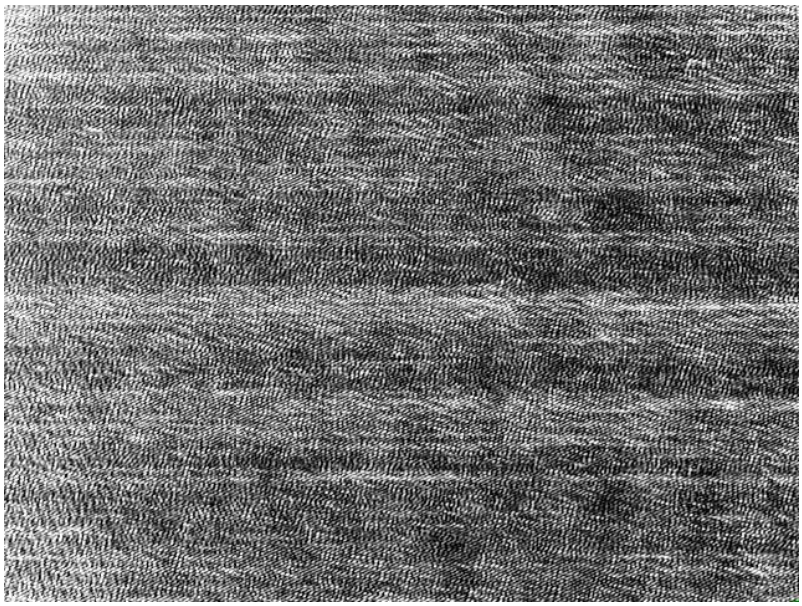

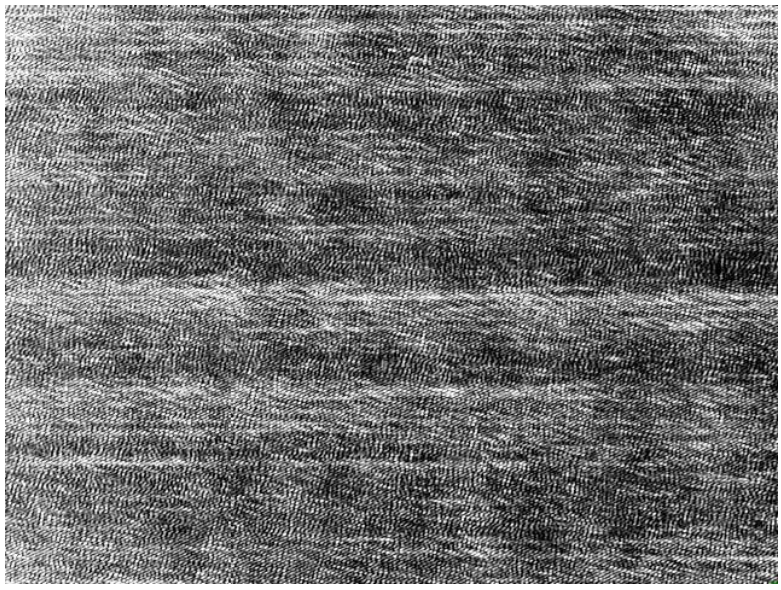

Figure G:The off-axis reflection configuration of the recorded interferogram of Augusto using negative lens.

Digitized by UCC, Library

Appendix G continued

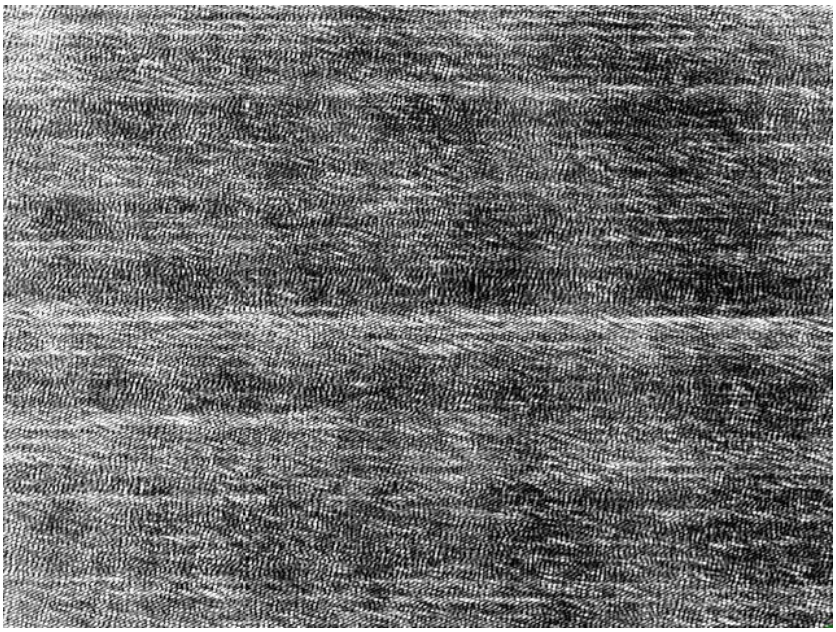

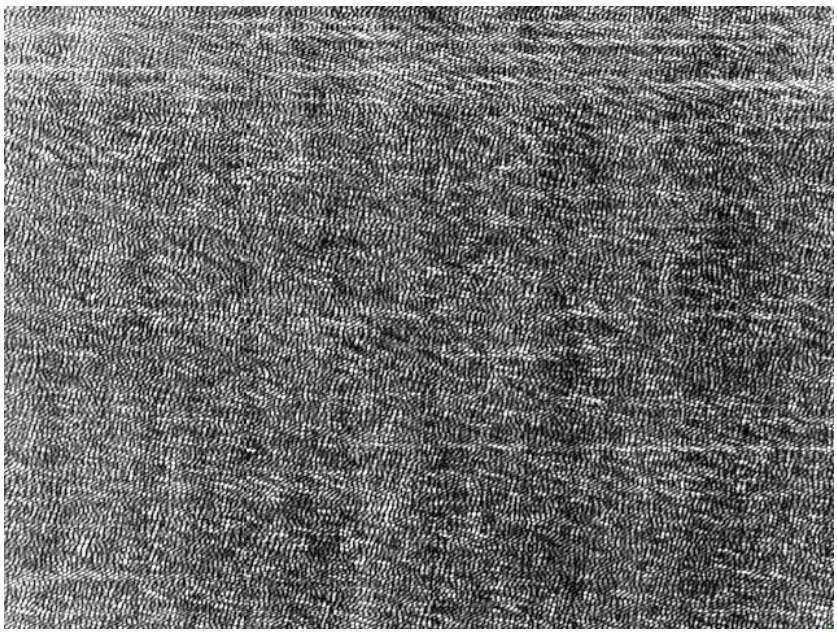

Figure G:The off-axis reflection configuration of the recorded interferogram of Augusto without negative lens.

Digitized by UCC, Library

Appendix G continued

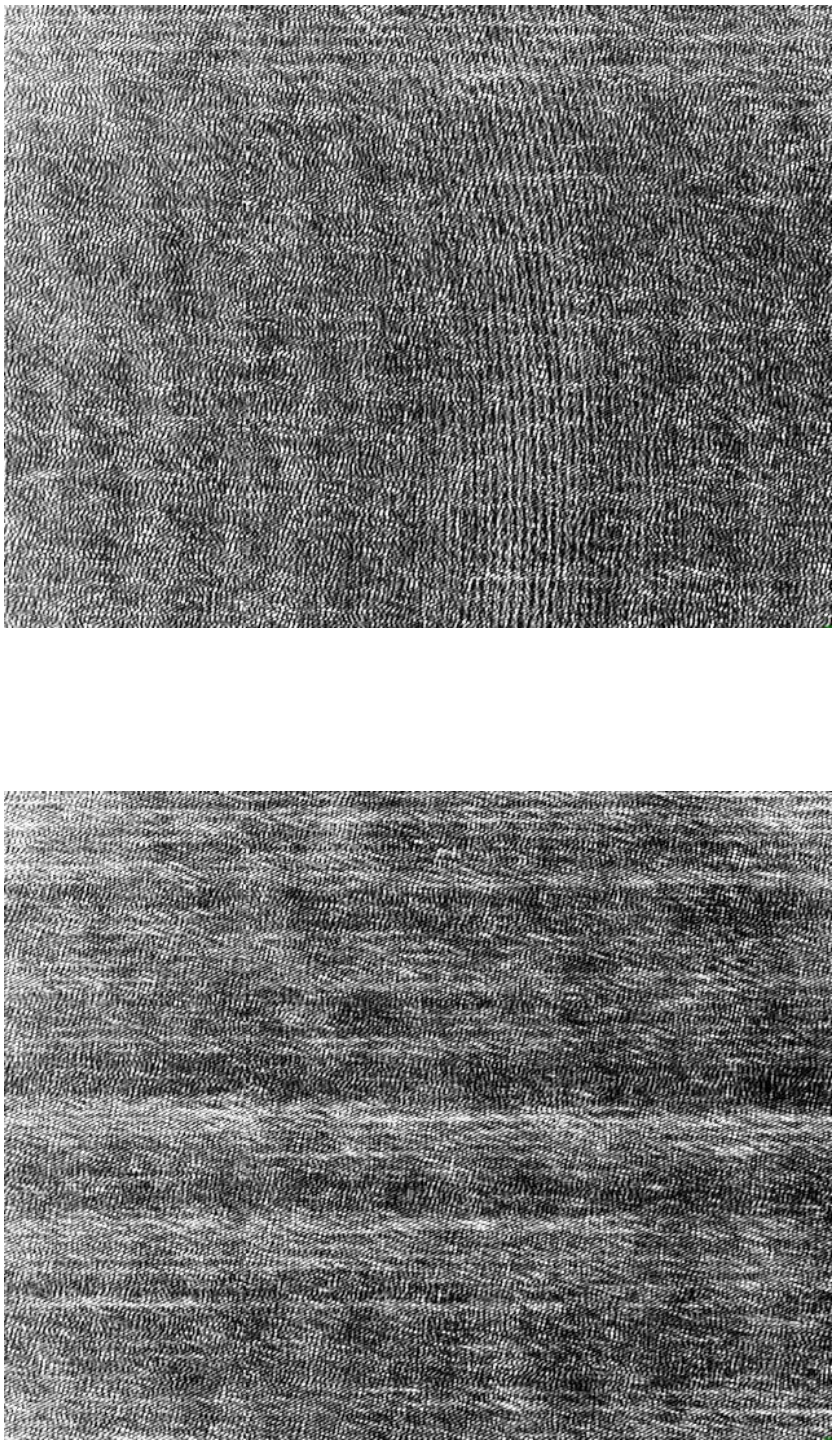

Figure G:The off-axis reflection configuration of the recorded interferogram of Augusto without negative lens.

Digitized by UCC, Library

Appendix G continued

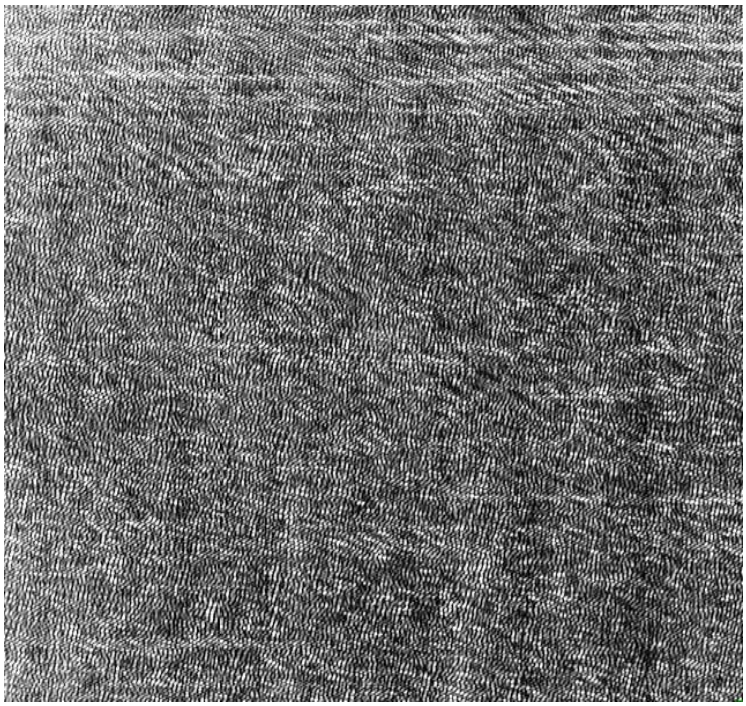

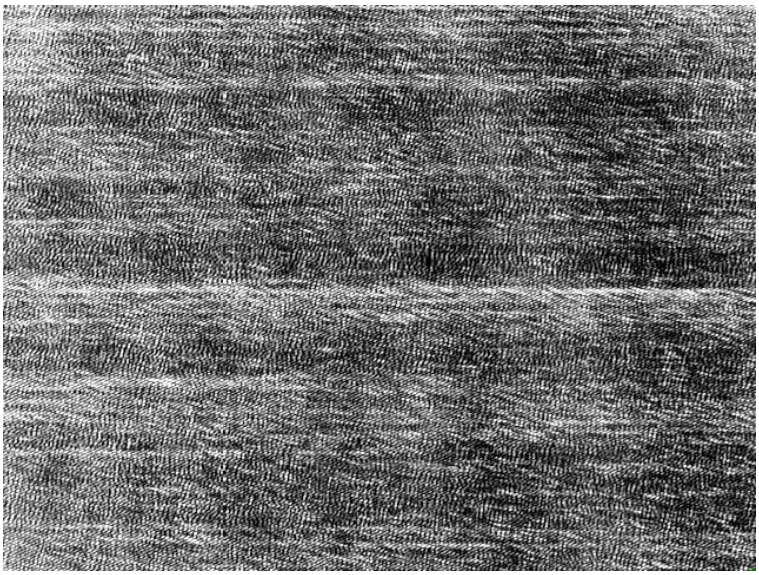

Figure G:The off-axis reflection configuration of the recorded interferogram of Augusto without negative lens.

Digitized by UCC, Library

Appendix G continued

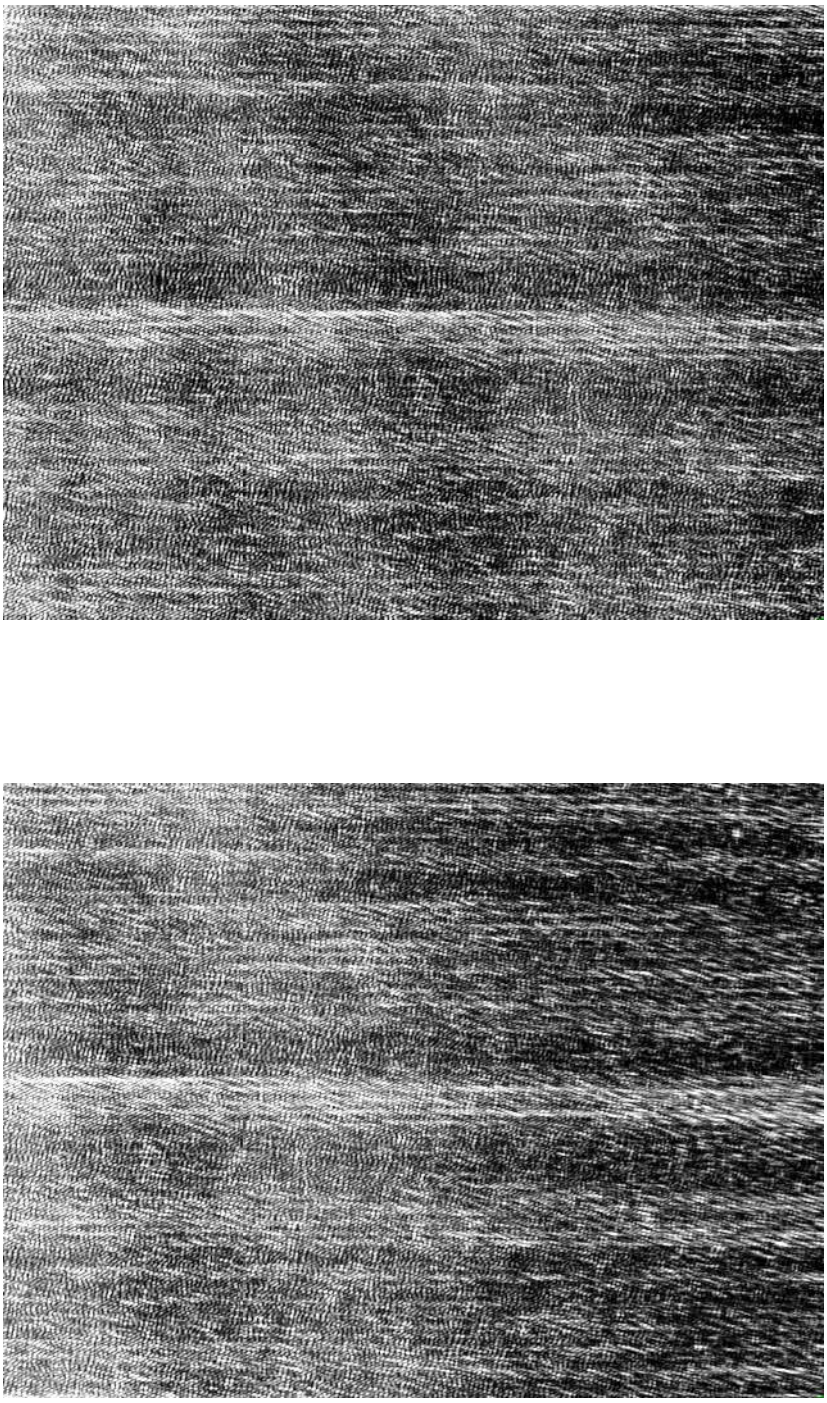

Figure G:The off-axis reflection configuration of the recorded interferogram of Augusto without negative lens.

Digitized by UCC, Library

Appendix G continued

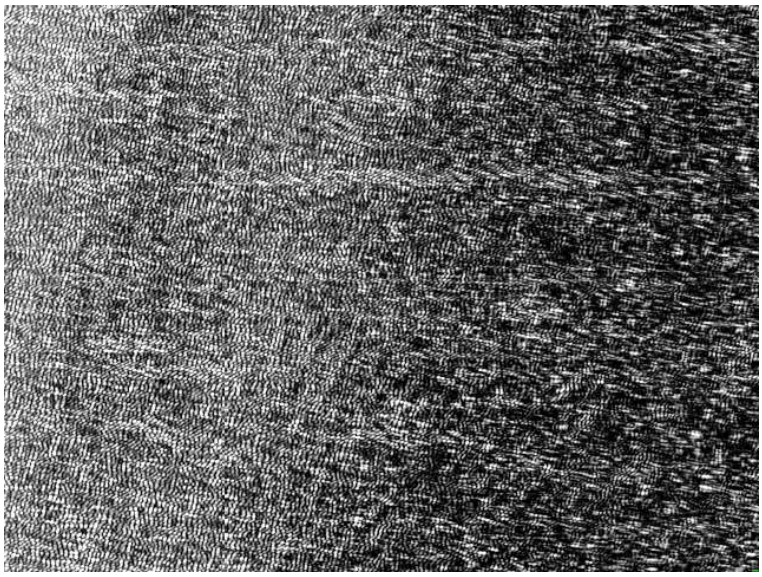

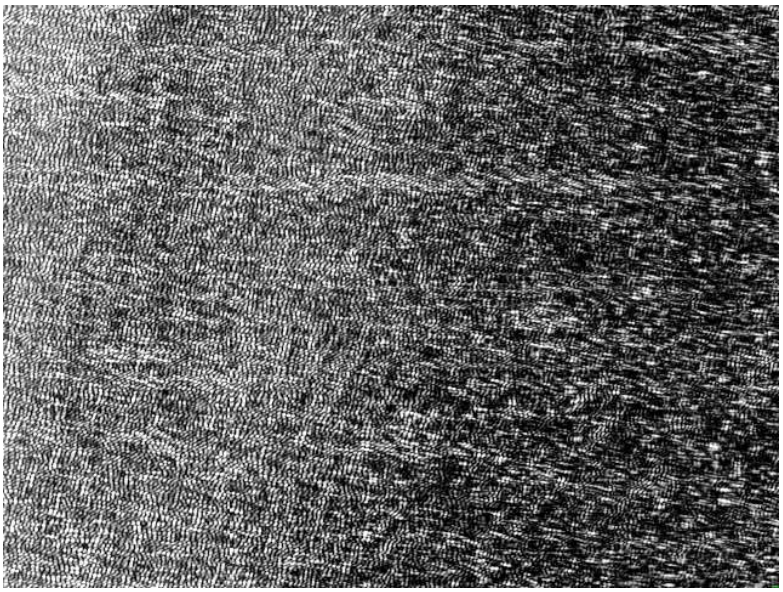

Figure G:The off-axis reflection configuration of the recorded interferogram of Augusto without negative lens.

Digitized by UCC, Library